THÈSE

En vue de l'obtention du

DOCTORAT DE L'UNIVERSITÉ DE TOULOUSE

Délivré par :

Institut National Polytechnique de Toulouse (INP Toulouse)

Discipline ou spécialité :

Micro-ondes, Électromagnétisme et Optoélectronique

Présentée et soutenue par :

M. EVELIO ESTEBAN RAMIREZ MIQUET

le jeudi 29 septembre 2016

Titre :

IMPLEMENTATION OF OPTICAL FEEDBACK INTERFEROMETRY FOR SENSING APPLICATIONS IN FLUIDIC SYSTEMS

Ecole doctorale :

Génie Electrique, Electronique, Télécommunications (GEET)

Unité de recherche :

Laboratoire d'Analyse et d'Architecture des Systèmes (L.A.A.S.)

Directeur(s) de Thèse :

M. JULIEN PERCHOUX

M. OSCAR SOTOLONGO COSTA

Rapporteurs :

M. ALAIN LE DUFF, GROUPE ESEO ANGERS

M. ERIC LACOT, UNIVERSITE GRENOBLE ALPES

Membre(s) du jury :

Mme ANNE HUMEAU-HEURTIER, UNIVERSITE D'ANGERS, Président

M. JULIEN PERCHOUX, INP TOULOUSE, Membre

Mme KARINE LOUBIERE, INP TOULOUSE, Membre

M. OSCAR SOTOLONGO COSTA, UNIVERSITE DE LA HAVANE, Membre

Doctorat de l'Université de Toulouse

Institut National Polytechnique de Toulouse

Implementation of optical feedback interferometry for sensing applications in fluidic systems

Evelio Esteban RAMIREZ MIQUET

Directeurs de thèse

Dr. Julien Perchoux

Prof. Oscar Sotolongo Costa

Abstract

Optical feedback interferometry is a sensing technique with relative recent implementation for the interrogation of fluidic systems. The sensing principle is based on the perturbation of the laser emission parameters induced by the reinjection in the laser cavity of light back-scattered from a distant target. The technique allows for the development of compact and non-invasive sensors that measure various parameters related to the motion of moving targets. In particular, optical feedback interferometers take advantage of the Doppler effect to measure the velocity of tracers in flowing liquids. These important features of the optical feedback interferometry technique make it well-suited for a variety of applications in chemical engineering and biomedical fields, where accurate monitoring of the flows is needed. This thesis presents the implementation of optical feedback interferometry based sensors in multiple fluidic systems where local velocity or flow rate are directly measured. We present an application-centered study of the optical feedback sensing technique used for flow measurement at the microscale with focus on the reliability of the signal processing methods for flows in the single and the multiple scattering regimes. Further, we present experimental results of *ex vivo* measurements where the optical feedback sensor is proposed as an alternative system for myography. In addition we present a real-time implementation for the assessment of non-steady flows in a millifluidic configuration. A semi-automatized system for single particle detection in a microchannel is proposed and demonstrated. Finally, an optical feedback based laser sensor is implemented for the characterization of the interactions between two immiscible liquid-liquid flowing at the microscale, and the measurement is compared to a theoretical model developed to describe the hydrodynamics of both fluids in a chemical microreactor. The present manuscript describes an important contribution to the implementation of optical feedback sensors for fluidic and microfluidic applications. It also presents remarkable experimental results that open new horizons to the optical feedback interferometry.

Keywords: Optical feedback interferometry; laser diodes; microfluidics, flow measurement; Doppler Effect.

Résumé

L'interférométrie par réinjection optique est une technique de mesure dont l'implémentation pour l'interrogation de systèmes fluidiques est assez récente. Le principe de mesure est basé sur la perturbation des paramètres d'émission du laser induite par la réinjection dans la cavité laser de lumière rétro-diffusée par une cible distante. La technique permet le développement de capteurs compact et non-invasifs qui mesurent différents paramètres liés aux déplacements de la cible. En particulier, les interféromètres par réinjection optique prennent avantage de l'effet Doppler pour mesurer la vitesse de traceurs dans les liquides en écoulement. Cet aspect important de la technique de réinjection optique la rend adaptée à une grande variété d'applications dans les domaines du génie chimique et du biomédical où un contrôle des écoulements est requis. Cette thèse présente l'implémentation de capteurs basés sur la réinjection optique pour différents systèmes fluidiques où la vitesse locale d'écoulement ou le débit sont directement mesurés. Nous présentons une étude centrée sur les applications où la réinjection optique est utilisée pour la mesure du débit à la micro-échelle avec en particulier une analyse de la robustesse des méthodes de traitement du signal propres aux régimes de diffusion simple et de diffusion multiple. Par ailleurs, nous présentons des résultats expérimentaux de mesures *ex vivo* où le capteur par réinjection optique est proposé comme alternative pour la myographie. Nous présentons également une implémentation temps réel pour l'estimation du débit instantané d'écoulements dynamiques dans une configuration milli-fluidique. Un système semi-automatisé de détection de particule unique dans un micro-canal est proposé et démontré. Enfin, un capteur basé sur la réinjection optique est implémenté pour la caractérisation des interactions entre deux fluides immiscibles en écoulement à micro-échelle et les mesures réalisées sont comparées à un modèle développé afin de décrire le comportement hydrodynamique des deux fluides dans un micro-réacteur. Le manuscrit décrit une contribution importante pour l'implémentation de capteur par réinjection optique pour des applications fluidiques et en particulier micro-fluidiques. Il présente également des résultats expérimentaux remarquables qui ouvrent de nouveaux horizons pour l'interférométrie à réinjection optique.

Mots clés: Interférométrie par réinjection optique; Diode laser; Micro-fluidique; Mesure de débit; Effet Doppler

Acknowledgments

I would like to express my deepest gratitude to those who contributed one way or another to the realization of the present thesis.

I thank Prof. Thierry Bosch for giving me the opportunity to join the OSE group at LAAS-CNRS. His continuous disposition and kindness will always be appreciated and remembered.

I have no words to express my gratitude and respects to my supervisor Dr. Julien Perchoux. Your constant guidance and advices pave the way to finally complete this goal. I sincerely say thanks for your tuition every step of the way. Likewise, I fully thank Prof. Oscar Sotolongo Costa for accepting to supervise my thesis work and for his continuous encouragements and wise advices through the course of these years. It was indeed an honor to have you both as my supervisors.

I wanna hereby acknowledge the contributions of my colleagues and friends who collaborated in the development of the present work, particularly those with whom I had the honor to work with: Lucie Campagnolo, Bendy Tanios, Adam Quotb, Antonio Luna Arriaga, Reza Atashkhooei, Raül da Costa Moreira and Yu Zhao. I really enjoyed the time we spent together in and outside the lab! The help provided by Véronique Conédéra and Rémi Courson in the clean room is equally appreciated.

To my dear fellows, I take a chance to reflect here that you will always be remembered as part of the greatest moments in my lifetime. Thank you for all we shared together my friends Jalal Al Roumy, Laura Le Barbier, Lavinia Ciotirca, Lucas Perbet and Blaise Mulliez, Fernando Urgiles, Harris Apriyanto and Mengkoung Veng. I equally appreciate the time spent with the *stagiaires* José Luis, Alejandro, Einar and Fadila as well as the research engineers Valeria, Allaoua and Gautier.

Likewise, the valuable help and technical assistance provided by Clément Tronche and Francis Jayat is highly appreciated. Thank you both for your disposition. Likewise, I show gratitude for Emmanuelle Tronche and the assistance provided with the intensive paperwork. I also thank the rest of the members of the OSE group: Francis Bony, Olivier Bernal, Hélène Tap and Han Cheng Seat.

This thesis is a final step in the research that I conducted in the field of Optical Feedback Interferometry, a technique I learned thank to my former supervisor Prof. Luis Martí López back in 2009.

The help provided by the *Centro de Aplicaciones Tecnológicas y Desarrollo Nuclear* in Havana is gratefully appreciated, especially from its former director Dr. Iván Padrón and the members of the Physics Department who guided me to the conceptualization and realization of the joint co-tuition of the present thesis.

… And the support and continuous encouragements of my family, especially my mother, Marlem, my grandma, my sister and Yancy who were there for me wherever it was necessary. Thanks!

I acknowledge the financial support provided by the French Embassy in Havana that allowed the funding of the present research work.

Contents

Introduction

Optics and photonics are present in everyday's life, in many technological devices recently introduced in worldwide markets. In addition, optical and photonic systems are still generating new discoveries, such as the relatively recent invention of the blue Light Emitting Diode, which led to three researchers to be awarded the Nobel Prize in Physics in 2014 as their discovery allowed the beginning of a new era in lighting applications. Last year was recognized by the United Nations as the International Year of Light and Light-based Technologies in a clear effort for emphasizing the top tanked role of optics, lasers and related disciplines in globalized world under continuous development.

With no doubt, the scientific community has found in optical sciences and photonic technologies a powerful tool to address cross-disciplinary research enabling the study, generation and development of new knowledge and applications in biomedicine, micro-nanotechnology and the environment.

Optical sensing and inspection has gained considerable attention over the last decades. Optical sensors are attractive for being precise and having non-contact nature. These elements make optics-based devices suitable for measuring physical parameters in non-destructive testing, where many other invasive techniques cannot be used or only with great difficulties. Optical techniques experienced a significant burst when lasers became available in the scene. The powerful

coherent light paved the way to the development of multiple interferometric and photonics related techniques that are employed today in diverse sensing applications. In this regard, the optical metrology took benefit from the particular features of lasers and their contribution to the development of multiple interferometric techniques that became part of routinely testing protocols in current manufacturing processes and worldwide production and maintenance.

In addition, the considerable size reduction of components and its combination with light technologies opens new promising perspectives for advanced imaging systems that can explore areas that where impossible to access before. This is the case of the tiny microscope developed recently and represents a major boost in non-invasive optical imaging of the brain [Kim, 2014].

Optical sensing techniques take benefit from the fact that they use light and non-destructive interaction with the inspected objects and therefore, they are well-suited as compared to many other electrical, mechanical, nuclear and chemical sensors with invasive measurements associated [Baldini, 2006].

Instrumentation and, in particular, optical instrumentation has been extensively projected as a tool in both laboratory environment and industry for addressing the measurement of flows. The need for accurate quantitative information of flows is recognized in the industrial world and laboratory environments.

Fluid flow measurements in microchannels and larger pipes and ducts are important in multiple processes in industry: chemical engineering, oil production, water treatment, but also in the biomedical field. To mention a few examples, microcirculation and blood perfusion in skin is closely related to anomalies in tissues and may be used as an indicator of potential malignant skin cancers such as melanomas. Blood flow monitoring in veins and arteries is used for the assessment of the circulatory system and angiography in human subjects as it may be used to prevent cardiac arrest. In chemical engineering, there is a vast use of flows for mixture, solution and transport. The use of flows in multiple applications in both macro and microscale was followed by the need of providing accurate velocity measurement in diverse scenarios. In this regard, several interferometric and image-correlation techniques exist which are widely used for quantitative and qualitative measurement of flows: speckle patterns, dual-slit, ultrasonics, particle image velocimetry, laser Doppler velocimetry and others are well-known and largely implemented techniques in fluid flow assessment.

The merge of optics and microfluidics is known as the cross-disciplinary field of optofluidics [Psaltis, 2007]. This rather recent denomination obeys to the fact that many groups dedicated to research on optical measurement technique achieve outstanding results to understand the behavior of flows at the microscale. Thus, the terminology optofluidics is nowadays referred to as the field of microfluidic technology assessed by optical means. Optofluidics has gained considerable

attention over the last years and has become a highly active area supported by a huge number of publications and developments that have revolutionized a wide range of applications in sensing and imaging [Fainman, 2009].

Although there is a vast amount of detection methods in microfluidics, including optical, electrical and mass spectrometry methods, the emerging field of microfluidic sensing has experienced a true fusion with optical measurement methods, which have become predominant in the field since its earliest developments [Wu, 2011]. Optical sensing comprise the direct detection of the flow in microfluidic devices by monitoring the light properties modulation due to the interaction light-flow.

Throughout this thesis, we propose to deploy optical feedback interferometry sensors for multiple sensing applications in fluidic systems, with strong emphasis in microfluidics. The experimental demonstrations presented in the frame of this manuscript accentuate the potential of this technique as an alternative optofluidic implementation system. We thereby utilize the capabilities of this technique for the interrogation of fluid flows with focus on the applicability in the chemical and biomedical field.

Several demonstrations of the potential applications of optical feedback effect and its use in optical sensing are provided and discussed in the present manuscript. The document is organized as follows:

Chapter 1 presents a review of the Doppler methods used for the analysis of flows. The main fundaments of the Doppler Effect are presented and the techniques using it explained in the frame of historical aspects, sensing system, recent developments associated and commercialization. We identified several largely used techniques and outline the relative aspects for every technique. The chapter presents Laser Doppler velocimetry, ultrasound Doppler velocimetry, optical Doppler coherence tomography, planar Doppler velocimetry, three-components laser two-focus velocimetry and finally optical feedback flowmetry. In the end of the chapter, a comparison of the techniques is provided as well as the main motivations of the present thesis manuscript are exposed.

The second chapter presents the sensing mechanism on which optical feedback interferometry is based. The chapter presents first the basics of the scattering theories and then the fundaments of the optical feedback effect. In the final part of the chapter, a section is dedicated to a detailed description of the characterization of the lasers used in this thesis.

Chapter 3 presents a huge portion of the experimental results obtained during the development of the present thesis. We describe the main processing methods used to quantify the flow velocity with optical feedback interferometry and present a complete analysis of the reliability of the flow measurement with this technique. The chapter continues with a demonstration of an ex-vivo flow mapping. Then, a

real-time system allowing the assessment of non-steady flows is presented and validated experimentally. The final section of the chapter presents a portion of an ongoing research work on single particle detection in microfluidic devices, which is proposed as a quality control system consisting on the inspection of fluids that should be free of particles.

The final chapter presents the implementation of the optical feedback interferometry sensing technique for the analysis of immiscible multiphase flows. A theoretical model based developed from the Couette flow approximation is proposed. The model is further validated with experimental measurements fluid velocity profile in microfluidic reactors.

In the end, a general conclusion is given and further perspectives are proposed.

Chapter 1

Doppler methods for flow measurements

In this chapter, some of the well-established techniques based on the Doppler Effect for flow measurements are reviewed and compared. In what follows, Laser Doppler Velocimetry, Ultrasonic Doppler Velocimetry, Optical Doppler Coherence Tomography, Planar Doppler Velocimetry, Three component laser-two-focus velocimetry and finally, Optical Feedback Flowmetry are reviewed to provide a general understanding of the historical and technological aspects that were developed to be part of the widely spread techniques allowing fluid flow assessment using the Doppler Effect.

The Doppler Effect

The Doppler Effect is defined as a change in the frequency of a wave when the reference observer moves towards or away from the source. It was named after

Christian Doppler, an Austrian scientist who proposed the first explanation of the phenomenon in 1842 in the frame of a meeting of the Natural Sciences Section of the Royal Bohemian Society of Sciences in Prague. Doppler's paper entitled "On the colored light of the double stars and certain other stars in heavens" was published in 1843 in the proceedings of the society [Doppler, 1843].

To provide a simple approach to the physics behind the Doppler Effect, let's consider a stationary light source emitting with a given wavelength λ and frequency f. The wave train with length λ needs a time $T = 1/f$ to pass a stationary observer. If the observer moves away from the light source the distance between them increases, and the waves would need more time ($T' > T$) to reach the observer. As the distance is modified, an equation describing this parameter can be set. The total distance cT' separating the observer and the source will be composed of the length λ plus the distance moved vT', where c is the speed of light and v is the velocity of the observer. The equation giving the distance is:

$$cT' = \lambda + vT' \tag{1.1}$$

which leads to

$$\lambda = (c - v)T' \tag{1.2}$$

Knowing that the new period is the inverse of the wave's frequency resulting from the displacement of the observer $T' = 1/f'$, $\lambda = c/f$ and substituting into equation 1.2, the relation between the orginal frequency and the one perceived by the observer is:

$$f' = \left[1 - \frac{v}{c}\right] f \tag{1.3}$$

From expression 1.3 follows that if the observer moves away from the source ($v > 0$) the new frequency is shifted to smaller values. If, on the contrary, the observer moves towards the source, the frequency shift increases.

1.1 Laser Doppler Velocimetry

The Laser Doppler Velocimetry (LDV) also referred to as Laser Doppler Anemometry was the first mature technique for flow measurement to be available for implementation. Since the sixties, soon after the laser appeared as a solution looking for problems, the LDV has been used in numerous applications ranging from aeronautics and turbomachinery to ophthalmology and other biomedical fields [Menn, 2004]. The main purpose of the technique lies in measuring the velocity and/or the length of moving surfaces.

1.1.1 History

Back in 1964, two scientists working on Rayleigh scattering modified a spectrometer with the idea of using the Doppler Effect to measure the velocity of particles flowing in a liquid. At that time, LDV was introduced by Yeh and

Cummins [1964]. In this work, the coherent light source was a He-Ne gas laser. Using optical elements, they split a laser beam and used one beam as a reference while the other was directed to illuminate a volume full of polystyrene spheres in water. After this interaction with the particles, the two beams were combined in a photomultiplier and the frequency shift was retrieved by processing the beat signal.

The original set-up employed by Yeh and Cumins is shown in Fig. 1.1. Using this system and pointing to the center of a cylindrical tube with 10 cm of diameter, they were able to measure part of the laminar velocity profile of particles in water. Also, they demonstrated the linear relation of flow rate with respect to the bear frequency, a validation used today in many fluidics applications. Since this first demonstration, the feasibility of LDV for flow measurements was evident and widely considered as a potential technique in the field.

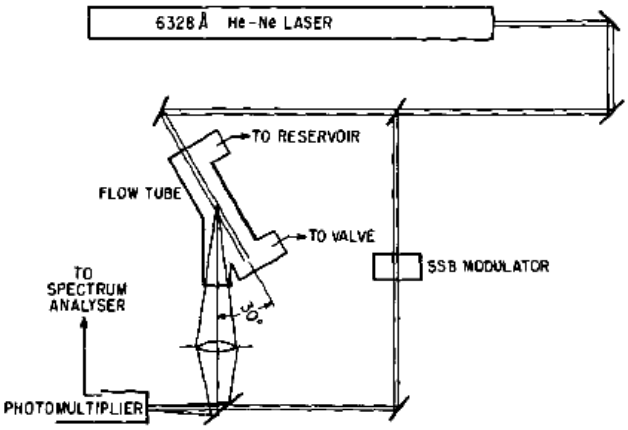

Fig. 1.1. Original Laser Doppler velocimeter set-up proposed by Yeh and Cumins in 1964.

Only one year after the original work presenting LDV was published, Foreman [Foreman, 1965] used the same technique for measuring gas flow using smoke as scattering particles, thus extending the potential application of LDV to measure the velocity of particles with random size and shape. In 1966, Foreman revised the configuration employed by Yeh and Cummins to develop a new version of the laser Doppler velocimeter [Foreman, 1966], where it was highlighted the potential use of LDV as an alternative to less powerful techniques available at the time for fluid flow measurements: the pitot tubes and hot-wire anemometers. Fig. 1.2 shows the set-up that allowed to cover 90% of the velocity profile in a circular tube with 1.1 cm internal radius.

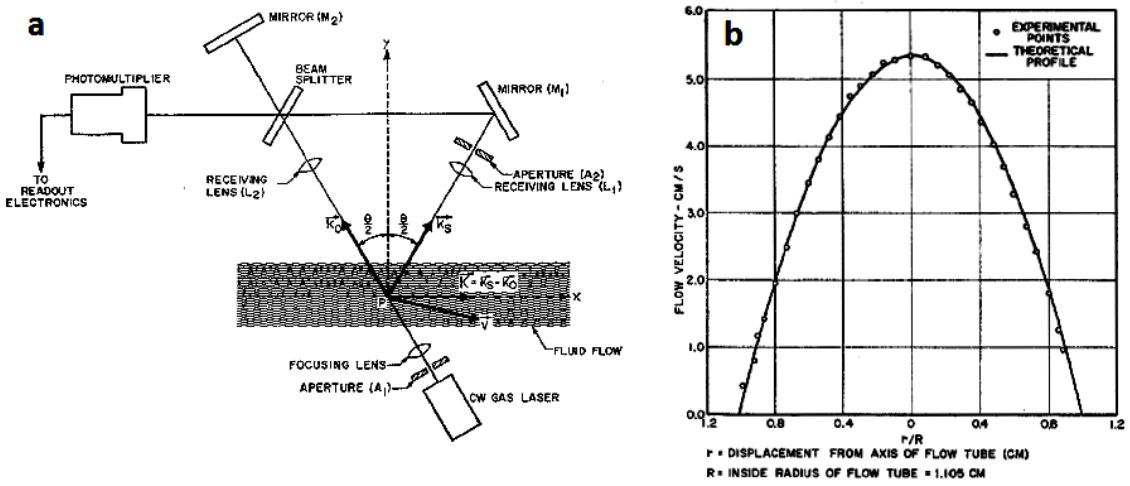

Fig. 1.2. LDV set-up employed by Foreman [1966] to measure gas flow (a). Measured velocity profile using this optical configuration (b).

1.1.2 Sensing principle

In LDV, small particles are immersed into the fluid to guarantee that they are subject to the hydrodynamic conditions of the carrier flow so that it is understood that they are tracers. Then, a laser beam is split into two identical parts using optical elements such as mirrors and both beams are directed together into a sensing volume, the so-called probe volume.

Fig. 1.3 provides a simple view of the principles on which the sensing scheme is based. As both beams illuminate a common area, an interference pattern is produced and dark and bright fringes become apparent in the probe volume.

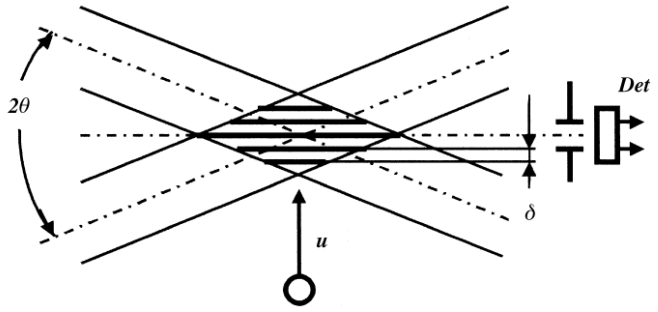

Fig. 1.3. Interference occurring in a probe volume in LDV. Scheme extracted from [Menn, 2004].

Fringes of the interference pattern are equally spaced and spacing δ is ruled by the angle θ so that:

$$\delta = \frac{\lambda}{2\,sin\theta} \tag{1.4}$$

where λ is the laser wavelength and θ is half the angle between the two split beams.

When a particle moves through the probe volume with velocity v_p, it crosses dark and bright fringes so that the intensity of the scattered light varies with a frequency f_p:

$$f_p = \frac{v_p}{\delta} \tag{1.5}$$

Photodetected signals contain information on the frequency, and the velocity of the particles in the probe volume is determined by:

$$v_p = \frac{\lambda}{2\,sin\theta} f_p \tag{1.6}$$

This detection system was first proposed by Rudd back in 1969 [Rudd, 1969].

Multiple optical arrangements of LDV systems were proposed. Some of them were review in detail by Wang [Wang, 1988]. In this paper, some of the possible configurations to collect the light scattered by particles in fluid are outlined: the so-called local oscillator heterodyne arrangement (shown in Fig. 1.4), the differential heterodyne arrangement depicted in Fig. 1.5 and the symmetric heterodyne arrangement represented in Fig. 1.6.

All these configurations are equivalent when measuring flows, but each of them has particular features in the way scattered light is collected. In the heterodyne system shown in Fig. 1.4, light is detected with narrow collection angle as only light scattered in the direction of the photodetector contributes to the signal. The scheme makes this configuration more suitable to detect the signal of highly reflective particles that may saturate the detection component.

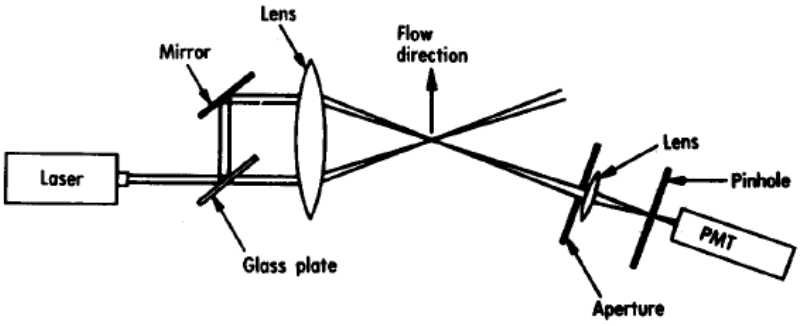

Fig. 1.4. Representation of the local oscillator heterodyne LDV arrangement. Figure is taken from Wang [1988].

In the differential heterodyne arrangement represented in Fig. 1.5, light coming with two different wave vectors is scattered from particles in the flow and collected with a large solid angle in a photodetector. This is of particular importance in the sense that low reflective particles acting as a non-cooperative target may be detected.

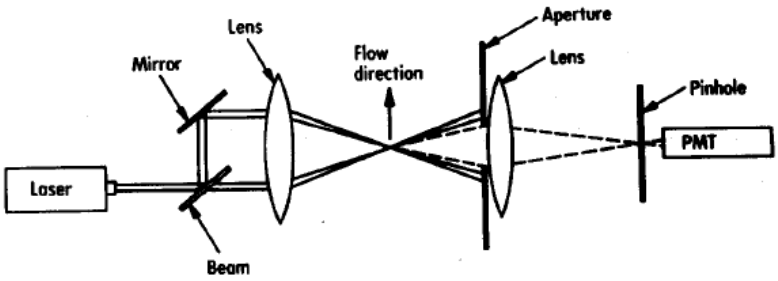

Fig. 1.5. Representation of the differential heterodyne LDV arrangement. Figure is taken from Wang [1988].

Finally, the symmetric heterodyne configuration depicted in Fig. 1.6 is an arrangement for which the probe volume does not result from the intersection of two beams. Light is scattered at the focus point, collected by a simple optics from two different directions and mixed in the photodetector. The interference pattern is generated in front of the photodetection device, thus imaging a moving fringe pattern. In other words, interferometric fringes move across the photodetector [Wang, 1974; Penner, 1970]. The signal to noise ratio is higher with this configurations and it is well suited for flow measurement in sub-millimetric channels.

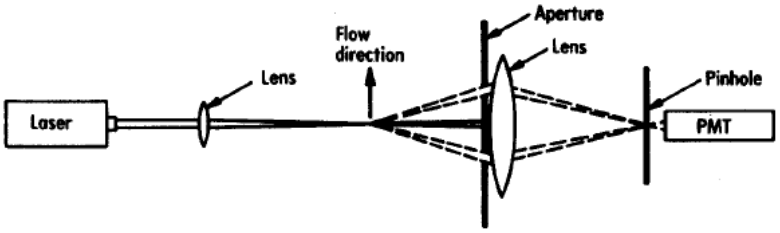

Fig. 1.6. Representation of the symmetric heterodyne LDV arrangement. Figure is taken from Wang [1988].

1.1.3 Recent developments and commercialization

Recent approaches use modified versions of different optical systems. That is the case of the configurations proposed by Voigt [2008] and König [2010], who used the LDV with convergent and divergent fringe patterns instead of using parallel fringes. This set-up increased the temporal and spatial resolution of previous LDV systems. It is reported that high resolution (4 μm) in one of the velocity components of the flow was achieved. The highest resolution for a LDV system was reported by Büttnerin 2010, who achieved a spatial resolution of 1.2 μm with associated uncertainty in the measurements of 0.25%.

Laser Doppler velocimetry is today a mature enough technology so that commercialization of industrial solutions are available from manufacturers from all over the world. Just to mention an example, Polytec developed a series of laser

Doppler velocimeters such as the LSV-6000. This velocimeter, depicted in Fig. 1.7a, uses an optical head incorporating an LDV system which enables non-contact measurement velocity of moving targets in real time with accuracy of 0.05 % and repeatability of 0.02 % with respect to the measurement value. Other LDV systems are used for continuous monitoring of flows using this technology. The FlowExplorer DPSS shown in Fig. 1.7b measures flow travelling at velocities as high as 600 m/s and measures with uncertainly as low as 0.067% of the detected speed. With more than fifty years since this invention was created, LDV is available to provide robust, accurate and reliable solutions for the scientific and technological developments and for sensing applications using laser light. However, in spite of its unquestionable advantages, the equipment using this technique is expensive and bulky for some specific applications where flow velocity measurement is a need. In addition, the LDV optical arrangements require multiple components acting as the interferometer, thus alignments of mirrors and beam splitters is necessary.

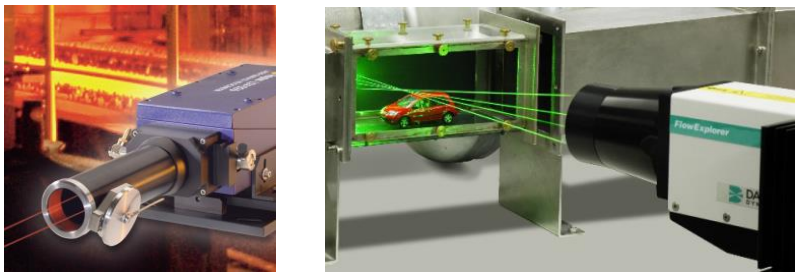

(a) **(b)**

Fig. 1.7. Polytec (a) and FlowExplorer DPSS (b) LDV commercially available products used currently in flow sensing.

1.2 Ultrasound Doppler Velocimetry

The Ultrasonic Doppler technique is a well-known and largely implemented method for non-contact measurement of flow velocity with accuracy. When used for this purpose, it is recognized as Ultrasound Doppler Velocimetry (UDV) [Takeda, 1999]. It presents the advantage that the carrier wave does not need to be transmitted only through a transparent or semitransparent pipe, so this technique can be used where light based Doppler techniques, such as Laser Doppler Velocimetry cannot be applied.

1.2.1 History

Ultrasound Doppler velocimetry had its early developments in Japan and the United States. The Institute of Scientific and Industrial Research of Osaka University developed the first Doppler ultrasound device for medical diagnosis [Satomura, 1957]. Using the promising results published in 1957 and based on this own experience, Satomura projected the utilization of the Doppler ultrasonography for exploring blood flow in percutaneous tissue. Together with

Kaneko, he reported the first ultrasonic flowmeter in 1960 [Satomura, 1960]. Parallel developments were performed at the University of Washington in Seattle, where a group headed by Rushmer and Franklin conceived and developed a continuous-wave prototype device using backscattered ultrasound frequency shift for blood flow measurement [Franklin, 1959]. The original system and methodology developed by the Seattle group is shown in Fig. 1.8 A refined version of this device was employed in clinical trials by Eugene Strandness [Strandness, 1967] during the mid-sixties, who could use a portable ultrasonic Doppler flowmeter for assessment of vascular diseases as part of his training as a vascular surgeon.

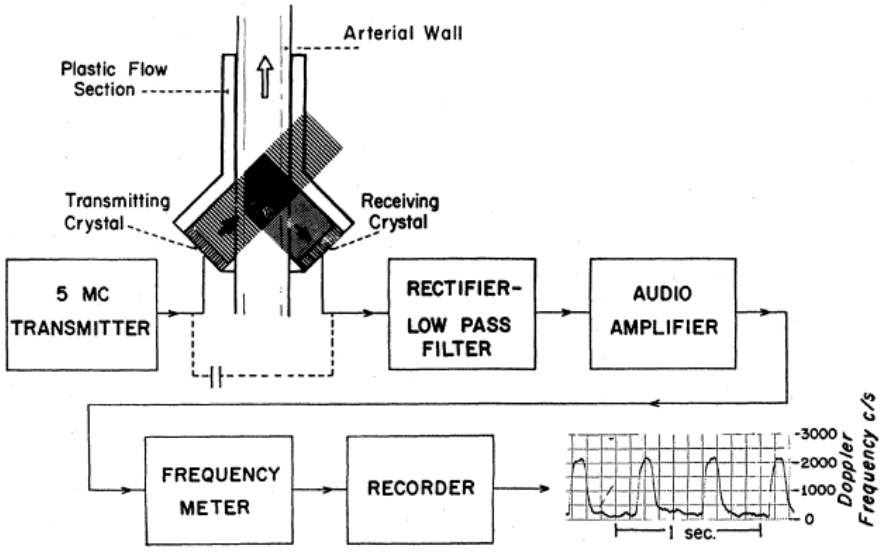

Fig. 1.8. Ultrasonic system using continuous-wave pulsing developed at University of Washington for blood flow measurements using the Doppler Effect. Picture extracted from [Franklin, 1959].

Pulsed-wave Doppler equipment was developed simultaneously by the Seattle group from 1966 on, and also by other groups in the United Kingdom and France [Baker, 1970; Wells, 1969; Peronneau, 1969]. A major advancement in the technique was obtained by the Seattle group when the duplex Doppler was invented. The duplex Doppler instrument contained a mechanical scanning head that enabled the ultrasound operator to determine the target of Doppler insonation. This development was revolutionary as it allowed the interrogation of deep-lying circulation in the human body. In terms of applicability to fluid flows assessment, this invention opened the possibility of using ultrasonic signals for the interrogation of corporeal circulators.

Continuous-wave Doppler ultrasonography characterized the implementation of Ultrasound Doppler in obstetrics, where it became a standard technique for fetal heart diagnosis. This is perhaps the most extended use of Doppler ultrasonography in medicine, where it has established as a major clinical diagnostic tool. Fully implemented Doppler velocimetry in obstetrics was first reported by FritzGerard and Drumm [FritzGerard, 1977], who published the first article in the field. Also,

McCallum and colleagues, who at the time were part of the Seattle group at University of Washington, pioneered the real time implementation of this technique [McCallum, 1977].

1.2.2 Sensing principle

Ultrasonic Doppler flowmeters operate using the frequency shift that a sound wave experiences due to the Doppler Effect. Usually, a transducer is employed to transmit a wave through a medium, and the moving components in the medium generate a shift in the carrier signal. The motion is measured after comparing frequency shift between the ultrasonic frequency source, the receiver and the fluid carrier.

The sound wave emitted by the transducer in the ultrasonic Doppler device travels from the face of the sensor to the flow stream. When the wave intercepts a moving particle merged in the flow, its frequency is shifted and consequently it differs from the original source frequency. Due to the Doppler Effect, if particles move toward the transducer, the Doppler-shifted wave will contain higher frequencies than the transmitted wave. In terms of mathematical representation, this process is described by the Doppler equation:

$$v = \frac{v_m(f_r - f_t)}{2 f_t cos(\varphi)} \tag{1.7}$$

where v_m is the velocity of the sound wave in the medium is, f_t is the transmitted wave frequency, f_r is the received wave frequency and φ is the angle between the transmitted ultrasound beam and the flow velocity vector. Equation 1.7 implicates that the angle φ should be precisely determined to obtain an accurate measurement of velocity.

Further developments included miniature sensors to measure the blood flow in animal aortas [Nakamura, 1986]. The system conceived a practical approach to *in-vivo* measurement of blood flow in small vessels that enabled the detection of induced heart failures. The schematic diagram used for the implantation is depicted in Fig. 1.9. Subsequent improvements in the technique were presented by Tamura and colleagues to overcome the dependence of the velocity measurement of the Doppler angle [Tamura, 1988; Tamura, 1987; Tamura, 1990].

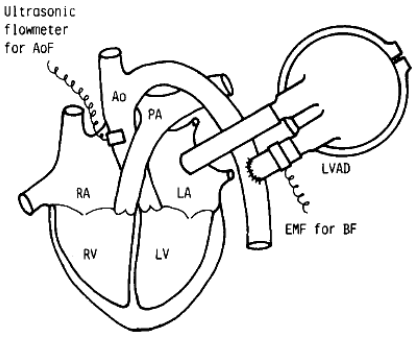

Fig. 1.9. Implanted Ultrasonic Doppler Flowmeter proposed by Nakamura *et al*. for in-vivo measurement of blood flow.

In 1986, Takeda presented an ultrasonic blood flowmeter capable of measuring the entire flow profile of millimetric channels with a spatial resolution of 0.7 mm.

Akamatsu developed an Ultrasound Doppler catheter insensitive to the angle of incidence of the source wave [Akamatsu, 1996]. Instead of using the classical expression represented in Eq. 1.6, they proposed a methodology considering a measurement at two different angles (α and α+Ω) thus obtaining a new expression for calculation of the flow velocity: $v = (v_1^2 + v_2^2)^{1/2}$ which becomes:

$$v = \frac{v_m}{2f_t}(\Delta f_1^2 + \Delta f_2^2)^{1/2} \tag{1.8}$$

While the theoretical fundaments were correct, the method has not been implemented, the main obstacle being that two separated beams need to be emitted to a common point with different Doppler angles.

1.2.3 Recent developments and commercialization

Other challenges related to UDV for flow assessment include the capability of measuring flow velocities higher than the maximum detectable velocity imposed in the Nyquist theorem. As the physical principle of supporting this technology depends on the velocity of propagation of the carrier ultrasonic wave, aliasing may arise as fast flows are measured.

Murakawa recently addressed this technical limitation. They proposed a method with dual-pulsed repetition frequency for ultrasonic flow measurements [Murakawa, 2015]. The method is aimed at overcoming the aliasing in the velocity detection, thus providing a way to extend the applicability of UDV to sense flow travelling at high velocities. In addition, the spatial resolution of the UDV sensing system achieved with this configuration ranges in between 0.74 and 2.96 mm.

Utrasound Doppler Flowmeters are accurate, non-contact liquid flow measuring devices. These devices are commercially available to satisfy the demands of the industry, where flows can be measured non-destructively even in adverse scenarios.

Research on UDV made possible that knowledge generated around the technique facilitated its implementation in commercial products available since many years. One can mention, for example, the Hitachi EUD-3B professional ultrasonic velocimeter capable to measuring flows [Nakamura, 1986]. Other technological UDV solutions are found in large water storage facilities, as for example the ISCO 4150 Doppler velocimeter which continuously measures the flow stream profile and automatically detects changes in the velocity distribution. Today, the technique is supported by a vast state of the art that enabled the extended use of UDV in laboratories, industry and as a valuable tool in in-field flow assessment.

1.3 Optical Doppler Coherence Tomography

Doppler Optical Coherence Tomography is a relatively recent technique using low-coherent light combined with the Doppler Effect to visualize and quantify mostly blood flow. Since early nineties, many studies have been performed to extract information on pathological structures and angiographic components in living subjects, where the utilization of this technique has provided the specialists with valuable data allowing diagnosis and assessment of morphology of tissue and microcirculation without any invasiveness. Thereby, implementation of this technique in medical studies opened promising perspectives in ophthalmology and angiography [Leitgeb, 2014] as well as in gastroenterology [Osiac, 2011].

1.3.1 History

The history of Optical Coherence Tomography (OCT) dates back to the early nineties, when it found its bases upon the development of low coherence interferometry. A group headed by professor Fujimoto from the Massachusetts Institute of Technology pioneered the first developments in the technique [Huang, 1991; Swanson, 1993]. OCT shares some similarities with ultrasound and both techniques are usually compared in experimental work reported in the literature. However, OCT is capable of providing high resolution cross sectional images allowing 3D mapping of samples. In early nineties, there was little availability for alternative imaging systems working at higher resolutions than the one allowed by high-frequency ultrasound and greater penetration depth than that of confocal microscopy [Drexel, 2004; Rajadhyaksha, 1999]. First applications included the study of tissue structure and targeted OCT's direct implementation in diverse medical domains, predominantly in ophthalmology.

Doppler OCT, also referred to as Optical Doppler Tomography (ODT) combines the fundamental principles of low coherence tomography and the Doppler Effect. It is an extension of classical OCT, aiming at outlining the morphology of tissue and providing values for the underlying microcirculation in this tissue. Moreover, ODT possesses a unique capability to be implemented for qualitative investigation of tissue shape and localization of vessels and arteries within living structures and

at the same time, it allows quantitative study of blood velocity associated with the circulatory system.

It should be noted, that most of research on OCT lies at the intersection of biomedical research and clinical diagnosis. As compared to other methods, OCT uses light in the visible and infrared region, so photons are less energetic than photons used in X-ray and gamma-ray systems widely used in medical imaging which have the inconvenient that they could damage biological samples [Boppart, 2004; Sun, 2013]. This makes OCT based diagnosis more suitable in clinical inspection and cancer diagnosis.

1.3.2 Sensing principle

ODT is non-invasive in nature as it uses low coherent light for inspection of the sample. The first set-up reported used a fiber Michelson interferometer associated to an automated translation stage for producing a three-dimensional image of tissue microstructures. This set-up is depicted in Fig. 1.10. Light emitted form a superluminescent diode (SLD) is partially directed into a reference arm in the interferometer and the other part is headed to the sample arm. The reference arm contains a mirror coupled to a longitudinal displacement mechanism and the sample arm allows displacement in the sense of the desired scan direction of the sample.

The sensing purpose of this technique lies in scanning the reference mirror arm and recording the amplitude of the interference pattern generated by the waves with similar path length. As stated above, ODT uses a combination of OCT with the information extracted from the Doppler Effect. Its first application in 2D imaging dates back to 1997, when the technique extended the use of OCT for obtaining quantitative values of blood flow velocity [Chen, 1997]. Light backscattered from moving elements (or particles) interferes with the light taken as a reference and its frequency is Doppler shifted in the interference pattern intensity. This shift is characterized by an amount given by [Chen, 1997]:

$$f_D = \frac{1}{2\pi}(\boldsymbol{k_s} - \boldsymbol{k_i})\boldsymbol{v} \qquad (1.9)$$

where k_i and k_s are wave vectors of incoming and scattered light respectively, and v is the velocity of moving particles.

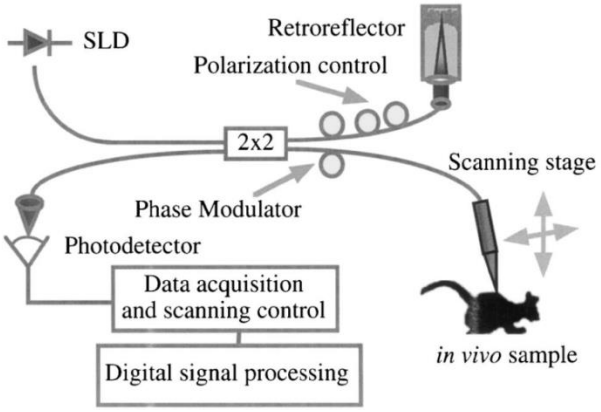

Fig. 1.10. DOCT system reported by Chen [1997].

The analysis of Doppler frequency extraction from OCT is straightforward. Light reflected by the sample is transmitted via the optic fiber in the reverse direction of the incident light and consequently $k_s = -k_i$. Then, Eq. 1.9 can be rewritten as [Wu, 2004]:

$$f_D = -\frac{2k_i v}{2\pi} = -\frac{2nv\,cos\theta}{\lambda} \tag{1.10}$$

where n is the refractive index of the medium surrounding the particles, λ is the light wavelength and θ is the angles of the Doppler shift, thus the angle between k_i and v. Equation 1.9 is the general form for light Doppler shift and expression 1.10 is identical to the general equation ruling Doppler detection systems as represented in the expression 1.6.

Using successive scans of the sample it is possible to generate a three-dimensional map describing the morphology of biological tissues and the velocity of flowing flows associated to the microcirculation undergoing in the biological sample. The values of velocity allow for the localization of vessels and arteries and their differentiation. Moreover, ODT is useful for *in vivo* flow profiling with micrometric resolution. Fig. 1.11 shows an OCT structural imaging of tissues surrounding a vessel, and the information of velocity associated to the flow inside it. The flow profile measured using ODT demonstrates the capabilities of this technique in measuring simultaneously parameters allowing clinical diagnosis with high resolution and accuracy.

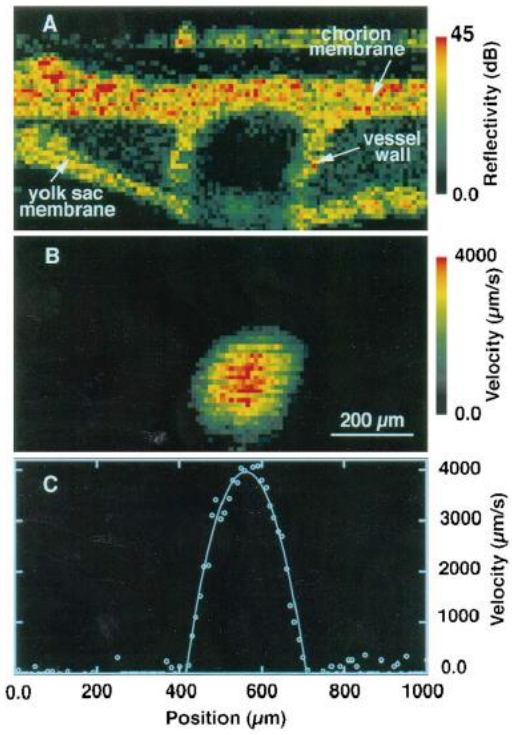

Fig. 1.11. Structural ODT imaging of biological tissue (a). Velocity of a vessel inside the tissue (b). Flow profile inside the vessel (c). Pictures correspond to Chen [1997].

1.3.3 Recent developments

Most of the technological advances and implementations of Optical Doppler Tomography have taken place in the biomedical field. Recently, a review by Leitgeb [2014] outlined the main promising introduction of ODT in quantifying blood flow. Wang [2011] used the technique in assessment of reduction of blood flow in retina in the presence of diabetes. Also, in the same work, ODT capabilities were employed to correlate the visual field loss with the reduction of the blood flow for patients with glaucoma.

In microfluidics, the intrinsic high resolution of ODT enabled a step forward in the analysis of mixtures as it allowed the study of secondary flows in microfluidic devices with a spatial resolution ranging from 2 to 10 μm [Ahn, 2008].

Application centered ODT has experienced a significant burst over the last years, and literature has references coming from a wide range of specific applications. The particular use of the Doppler effect combined with OCT has facilitated the recent advances experienced in medical diagnosis. In the last years, huge progress has witnessed the biomedical optical community as reviewed by Leitgeb [2014]. Most of the experimental work associated to ODT is subject of current research on biomedical optics, thus this technique has become a yardstick in routinely medical procedures with excellent spatial resolutions reported in the order of 1-10 μm [Raghunathan, 2016]. Blood flow is used as an indicator in clinical diagnosis due to its connection with neural activation in a phenomenon called neurovascular

coupling [Attwell, 2010]. Also, this technique provided sensitive quantitative data for the study of retinopathy and the influence of diabetes in it [Wang, 2009].

1.4 Planar Doppler velocimetry

The experience generated with the advent of the laser and its use in flow measurements pioneered by Yeh and Cummins [Yeh, 1964] pave the way to further developments integrating the Doppler Effect with optics and laser technology and its potential utilization in measuring flow velocity. Planar Doppler Velocimetry (PDV), also known as Doppler Global Velocimetry is another optical technique with relative recent presence in the analysis of flows. This technique uses a planar imaging configuration of the light emitted by a laser that illuminates a medium with particles. The scattering produced by these particles is used for the measurement of a Doppler frequency shift of backscattered light to further turn it into an intensity distribution.

1.4.1 History

In 1991, Komine and Brosnan developed the original Global Doppler Velocimeter using a molecular filter to identify the Doppler shift in scattered light generated by particles in a flow illuminated with a laser [Komine, 1991]. The idea is based on the concept of the filtered scattering produced by small particles and molecules in the flow [Miles, 1990]. The technique was rapidly introduced in the analysis of mixing [Elliot, 1992] and flows travelling at high velocities [Elliot, 1994].

McKenzie explored PDV in flow assessment using a pulsed laser [McKenzie, 1996] and presented the capabilities of the technique in measuring slow flows [McKenzie, 1997]. Several groups accelerated the implementation of PDV to visualize fast processes in fluid, including velocity measurements of supersonic jets [Clancy, 1997; Clancy, 1999]. During the development and consolidation of the technique, authors started to denominate it as Planar Doppler Velocimetry, that was found to be more precise than Doppler Global Velocimetry, but any of these terms is found in the current literature.

1.4.2 Sensing system

The global idea of this technique lies in the measurement of the scattered light produced by particles in a fluid when a laser illuminates them using a sheet forming optics. The word planar refers to an illuminated interrogation region that is monitored by a full-field visualization device. Then, backscattered light is transmitted through a beam splitter and two 50 % components of the laser beam are redirected towards a camera. A graphical representation of the system is depicted in Figure 1.12a. The purpose is to divide the light beams and to propagate one of them into an iodine filter with known transmission function. The laser is tuned to produce Doppler shift in the region close to a midpoint between the transmission and the absorption of the molecular filter. In this way, the

variations of the intensity of light are proportional to the Doppler shift produced by the scattering centers of the flow. Both intensity images obtained with the cameras are compared and by normalizing the intensity values the variations of the flow velocity can be quantified.

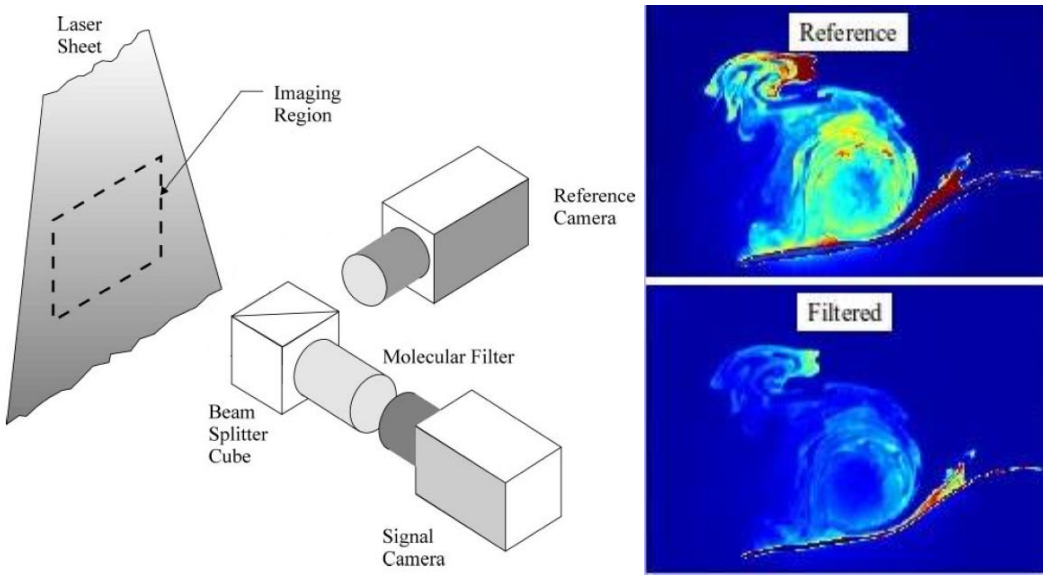

Fig. 1.12. PDV system for flow measurements using a reference camera and a signal (filtered) camera (a). Measured qualitative velocity (b).

In its simplest configuration, this set-up can be used for quantifying complex flows fields using the rate capabilities of a visualization device such as cameras [Meyers, 1992]. Since the early introduction of this technique, it has been considered as a step forward towards full-field flow measurements beyond single point measuring scheme. Is this particularly useful in the qualitative visualization of vortex trajectories and other features of complex flow that are difficult to measure [Samimy, 2000; Elliott, 1999]. The Doppler shift of scattered light is then measured using the expression 1.6.

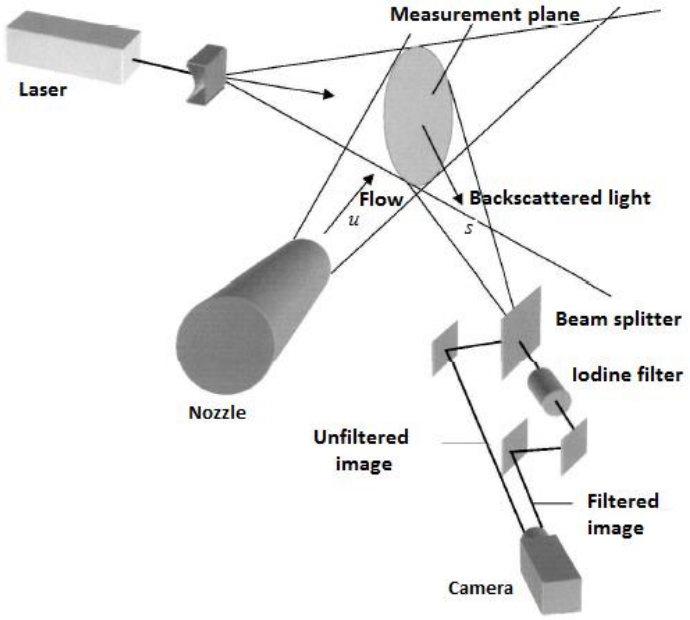

Fig. 1.13. PVD systems based on a single visualization system. Image belongs to reference [Samimy, 2000].

However, it should be pointed out, that measuring the Doppler shift is necessary in the implementation of the technique but not fully sufficient for measuring the desired velocity of the flow. The set-up described in Figure 1.13 is sensitive to obtain velocities components in the direction $(s-u)$. In order to measure all possible components of flow velocity the detection system needs to be modified so that the scattering produced by particles is observed from three different directions. This configuration was explored by Clancy [1999]. Another setup proposal was explored by Roehle [1998]. This design consisted in bringing the laser sheet from three different directions and observing the scattering components with the configuration shown in Figure 1.14. Generally, the system configuration used by Clancy is considered to be simpler in spite of requiring multiple visualization devices. The schematic representation of Clancy's configuration is presented in Fig. 1.14.

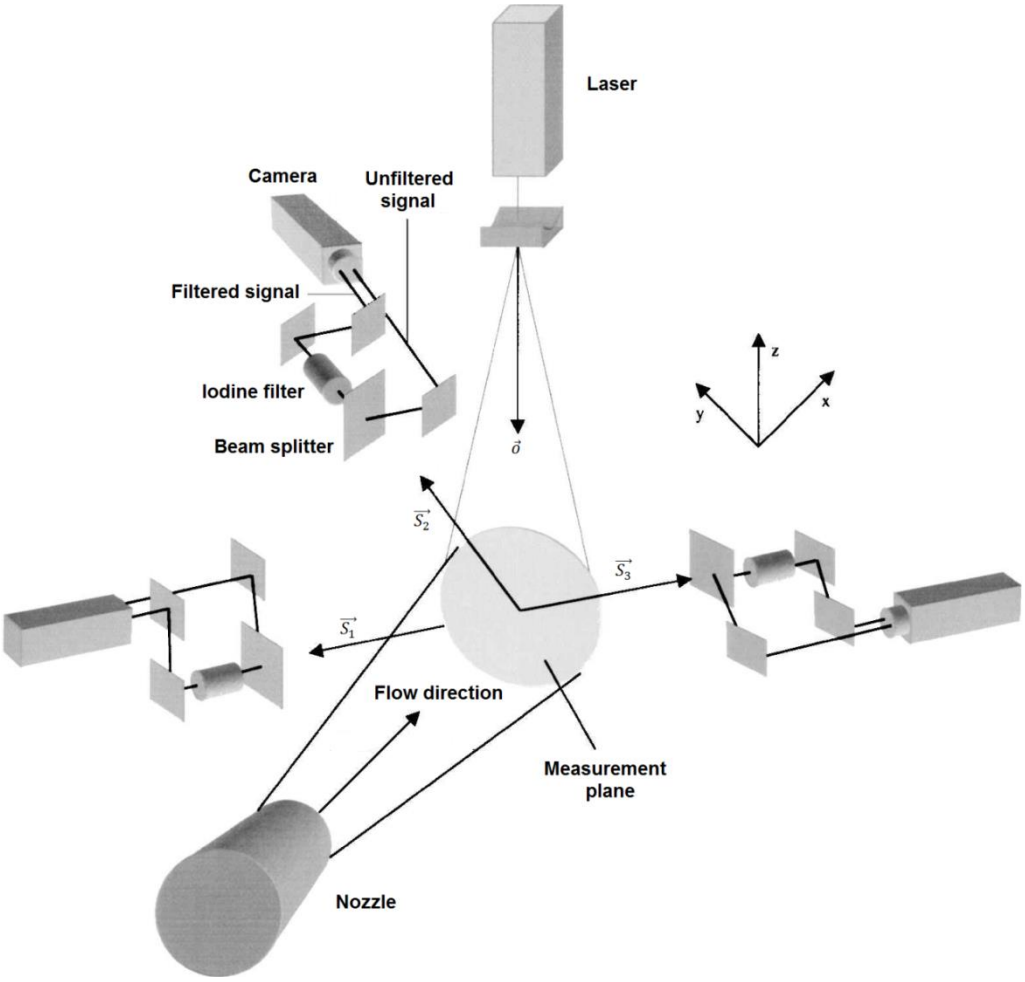

Fig. 1.14. PVD system proposed by Clancy in 1999. The PDV setup consisted of multiple cameras for retrieving the velocity components of the flow. Image belongs to reference [Samimy, 2000].

1.4.3 Recent developments and commercialization

Planar Doppler Velocimetry is used nowadays as an alternative sensing technique to Particle Image Velocimetry, a well-established technique widely employed in flow measurement and instrumentation while huge progresses are demonstrated in the frame of application-centered research. Recently, an improved frequency modulated PDV system was proposed to measure non-steady spray flows [Fischer, 2014]. In addition, a cross correlation processing of the signals generated from a PDV setup allowed the measurements of fast flow stream, with mean velocities measured in the order of 600 m/s, with significant reduction of uncertainty in the measurements [Cadel, 2015].

The PDV setup is complex to assemble and manipulate. Therefore, rather than widely commercialized equipment, technological facilities offering precise and accurate velocity measurements are established as for example The Virginia Tech Doppler Global Velocimeter [Jones, 2001]. Also, German automotive engineering services providers such as IAV, established PDV services to measure turbomachine flows and developed the software *DGV Evaluator* for the analysis

of the three components of the flow fields. According to Harald Müller from PTB in Germany, PDV "has become a promising flow field diagnostic tool for research and development tasks in aerospace and car industry".

1.5 Three-Component-Doppler-Laser two-focus Velocimetry

1.5.1 Laser two-focus velocimetry

The Laser two-focus (L2F) velocimetry is another method to measure flow velocity, also known in literature as Laser Transit Anemometry. It shares some elements with Laser Doppler Velocimetry and Planar Doppler Velocimetry such as the use of particles merged in the flow and its use in applications with fast flows.

This method was demonstrated for the first time in 1968, when Thompson introduced the original idea outlining the fundamental principle behind this technique [Thompson, 1968]. In this seminal paper, the author highlighted the potential of Laser Doppler Velocimetry and presented some drawbacks inherent to this technique. Based upon those elements, he proposed the original Laser two-focus velocimeter, depicted in Fig. 1.15 and conceived it for measuring dust particles in a turbine flow.

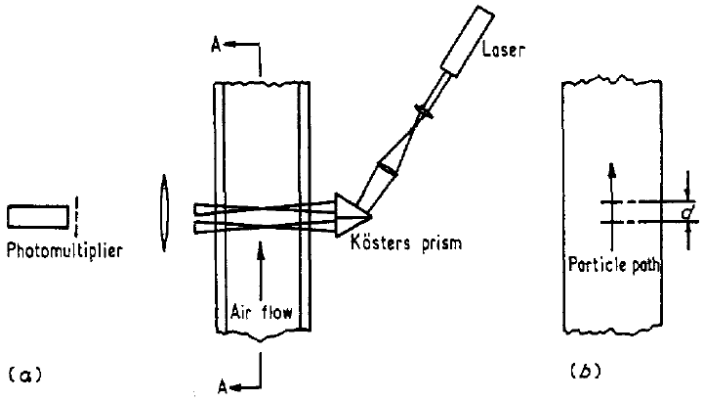

Fig. 1.15. First Laser two-focus system proposed by Thompson [Thompson, 1968].

L2F works with a simple principle. Tracer or suspended particles travel between two laser beams and their transit time is measured. Since the coherent beams are focused in a small volume where they are parallel and the distance separating them is perfectly known, the velocity is directly correlated to the transit time, so this interval serves as the quantitative value for determining the velocity parameter. The fact that the measurement takes place using a focused light, the intensity in the scattering is higher than in Laser Doppler Velocimetry, and this enables that particles with diameters smaller than 0.1 μm can be detected [Schold, 1980].

The capabilities of L2F have been tested in many scenarios, including wind speed, water pumps and stream flows. However, probably the most widespread

application is in experimental turbomachinery, where it is used in the analysis of turbulence [Kost, 1997] and vorticity in highly complex flows [Ball, 1988].

However, there are some specific applications where the optical access to flow is hard and applying L2F to measure three component of velocity is cumbersome or simple impossible. For those cases, a combination with other techniques is a reliable solution.

1.5.2 3C-Doppler-L2F Velocimetry

L2F is itself a non-Doppler technique. It became part of the Doppler methods for flow measurement when it was first combined with the Planar Doppler Velocimetry in what it now known as Three Component Laser two-focus Doppler Velocimetry [Förster, 2002]. By merging the features of PDV and L2F, the sensing system developed by Förster is capable of measuring every component of velocity. Two velocity components of the in-plane movement orthogonal to the laser propagation axis are measured with the optically setup of L2F. The third component is measured from the analysis of the Doppler-shifted backscattered light as used in PDV systems [Roehle, 1999]. This system was originally conceived and developed in the Institute of Propulsion Technology in Germany as part of the research in Aerospace Engineering.

In spite of the number of optical elements, this technique is relatively simple as the contribution of PDV necessitates only one single visualization system, so the overall need for measuring three-components of velocity is fully satisfied with this combination of two subsystems working in their simplest configurations.

A graphical representation of the system is depicted in Fig. 1.16.

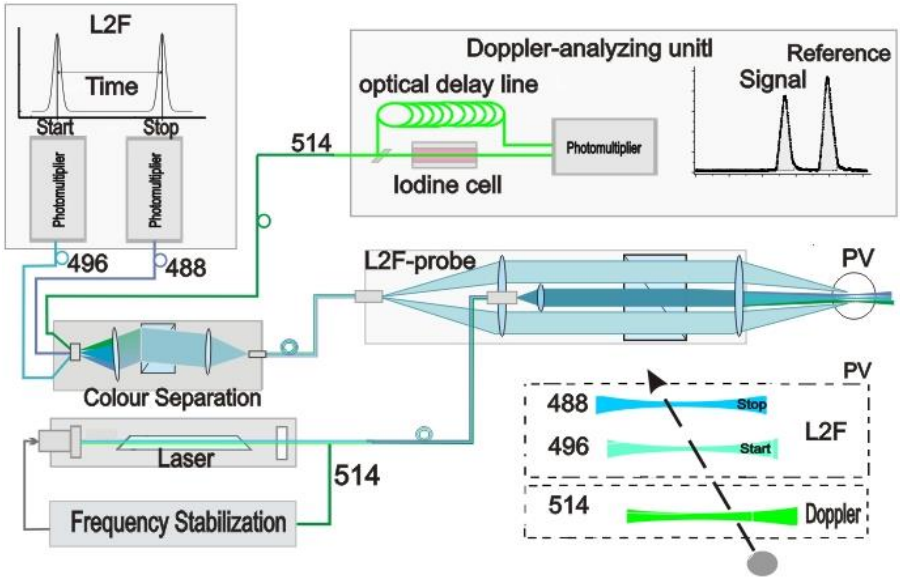

Fig. 1.16. Three component Doppler-L2F system [Förster, 2002].

1.6 Optical feedback flowmetry

Optical feedback interferometry (OFI) is an interferometric technique with recent implementation in fluidics and flow measurements. It uses a laser as a sensing device with minimal optical components. OFI's physical principle is based on the interferences generated by the back-scattered light inside the laser's resonant cavity to extract information on the sensed object. When used for sensing purposes in fluidics applications, it is denominated Optical Feedback Flowmetry.

1.6.1 History

The history of optical feedback started almost immediately after the invention of the laser. In most cases optical feedback, or the self-mixing of an electromagnetic waves in the laser cavity after being back-scattered by an external object, was considered as a parasitic effect affecting both laser's frequency and amplitude. The first demonstration of the potential capabilities of the technique in sensing applications started in 1963 with the work of King and Steward [King, 1963; Hilsum, 1963]. Their articles demonstrated the feasibility of optical feedback to measure displacement even though as little as 0.1 % of scattered light from an object distant up to 10 m entered back inside the lasing cavity. In a clear attempt to extend the utility of the phenomenon of optical feedback in lasers in the general field of metrology, King and Steward filed a patent application in 1968 that introduced a general discussion on the potential of optical feedback interferometry for measuring physical parameters [King, 1968].

During the sixties, optical arrangements where designed and mounted in order to avoid the effect of external feedback entering back in the resonant cavity of the laser [Servagent, 1998]. The first application in velocimetry was reported as early as 1968 when Rudd proposed the first Doppler velocimeter using self-mixing effect in He-Ne gas laser [Rudd, 1968].

Gas laser were continuously used in the seventies. In 1972, Honeycutt and Otto reported the utilization of a CO_2 laser for range finding [Honeycutt, 1972]. A few years later, a feedback-induced device was reportedly employed in reading a compact disc [Seko, 1975]. A self-mixing displacement sensor was proposed by Donati in 1978 using a combination of analog circuitry with an He-Ne laser [Donati, 1978].

It was in the eighties when OFI started to be employed in sensors incorporating semiconductor lasers, thanks to the advent of laser diodes. In 1980, Lang and Kobayashi [Lang, 1980] conducted a study on the phenomenon of external feedback in laser diodes and developed the equations ruling the behavior of lasers while subjected to optical feedback effect. Later on, Shinohara used laser diodes for velocity measurements [Shinohara, 1986].

For many years, optical feedback has been used in diverse scenarios as an alternative tool allowing precise measurements of vibration, absolute distance and velocity. OFI's ability to measure velocity led to its implementation for sensing purposes in diverse fluidic applications. Koelink and de Mul proposed and demonstrated the first self-mixing flowmeter in 1992 [Koelink, 1992; de Mul, 1992]. The first optical feedback flow sensor accurately measured the flow velocity and these measurements were validated with a linear relationship obtained between flow rate and measured velocity. Since then, OFI sensors have been tested and implemented in flow assessment in fluidics, microfluidics and general flowmetry with interest in chemical and biomedical engineering. It has been employed in the past for measuring blood flow over skin [Özdemir, 2008], blood perfusion in tissue [de Mul, 1993; Figueiras, 2013] and drop measurements [Norgia, 2015]. Moreover, this technique is currently being actively employed for the study of flows in small channels [Campagnolo, 2013] with direct implementation as an optofluidic alternative sensing technique [Nicolić, 2013].

1.6.2 Sensing principle

Optical feedback interferometry uses a reinjection scheme. Light emitted by a laser impinges in a moving target and a part of the scattered light is fed back inside the laser cavity. This reinjection causes variations in the laser emission power and junction voltage that can be employed to obtain information on the target and describe kinematic features of the external object such as its velocity or vibration frequency.

In Optical Feedback Flowmetry, the external feedback is generated by particles flowing in a fluid. Light scattered by those tracer particles enters back in the laser and modulate its lasing properties. As in Laser Doppler Velocimetry, this Doppler frequency f_D is related to the particle's velocity as explained in expression 1.6.

The fundamental aspects of OFI's sensing scheme will be exposed throughout this thesis. Thereby, it will be provided the basics of the phenomenon behind this technique as well as applications in sensing and interrogation of fluid flows.

1.6.3 Particular features of optical feedback interferometry

In OFI based sensing systems, a laser is used as the light source, interferometer and receiver and for many applications very few optical components are needed. This makes OFI sensors generally compact when compared to other sensing devices. Other advantages include its self-alignment, thus avoiding complex alignments required by classical interferometry. In addition, taking advantages from the light amplification in the laser cavity where the interferences take place, OFI is sensitive to very low levels of back-scattered optical power.

OFI can be considered as a consolidated and mature interferometric technique in mechatronics, typically for velocity, vibration and displacement measurements

[Atashkhooei, 2014; Arriaga, 2016] and as an alternative method for multiple biomedical studies [Donati, 2014; Bakar, 2013]. A recent review summarizes most of the known applications [Taimre, 2015]. Moreover, current trends in OFI's implementation for multiple biomedical applications are described in a recent publication [Perchoux, 2016].

1.7 Comparison of the methods and key features

The main features of the techniques presented in this chapter are outlined in Table 1. Key parameters inherent to the measurement scheme utilized by the detection system are detailed in terms of technical and economic relevance. To this end, this table provides a general overview of the advantages and constraints relative to the Doppler measurement techniques used in fluid flow assessment and quantification.

LDV and ODT perform accurate velocity measurements with high resolution. This is particularly interesting as this resolution is comparable to the typical resolution that optical feedback interferometry sensors hold for many applications in fluid flow measurements, which is utmost important for sensing at the microscale. However, both LDV and ODT require complex optical arrangements resulting in bulky equipment that makes complicated its direct implementation for microscale fluid measurements.

Ultrasound Doppler flowmetry measures flow velocity in channels and pipes without direct dependence on the transparency of the flowchannel, thus it can perform valid measurements where the rest of the optical methods exposed in this chapter may not. However, this technique has the drawback that it does not offer high resolution in the measurements when compared to the characteristic resolution of the optical Doppler methods reviewed here.

Finally, PDV and 3C-L2F velocimetry are complicated to be implemented, difficult to mount and require many optical and visualization components. However, these techniques are capable or measuring with good accuracy and resolutions comparable to that of OFI systems.

Table 1.1. Comparison of the Doppler methods for flow measurements

Technique	Spatial Resolution	Costs	Simplicity	Published In-vivo Implementation	Type of Target
Laser Doppler Velocimetry	1 μm	Expensive	No, many components are necessary and requires complex alignments	Yes	Solid/Fluid
Ultrasound Doppler Velocimetry	740 μm	Expensive	No	Yes	Fluid
Doppler Optical Coherence Tomography	5 μm	Expensive	No, it requires optical alignments and components	Yes	Tissue/Fluid
Planar Doppler Velocimetry	100 μm	Expensive	Easy mounted	No	Fluid
Three-Component Laser-2-Focus Velocimetry	10 μm	Expensive	No, it requires the synchronization of two independent measurement techniques	No	Solid/Fluid
Optical Feedback Interferometry	10 μm	Cost-reduced	Yes	Yes	Solid/Fluid

1.8 Motivations of the present thesis

Optical feedback interferometry, as any other interferometric technique, is limited in the detection scheme and consequently in sensing applications. One can mention, for example, the impact of speckle effect in the amplitude of self-mixing signals, the susceptibility of signals to extraneous parasitic vibrations and therefore, the complexity of designing optical feedback sensors for compensation of externally affected signals to successfully retrieve the displacement when measuring vibrations. These issues were subject of research of several authors extensively addressed in their thesis dissertations [Arriaga, 2014a; Zabit, 2010]

In the case of optical feedback flowmetry, the signal processing may vary depending on the concentration of particles in the sensing volume. It is distinctive the shape of the spectrum at low particle concentration, the so-called single scattering regime, as compared to the power spectral density of highly concentrated particles, the multiple scattering regime. So, it is of great interest to study when a particular signal processing is suitable for sensing in one regime or the other, and the reliability of each signal processing in *in-situ* sensing applications. Throughout this thesis, we drive our attention at exploring experimentally the optical feedback flowmetry in both single and multiple scattering regime to further discern when a signal processing can successfully sense in either regime.

In an effort to conceive OFI-based online measurements, we explored the capabilities of this technique in detecting suspended monoparticle in microfluidic devices. We propose a methodology enabling particle tracking, localization and size estimation. Single particle detection is the extreme limit of detection in the single scattering regime, where signal processing is straightforward.

Taking advantages of the fact that signal processing associated to the single scattering regime in optical feedback flowmetry is relatively simple, we have performed a study on the ability of OFI sensors in ex-vivo characterization of flow inside a vessel, which is proposed as pressure myograph sytem useful to investigate hemodynamics in microcirculation.

Being able to sense in single or multiple scattering extends the utility of optical feedback interferometry sensors in fluidics applications in both micro and macroscale, thus providing the chemical, biomedical and biotechnological industry with new alternative non-contact, non-destructive tool utilizing only a laser for sensing purposes.

As part of this thesis dissertation, we developed an OFI sensor allowing the analysis of non-steady flows in the multiple scattering regime. Unsteady flows are present in many cases in industry

Also, proposing this kind of sensors for the assessment of multiphase flows is of actual relevance as most of the experimentation in this regard depends strongly on visualization systems. We extensively explore OFI for the interrogation of two-phase immiscible liquid-liquid interactions using the flow profile characterization from parameters of fluid motion. This is a first step in the implementation of OFI sensors in the analysis of two-phase flows, which has been up to now unexplored.

Chapter 2

Optical feedback interferometry for flows: theoretical fundaments

In this chapter, we present the different scattering mechanisms that are present as a consequence of the interaction of the laser used in the optical feedback interferometry sensing technique with a moving target. We focus our attention towards the implications of the nature of the target on the optical feedback departing from the main theoretical fundaments of on which the phenomenon is based applied to semiconductor lasers.

When the laser light interacts with a moving object, part of the backscattered radiation re-enters the laser cavity and mix with the original emitted wave. Due to the Doppler Effect, this reinjection in the laser affects directly its emission power and spectral properties. The amplitude and frequency fluctuations are due to a "parasite" feedback, other than the feedback by the mirrors of the laser resonator, caused by reflection (diffuse or not) on external surfaces.

In what follows, we examine the optical feedback in the case of the interaction of the laser beam with flowing particles in a fluid, and its impact in the behavior of the laser subject to feedback generated by those particles.

2.1 Optical feedback phenomenon for flow measurements

Optical feedback interferometry has been extensively studied and applied in mechatronics. However, its implementation in fluid flow measurement systems is rather recent. Most of the work developed to implement OFI sensors in fluidics circumscribes in the frame of velocimetry. Still, measuring velocity with accuracy is challenging and at the same time an increasing need for the biomedical, chemical and industrial communities.

Unlike solid targets, light scattered by small particles in a flow generate a diffusion pattern where the scattered electromagnetic field vectors are randomly distributed all over a round solid angle. Typically in solid targets light is scattered preferentially in the direction of the laser beam propagation.

This section presents the basic principles of OFI applied to velocity measurements of flows. The main features of the interaction of the laser beam with the carrying scattering particles are posed and analyzed.

2.1.1 Particular features of the interaction laser-fluid

The sensing mechanism of the optical feedback interferometry technique applied to flow measurements depends on the interaction of a laser beam and the particles embedded in the flow. There are particular features that models and approximations need to consider. The following aspects are distinctive:

- Light travels through a gradient of refractive indexes as it passes from different materials until it reaches the particles in the flow.
- Many particles in the flow may be illuminated at once; hence the contribution to the optical feedback signal has a frequency signature characterized by a distribution of frequencies correlated to a plurality of particles travelling at different velocities.
- The illuminated volume where particles in the flow contribute to the optical feedback affecting the laser has three dimensional spatial components.
- The scattering angle is 2π. This means that light is scattered in all directions, not only in the direction towards the laser as in the case of solid targets. This implies that the detection of light from fluidic systems interrogated by optical feedback interferometry is poor with respect to the sensing of solid targets.

It is important to take into consideration also that particles may behave different from the fluid so that they do not follow perfectly the flow hydrodynamics.

2.1.2 Theoretical approaches for laser-particles interaction: scattering theories.

The information obtained in optical feedback interferometry from the fluid is provided by particles acting as scattering centers embedded in the flow. Depending on the particle's size, different theories should be considered. Most of the theories developed for describing light-particle interaction assume that particles are spherical bodies ranging in size from diameters smaller than the incident light wavelength to sizes bigger than the wavefront wavelength.

In other words, for a given laser source, the validity of the model would depend directly on the particles sizes. Considering that scattering of particles may occur in all directions, the behaviors of scattered waves will be given by the ratio of the particles radius r_p and the incident wavelength λ_i:

$$\sigma_s = \frac{2\pi r_p}{\lambda_i} \tag{2.1}$$

σ_s determines the theory that is applicable to each case of scattering. It is accepted in literature to classify the three cases as follows [Bohren, 2004]:

- If $\sigma_s < 0.3$ the Rayleigh scattering dominates the interaction. In such a category are small molecules (DNA, around 2 nm in size), pigments for printing (around 100 nm [Ortalano *et al.*, 2015]), small molecules of the atmosphere (O_2, N_2 and Ar, sizes around 0.3 nm), soot particles produced in combustion engines (typically produced with mean diameters from 60 to 120 nm [Harris, 2001]) and cloud droplets (sizes ranging between 5 and 50 nm).
- If $0.3 < \sigma_s < 30$ the Mie scattering model rules the interaction. Common examples of particles producing Mie scattering are blood microparticles (≤ 1.5 µm [Shet, 2008]), red blood cells (with average diameter of 7.5 µm [Turgeon, 2004]) and fat content in milk (sizes range from 1 to 10 µm [Michalski, 2001]).
- For $\sigma_s > 30$ the interaction is based on geometrical optics and is comparable to a moving solid target.

For the work related to flow measurements and particle detection presented in the frame of this thesis, only microparticles in the range of σ_s corresponding to the Mie scattering are used as, to our knowledge, OFI has never been demonstrated in the Rayleigh diffusion regime.

It should be pointed out that the shape of the scattering pattern varies from the case of Rayleigh to Mie theories. Figure 2.1 shows the Rayleigh intensity scattering pattern in polar plot for particles with radius of 2 nm, 10 nm and 60 nm illuminated with an unpolarised laser emitting 785 nm. As can be appreciated, the

scattering distribution is symmetrical and intensity is homogeneous in space. The intensity of the scattered light represented in the graph in logarithmic scale for each particle size is respectively: $7.1 \cdot 10^{-13}$ W/m^2, $1.09 \cdot 10^{-8}$ W/m^2 and $5.1 \cdot 10^{-4}$ W/m^2.

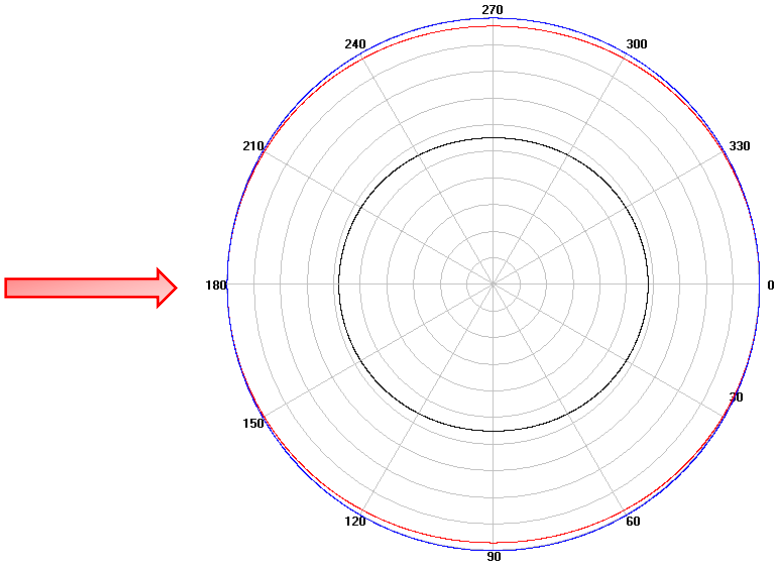

Fig. 2.1. Rayleigh intensity scattering in of particles with different sizes: 2 nm (black), 10 nm (red) and 60 nm (blue). Patterns correspond to a scattering produced when illuminating the particles with an infrared laser emitting at wavelength 785 nm. The arrow indicates the laser propagation direction.

The backscattered power in the direction of the laser in linear scale for those nanoparticles is represented in Fig. 2.2. The values of the power backscattered by the particles are extremely low and the Rayleigh scattering produced is so weak that is unlikely to be detected by the sensing methods described in the first chapter.

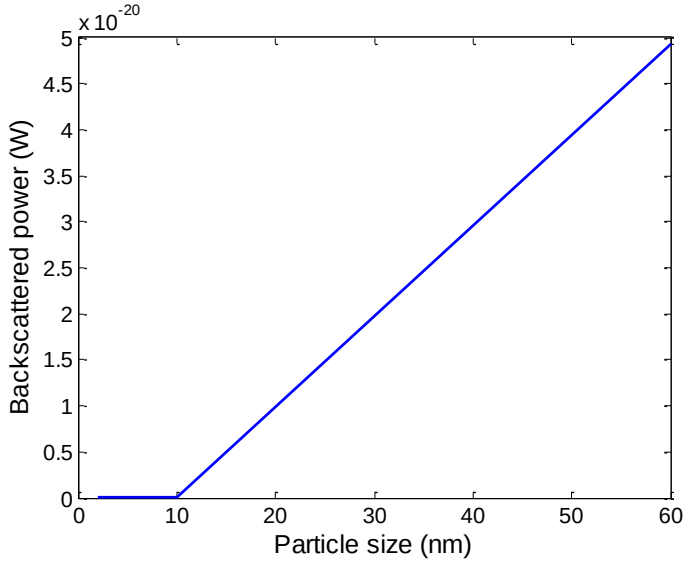

Fig. 2.2. Backscattered power in the direction of the illumination point source emitting 7.6 mW at 785 nm.

Likewise, the Mie intensity scattering patterns for microparticles with different radius (2 µm, 10 µm and 60 µm) illuminated with an unpolarised laser emitting at 785 nm is presented in Fig. 2.3. As can be appreciated in this figure, the scattering distribution is asymmetrical and most of the power is forward-scattered in the direction of the propagation of the light emitted by the laser. The intensity values represented in the graph in logarithmic scale for each size of the microparticles are respectively: $3.19 \cdot 10^{4}$ W/m^2, $1.07 \cdot 10^{7}$ W/m^2 and $1.36 \cdot 10^{10}$ W/m^2

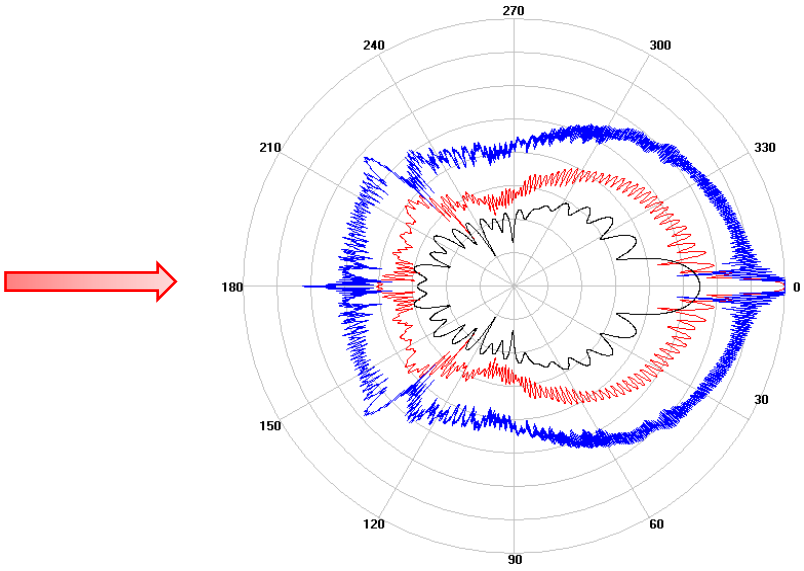

Fig. 2.3. Mie scattering in of particles with different sizes: 2 µm (gray), 10 µm (red) and 60 µm (blue). Patterns correspond to a scattering produced when illuminating the particles with an infrared laser emitting at wavelength 785 nm. The arrow indicates the laser propagation direction.

Figure 2.4 presents the backscattered power in the direction of the laser produced by the microparticles in linear scale. As can be seen, the Mie scattering generates a power that is higher by several orders as comparted to the Rayleigh scattering, which is probably the explanation of the extended use of microparticles in the optical feedback flowmetry.

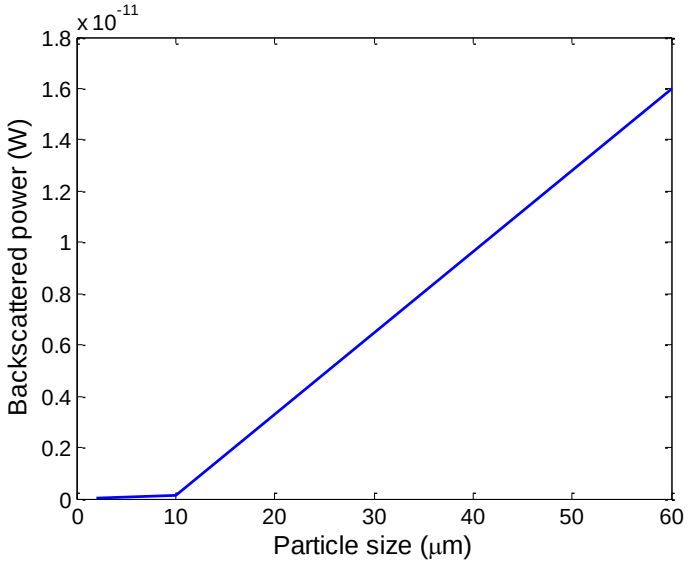

Fig. 2.4. Backscattered power in the direction of the illumination point source emitting 7.6 mW at 785 nm.

2.1.3 The scattering regimes

Most of the research on the scattering generated by flowing particles has considered a model interaction system where each photon is scattered by only one particle, so the photons are Doppler-shifted only once during the interaction time. In such a case, it is considered that the system works in the single scattering regime. Single scattering of light is produced when particles are sufficiently far from each other, so that they can be considered as isolated scattering centers in the flow. Thereby, the Doppler shifted light, contributes to the optical feedback with the information of a single particle's velocity.

According to Quirantes *et al*. [Quirantes, 2001], when illuminated particles in a volume are separated a distance comparable to four times their radius, it can be assumed that each of them will scatters one photon as a result of the interaction and that independent scattering would dominate the light detection.

The signal processing associated to the single scattering regime is rather simple and straightforward as the frequency distribution is distinctive and can be easily associated with, for example, the velocity of moving particles in a flow. In this case, a Doppler shift can be identified in the power spectrum as a frequency distribution that has a maximum correlated to the maximum velocity of the moving object generating the shift. Alexandrova *et al*. recently used the optical feedback interferometry sensing technique to measure the velocity of micrometric titanium particles merged in small quantities in a flow ranging from 0.03 to 0.8 % by mass, thus guaranteeing a very independent scattering contribution of the seeded flow and a simple processing of the data [Alexandrova, 2016]. A simple model for single scattering applied to optical feedback flowmetry was proposed by Campagnolo in her doctoral dissertation [Campagnolo, 2013b]. The model

reproduced the power spectrum of a fluid moving at a given known flow rate using the equivalent reflection coefficient from the theory optical feedback.

If the number of obstacles in a medium where light propagates is large, then the wave interacts multiple times with the bodies in the medium. In this case, the phenomenology is understood as an interaction process in the multiple scattering regime. Perhaps the closest example attributable to a sensing scheme in the multiple scattering regime is the measurement of blood perfusion in tissue and the measurement of blood flow in veins and arteries. Also, many experiments use phantoms based on milk or intralipid to mimic light interaction with living tissue. I this regard, many techniques devoted to measure any activity related to the tissue use the Doppler Effect to retrieve information on the flow, perfusion and microcirculation.

The multiple scattering regime in the case of a laser impinging a medium with flowing particles is applicable when in the concentration of scatterers is high and photons experience multiple reflections with the particles in the medium and they suffer several Doppler shifts before they propagate towards the laser cavity. In this case, the spectral properties of the optical feedback signal are highly random and the frequency distribution has a complex statistical behavior. The multiple scattering effect is a complex phenomenon involving random interactions between the light wave and matter that has been addressed by different approaches depending on the nature of the scattering particles. As explained in the previous section, the size of the particles influences the scattering pattern associated to the type of interaction. However, the problem of retrieving the quantitative information of moving particles has been a major challenge using different techniques in the multiple scattering regime such as laser speckle contrast imaging and Doppler optical coherence tomography.

A scattering model presented by Bonner *et al*. [Bonner, 1981] proposed to consider the spectrum of the time autocorrelation function of detected photons experiencing multiple collisions in a tissue as it is related to the scattering function. The normalized scattering function is composed of the sum the product of the probability that photons undergo several collision on the tissue and the autocorrelation function for an equal number of collisions. Then, for a wave interacting with the medium, the center of mass of the moving scatterers is continuously changing and as a consequence, the wave is Doppler-shifted. The model yielded a direct relation of the first order moment of the spectrum with the radius of the particles in the flow, the velocity of the scattering centers and the number of particles generating scattering. This physical approximation allows for the interpretation of the mean frequency of a spectrum. The signal's spectrum can be assimilated as a probability density function related to the velocity of particles embedded in the flow. Those particles scatter a portion of the incident light, which is Doppler shifted. By summing up the contribution of each interaction the mean

frequency can be calculated from the center of mass of the power spectrum. The sense of the center of mass of a frequency distribution was exploited by de Mul *et al*. in the development of an instrument to measure directly the blood flow velocity [de Mul, 1984]. In addition, Nilsson conceived and developed a signal processor for flow measurement [Nilsson, 1984] and Norgia *et al*. measured extracorporeal flows using the same principle [Norgia, 2010].

Using Monte Carlo simulations Davis *et al*. studied the photon propagation in tissue with vasculatures and the implications of multiple scattering in the interpretation of the laser speckle contrast imaging (LSCI) [Davis, 2014]. LSCI uses backscattered light to image a changing structure that generates a blurring effect in those regions with flow or evident microcirculation associated. They found that a large percent of photons, more than 75 %, experience multiple scattering for various values of the scattering coefficient. Their work, demonstrated that existing models that consider only single scattering in functional vessels may fall into a wrong approximation for blood flow assessment.

The effects of multiple scattering are associated to the interaction of the light source with the moving elements in the flow. However, multiple scattering arises as light propagates through a medium before interacting with the flow stream. Moger *et al*. analyzed the effect of multiple scattering in the velocity profile of blood measured by Doppler optical coherence tomography [Moger, 2005]. Their study consisted on mimicking a flow under a high-scattering medium by adding phantoms with different thickness. In this way, it is possible to measure the influence of the scattering regime in the ability of the technique to measure the velocity in depth by immersing the tube carrying the fluid in water and in a 20 % solution of intralipid. The comparative results concluded that for a scattering layer of intralipid thicker than 150 μm, multiple scattering effects introduce systematic errors in the measured velocity profile and rigorous fitting needs to be performed to accurately fit the experimental results with an analytical expression of the profile.

Kalkman *et al*. investigated the effect of multiple scattering of blood in the Doppler OCT using different dilutions of hematocrit ranging from 0 % to 15 % [Kalkman, 2012]. From a set of Monte Carlo simulations of the ODT signals, they explained the influence of multiple scattering and the scattering anisotropy in signals for blood flowing in a cuvette. The simulations considered the sum of all photons and the contributions of several scattering events in the sample. Good coincidence was found between their simulation outcomes and the experimental results, which demonstrated that photons may experience more than 20 scattering events in the flow.

As multiple scattering effects are complex, the use of high concentration of particles in liquids is usually avoided as much as possible [Kliese, 2010; Campagnolo, 2013a; Norgia, 2012]. Doppler methods take advantage of the

relatively simpler processing of the data in the single scattering regime. In many cases, the theoretical framework present in the literature is limited to flow sensing in the single scattering regime and assuming that multiple scattering effects are negligible. In addition, very few is found in literature to explain how the multiple scattering effect may impact the measurement of velocity using Doppler methods.

While there is an ongoing active research in scattering models and how they would fairly reproduce the information observed in the experiments, we will focus on presenting the working principle of the optical feedback interferometry sensors for flow measurements in the following section and we will address experimentally the potential applications of the single scattering in the third and fourth chapter of the present thesis and present a processing analysis from single to multiple scattering in the third chapter.

2.2 Theory of the optical feedback applied to multiple scatterers

In this section, the fundamental equations of the laser under external feedback are presented and the model is developed to determine the impact of multiple scatterers to the laser amplitude changes.

Two options are possible to describe the behavior of the laser diode under optical feedback: first, the three mirror cavity (the third mirror being the target) can be reduced to a two-mirror equivalent cavity from which the laser rate equations can be deduced [Petermann, 1991]; second, the optical feedback can be seen as a perturbation of the established lasing systems and, in this case, an additional term can directly be added to the field or photon rate equation that represents the contribution of the back-scattered light. This second way is known as the Lang and Kobayashi model [Lang, 1980]. A discussion on the advantages and the inconveniences of both modeling methods is presented in [Kane, 2007]. The conclusion of this study shows that, despite the equivalent cavity method is the most exact method, the Lang and Kobayashi perturbation approach is well suited for low feedback levels and quasi steady state analysis of the optical feedback phenomenon.

In the case where the optical feedback is due to small particles flowing in fluids, where the back-scattered power is described by the Mie theory, the optical feedback level remains very low. Despite Campagnolo [Campagnolo, 2013] has demonstrated the contribution of multiple scatterers based on the equivalent cavity model, we have derived the Lang-Kobayashi method as originally proposed by Zakian [Zakian, 2005].

The modeling approach is based on the description of the established electric field propagating inside the laser cavity E that is subject to an external perturbation:

$$\frac{\mathrm{d}}{\mathrm{d}t}[E(t)\exp(\mathrm{j}\omega t)] = \left[\mathrm{j}\omega_N + \frac{1}{2}\Gamma G(N - N_{\mathrm{tr}})\right] E(t)\exp(\mathrm{j}\omega t) + \boldsymbol{F}(\boldsymbol{t}) \qquad (2.2)$$

where ω is the laser mode angular frequency, ω_N is the cavity mode angular frequency ($\omega_N = k\pi c/n_c L_c$ with k an integer, L_c the laser cavity length and n_c the refractive index), Γ stands for the laser mode confinement factor, N is the carrier density, N_{tr} is the carrier density at transparency, G is the stimulated emission gain and $F(t)$ is the feedback induced perturbation term. Depending on the nature of the target, $F(t)$ can adopt different formulations :

- In the case of a unique and fixed target located at a distance L_{ext} from the laser cavity,

$$F(t) = \frac{\kappa}{\tau_C} E(t-\tau)\exp[\mathrm{j}\omega(t-\tau)], \qquad (2.3)$$

where τ is the external cavity roundtrip time of flight ($\tau = 2n_{\mathrm{ext}}L_{\mathrm{ext}}/c$), τ_c is the laser cavity roundtrip time of flight ($\tau_C = 2n_C L_C/c$) and κ is the feedback coupling coefficient defined as

$$\kappa = \frac{1}{\tau_C}(1 - r_2^2)\frac{r_{\mathrm{ext}}}{r_2} \qquad (2.4)$$

with r_2 the reflectivity of the laser front mirror and r_{ext} the ratio of the back-scattered power actually re-entering the laser cavity over the emitted power.

- In the case of a unique target in translation that induces a Doppler shift

$$f_D = \frac{\omega_D}{2\pi} = \frac{\omega}{2\pi}\frac{2V}{c+V} \qquad (2.5)$$

is dependent on the target's velocity V and the feedback contribution becomes

$$F(t) = \frac{\kappa}{\tau_C} E(t-\tau)\exp[\mathrm{j}(\omega+\omega_D)(t-\tau)]. \qquad (2.6)$$

- In the case of multiple targets, each one scatters back toward the laser cavity its own contribution so that:

$$F(t) = \sum_i F_i(t), \qquad (2.7)$$

with each $F_i(t)$ that can be written as :

$$F_i(t) = \frac{\kappa_i}{\tau_C} E(t-\tau_i)\exp\left[\mathrm{j}(\omega+\omega_{D,i})(t-\tau_i)\right] \qquad (2.8)$$

That takes into account the fact that each particle is located at a specific distance from the target which induces a particular time of flight τ_i, that the reflectivity of each particle is its proper characteristic so that

$$\kappa_i = \frac{1}{\tau_C}(1 - r_2^2)\frac{r_{\text{ext},i}}{r_2}, \tag{2.9}$$

and that each particle has its proper velocity projection along the optical axis inducing

$$\omega_{D,i} = \omega\frac{2V_i}{c + V_i}. \tag{2.10}$$

Thus considering equation (2.2) with the perturbation *F(t)* described as (2.8) obtaining the variation of the laser output power induced by the particle optical feedback consists in solving the set of rate equations that describe the laser by separating the real and the imaginary part of the field equation and introducing the carrier density equation. In the meantime, considering the Doppler shift induced by the particle velocity is at very low frequency when compared to the laser optical frequency, the usual approximations of the quasi-steady state regime can be done : $E(t-\tau) \sim E(t)$, thus :

$$\frac{\mathrm{d}E(t)}{\mathrm{d}t} = \frac{1}{2}\Gamma G(N - N_{\text{tr}})E(t) + \sum_i \frac{\kappa_i}{\tau_C}E(t)\cos\left(\omega_{D,i}t + \phi_i\right), \tag{2.11}$$

$$\frac{\mathrm{d}\Phi(t)}{\mathrm{d}t} = \frac{1}{2}\alpha\Gamma G(N - N_{\text{tr}}) + \sum_i \frac{\kappa_i}{\tau_C}\sin\left(\omega_{D,i}t + \phi_i\right), \tag{2.12}$$

$$\frac{\mathrm{d}N(t)}{\mathrm{d}t} = \frac{I}{qV_a} - G(N - N_{\text{tr}})S - \frac{N}{\tau_n}, \tag{2.13}$$

where α is the linewidth enhancement factor, Φ is the phase term of the electric field E, ϕ_i is a random phase, q is the elementary charge, V_a is the laser active volume, τ_n is the carrier lifetime and S is the photon density which is linked to the field amplitude by :

$$S \propto E \cdot E^*, \tag{2.14}$$

which allows to re-write (2.11) as

$$\frac{\mathrm{d}S(t)}{\mathrm{d}t} = G(N - N_{\text{th}})S(t) - \frac{S(t)}{\tau_S} + \sum_i \frac{\kappa_i}{\tau_C}S(t)\cos\left(\omega_{D,i}t + \phi_i\right), \tag{2.15}$$

In (2.15), τ_S is the photon lifetime and N_{th} is the carrier density at threshold.

Solving the set of equations (2.11)-(2.15) in the case of the quasi-steady state regime has been exposed in many ways [Kane, 2005], [Taimre, 2015]. Following the exact same methodology leads to write the following equations for phase and amplitude respectively:

$$\omega_F - \omega_0 = \alpha \sum_i \frac{\kappa_i}{\tau_C} \cos\left(\omega_{D,i} t + \phi_i\right) + \sum_i \frac{\kappa_i}{\tau_C} \sin\left(\omega_{D,i} t + \phi_i\right), \tag{2.16}$$

$$S_F = S_0 \left[1 + 2\frac{\tau_S}{\tau_C} \sum_i \kappa_i \cos(\omega_{D,i} t + \phi_i)\right] \tag{2.17}$$

where ω_F and ω_0 are the laser angular frequency with and without feedback respectively and S_F and S_0 are the photon densities under similar hypothesis.

Eq. (2.16) can be simplified in

$$\omega_F - \omega_0 = \sqrt{1 + \alpha^2} \sum_i \frac{\kappa_i}{\tau_C} \sin\left(\omega_{D,i} t + \phi_i + \arctan \alpha\right), \tag{2.18}$$

while (2.17) directly provides a simple and easy relationship for the laser emitted power variations that are proportional to the photon density

$$P_F = P_0 \left[1 + \sum_i m_i \cos(\omega_{D,i} t + \phi_i)\right], \tag{2.19}$$

where the m_i is the modulation indexes relative to the ith particle:

$$m_i = 2\frac{\tau_S}{\tau_C} \kappa_i. \tag{2.20}$$

It shall be noted that despite the Doppler shift $\omega_{D,i}$ is function of ω_F, in the case of optical feedback in fluids where the low back-scattered power requires a short range of operation (usually a tens of millimeters), the changes in laser frequency can be neglected for the calculation of the optical power variations.

To validate the model, the equation (2.19) has been implemented with Matlab™ for a 1D - distribution of velocities along the optical axis that follows Poiseuille's law for velocity distribution in a circular duct (Fig. 2.5(a)). The laser and target parameters for simulation are presented in the table 1. The flow parameters are as follows: the maximum velocity in the 320 µm diameter channel is 0.1 m/s, the flow direction makes an angle of 80° with the optical axis. The light absorption in the fluid has been fixed so that the penetration depth is 1 mm. A random phase ϕ_i has been given for each position as originally proposed by Nikolić *et al.* [Nikolić, 2014] that takes into account both the phase shift induced by the time of flight in the external cavity and the random phase shift induced by the scattering effect on the particle. Also, for sake of understanding of the signal spectrum a white Gaussian noise has been added to the signal through Matlab's *rand* function.

As expected the time domain signal presented in Fig. 2.5(b) is clearly not deterministic and the unique manner to obtain the information on the velocity of the fluid is the spectral analysis. The flow maximum velocity, considering the incident angle and the laser wavelength is expected to produce a Doppler shift of 44.2 kHz which corresponds roughly to the maximum observed frequency in the distributed spectrum of Fig. 2.5(c).

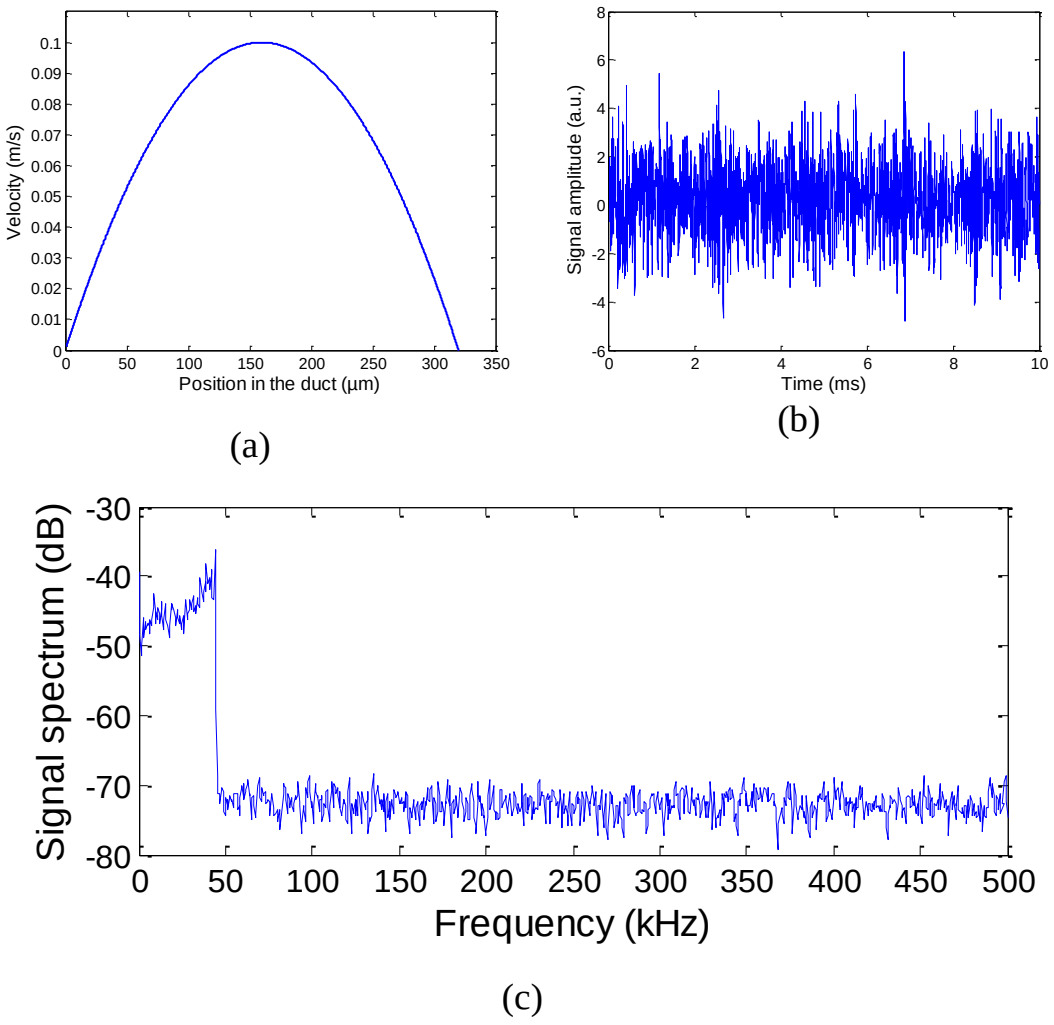

Fig. 2.5. Simulation of equation (2.19) : (a) velocity distribution along the optical axis in the duct (b) time domain representation of the OFI signal (c) Frequency domain representation of the OFI signal

Table 2.1: Laser and target parameters used in the modeling			
Parameter	**Definition**	**Unit**	**Value for model Fig 2.5**
E	Electric field amplitude	V/m	
ω	Electric field angular frequency	rad/s	$2.4 \cdot 10^{15}$ (λ=785 nm)
ω_N	Cavity mode angular frequency	rad/s	
Γ	Laser active area confinement factor		
G	Stimulated emission gain	s^{-1}	
N	Carrier density	m^{-3}	
N_{tr}	Carrier density at transparency	m^{-3}	
n_c	Refractive index in the laser cavity		3.5

L_c	Laser cavity length	m	3.10^{-4}
τ	External cavity round-trip time	s	
n_{ext}	Refractive index in the external cavity		
L_{ext}	External cavity length	m	0.1
r_2	Reflexion coefficient of the front mirror of the laser		5%
r_{ext}	External cavity reflexion coefficient		10^{-9}/x position
ω_D	Doppler angular frequency shift	rad/s	
V	Projection of the target velocity along the optical axis	m/s	
Φ	Instantaneous phase of the electric field	rad	
ϕ_i	Phase shift of the back-scattered electric field	rad	
α	Linewidth enhancement factor		
V_a	Active area volume	m^3	
I	Laser injection current	A	
S	Photon density	m^{-3}	
τ_n	Carriers lifetime	s	
N_{th}	Carriers density at threshold	m^{-3}	
τ_s	Photon lifetime	s	10^{-9}
ω_F (ω_0)	Electric field angular frequency in presence (absence) of feedback	rad/s	
S_F (S_0)	Photon density in presence (absence) of feedback	m^{-3}	
P_F (P_0)	Laser power in presence (absence) of feedback	W	
m	Modulation index of the optical power		

2.3 Laser characterization under weak feedback level

As can be seen in the model developed above, the OFI sensing scheme is extremely dependent by nature on the laser source used as the sensor. As will be discussed in the following chapters, depending on the application, different laser diodes may be chosen. The lasers used in this thesis were characterized prior to be used in the experimental conditions. In what follows, we detail the experimental study of useful parameters for designing optical feedback interferometry sensors. The main difficulty while performing the characterization of various laser diodes with different emission properties is to design a robust and reliable setup so that characterization results are stable and reproducible and that comparison between laser sources is meaningful.

The setup employed for the lasers characterization is depicted in Fig. 2.6. The laser diode under test is held by an Arroyo laser mount which provides two switches allowing operation with any possible pin configuration. The electronics associated to the laser are custom made and are presented in Fig. 2.7:

- the laser driver is based on MOSFET as the current source. A closed loop ensure for current control for manual control of the injection current using a potentiometer or for external control using a voltage source.
- the photodetected current amplification is ensured by a multistage amplifier based on low-noise operational amplifiers. The first stage is standard transimpedance amplifier where the operational amplifier is fedback by a 1 kΩ resistor. This stage amplifies the DC photocurrent and the output is connected to an output SMA connector in order to perform P(I) measurement. Two other voltage amplifier with band-pass filtering allow full recovery of the OFI signal. The gain of each stage are 60 $dB_{V/A}$, 26 dB and 26 dB achieving a total gain of 112 $dB_{V/A}$.

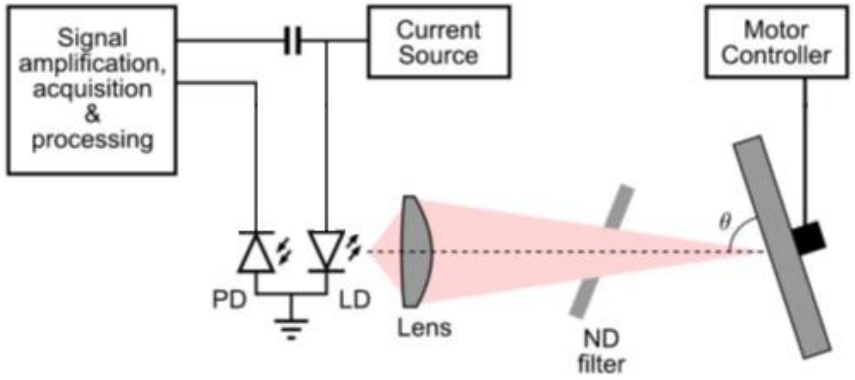

Fig. 2.6. Setup for characterization of the laser diodes. The ND filter used as an attenuator (Thorlabs NDC-50S-3) is positioned in between the rotating target and the focusing lens. The angle between the laser propagation axis and the wheel is 80º.

The laser beam is focused by a single lens on a duralumin rotating disk. The disk surface has been polished to ensure the most uniform surface roughness. In the opto-mechanical system, the disk and the lens holder have a fixed pre-determined position. Only the laser mount is mobile and the laser position is adjusted using a XY micrometric translation stage. To ensure that the Doppler shift is constant and reproducible at each laser test, a mobile needle used as a knife edge system allows guaranteeing the focus position on the disk. Meanwhile, the disk is mounted on a step motor which velocity is controlled by a custom made proportional-integral-derivative controller. The system is mounted in a vibration-isolated optical table.

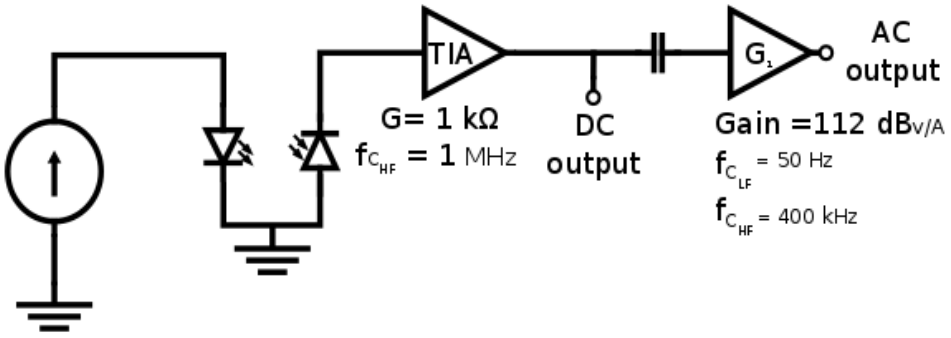

Fig. 2.7. Electronic diagram of the custom made laser driver and signal amplification.

Since the comparison criteria between the laser diodes is the sensitivity to optical feedback by measuring the strength of the Doppler frequency peak in the spectral domain, it is important to ensure that all the energy carried by the OFI signal is concentrated in the fundamental frequency. It means that the laser has to operate in the very weak feedback regime were Doppler fringes are sinus functions. Round step neutral density filters are set in the optical path between the laser and the disk to ensure that the Doppler frequency is attenuated enough so that the harmonics do not appear in the spectrum.

2.3.1 Infrared laser characterization

The laser Thorlabs L785P090 is used in the present thesis in chapters 3 and 4. This laser is an AlGaAs simple Fabry-Pérot cavity mounted in a TO-18 package where a monitoring photodiode is included. The emitted power at the operational current (120 mA) is 90 mW centered at a wavelength of 785 nm. At this power emitted in the front facet, the monitor photodiode that is located at the rear facet of the laser diode delivers a photocurrent of 280 µA. The neutral filter Thorlabs NDC-50S-3 is used during the characterization of the laser. The possible optical density values range between 0.04 and 3, and the optical density employed was 3, thus attenuating a million times the signal in the roundtrip.

The emission power (or rather the amplified photocurrent) against the injection current is presented in Fig. 2.8.

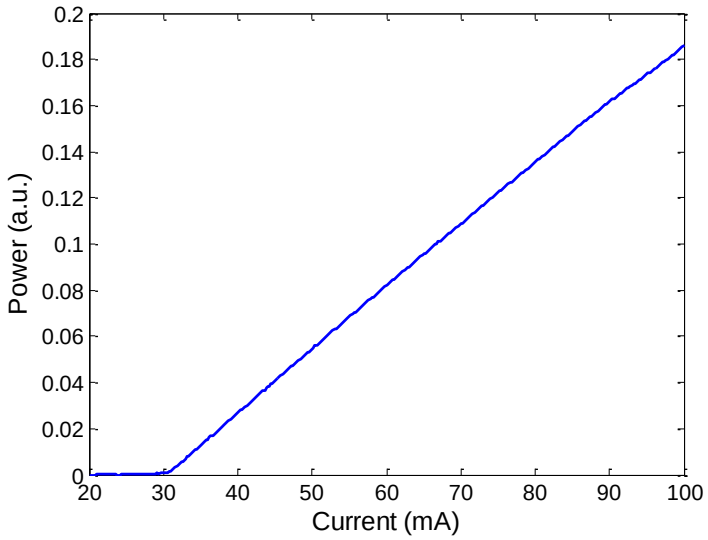

Fig. 2.8. Light-current curve of the laser L785P090. The power is represented by the photocurrent amplified through the first stage transimpedance amplifier, which has a gain of 1 kΩ.

The threshold current for this infrared laser is about 32 mA. For the characterization, the current was varied from 20 to 100 mA in steps of 0.2 mA. The Figure 2.9 shows the spectrums of signals sampled at 1 MHz for 400 different current values. As the current provided to the laser increases and passes the threshold value, a Doppler peak appears in the photodiode signal. This Doppler peak is related to the target's velocity.

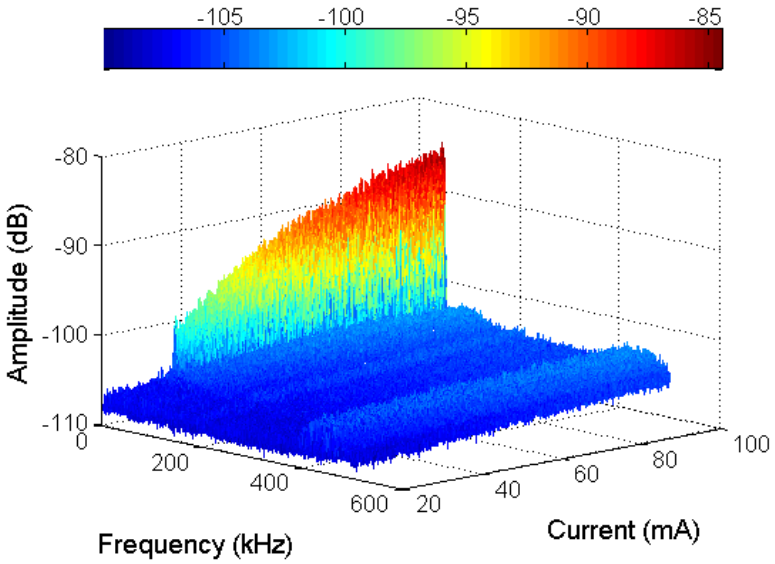

Fig. 2.9. Spectrum evolution as a function of current provided to the laser L785P090. The graph shows 400 spectrums and the fundamental Doppler peak is found as the current passes the threshold for the laser.

The Doppler peak is then fitted to a Gaussian function in order to automatically extract the signal-to-noise ratio. The Gaussian equation is given by:

$$f(x) = A_0 + Ae^{-\frac{(f-b)^2}{2{c_1}^2}}, \tag{2.21}$$

where A is the amplitude of the function, b is the position of the maximum, c_1 accounts for the full-width at half maximum while A_0 is the floor noise of the spectrum. The variable f represents the frequency. An example of the fitting is presented in Fig. 2.10, which corresponds to the Doppler peak obtained at current of 120 mA.

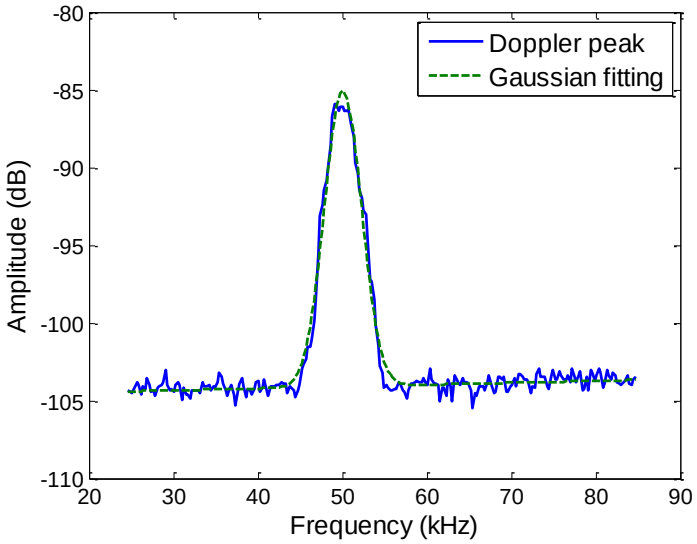

Fig. 2.10. Doppler peak in the spectrum fitted to equation 2.21. The spectrum corresponds to a current of 120 mA.

The evolution of the noise and the maximum of the Doppler peak is represented in Fig. 2.11(a) and their difference, the signal-to-noise ratio (SNR) is plotted in Fig. 2.11(b).

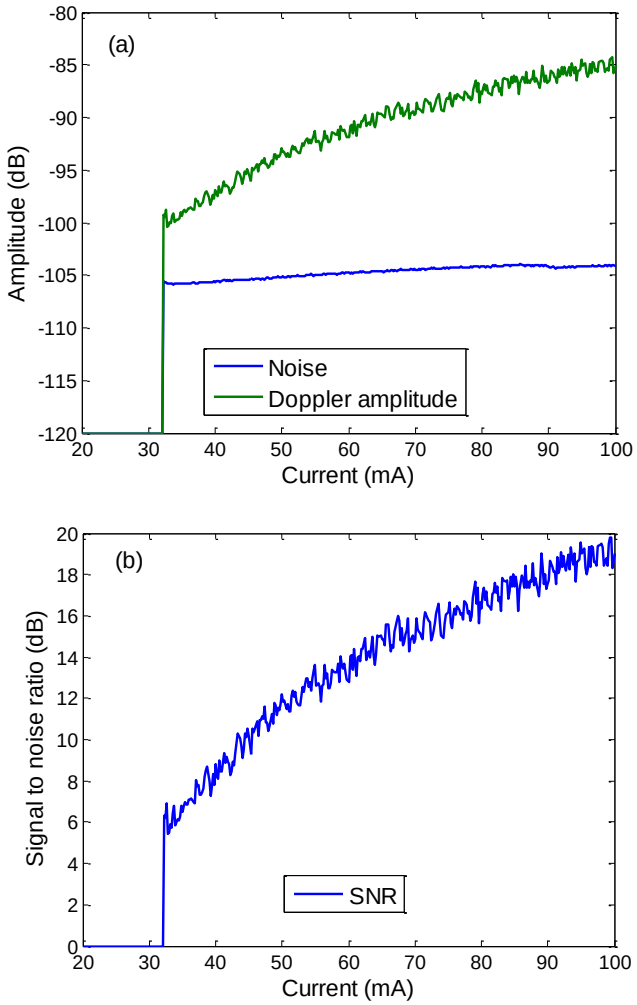

Fig. 2.11. Amplitude of the Doppler peak and the noise for different values of current (a). Signal to noise ratio of the signal.

As can be appreciated from these graphs, the signal's SNR reaches around 20 dB when it is driven by an injection current of 100 mA. Considering that the measured attenuation introduced by the optical densities is 60 dB over the roundtrip, it means that the equivalent SNR is 80 dB distributed between the fundamental peak and its harmonics.

2.3.2 Blue-violet laser characterization

The blue-violet laser (Panasonic DL5146-101S) used in some of the experiments that will be described in chapter 4 is characterized. It is a GaN laser emitting at 405 nm. At the operational current (90 mA), this laser emits a power of 40 mW. The scheme presented in Fig. 2.6 is used during the characterization of the laser. For the characterization of this laser, the ND filter represented in the figure is replaced by a set of two neutral filters Thorlabs NDC-50S-3 and NDC-50S-1, both in position 6. This combination attenuates the power a thousand times in the roundtrip and guarantees a single Doppler peak in the spectrum.

The emission power interpreted as the amplified photocurrent as a function of the injection current is depicted in Fig. 2.12.

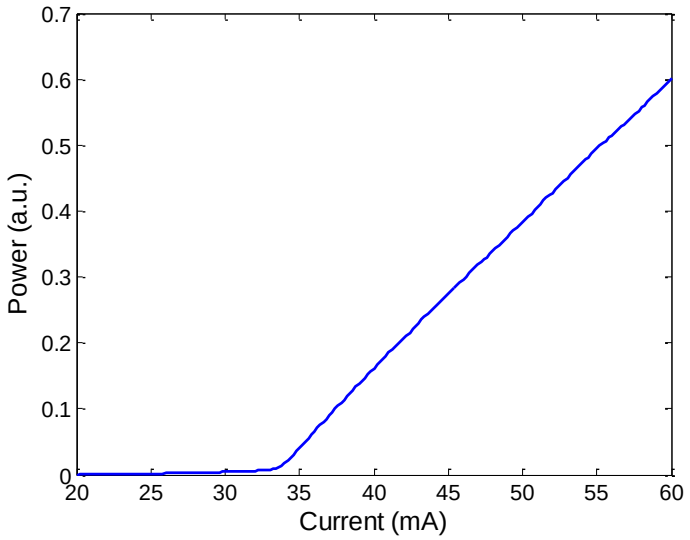

Fig. 2.12. Light-current curve of the laser DL5146-101S. The power is represented by the photocurrent amplified through the first stage transimpedance amplifier, which has a gain of 1 kΩ.

For the characterization of the blue-violet laser, the injection current was varied from 20 to 60 mA in steps of 0.2. The spectrums of the signals sampled at 1 MHz for 200 different values of current are presented in Fig. 2.13.

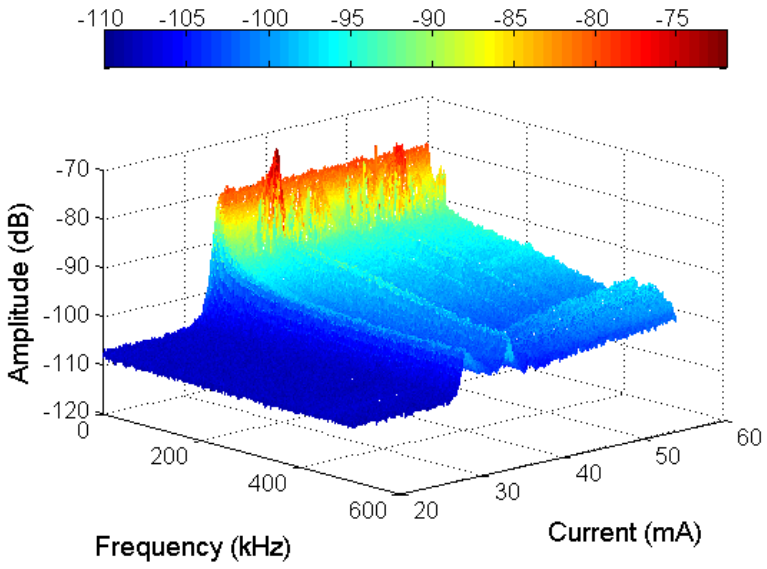

Fig. 2.13. Spectrum evolution as a function of current provided to the laser DL5146-101S. The graph shows 200 spectrums and the fundamental Doppler peak is found as the current passes the threshold for the laser.

The Doppler peak is related to the target's velocity. Figure 2.14 shows the spectrum for 60 mA. The function to fit the amplitude of the peak is similar to the

one used for the infrared laser with new terms included to account for the evident slope in the spectrum as follows:

$$f(x) = A_0 + Ae^{-\frac{(f-b)^2}{2{c_1}^2}} - pf + q, \qquad (2.22)$$

where the terms p and q are the slope and the interception with the vertical axis.

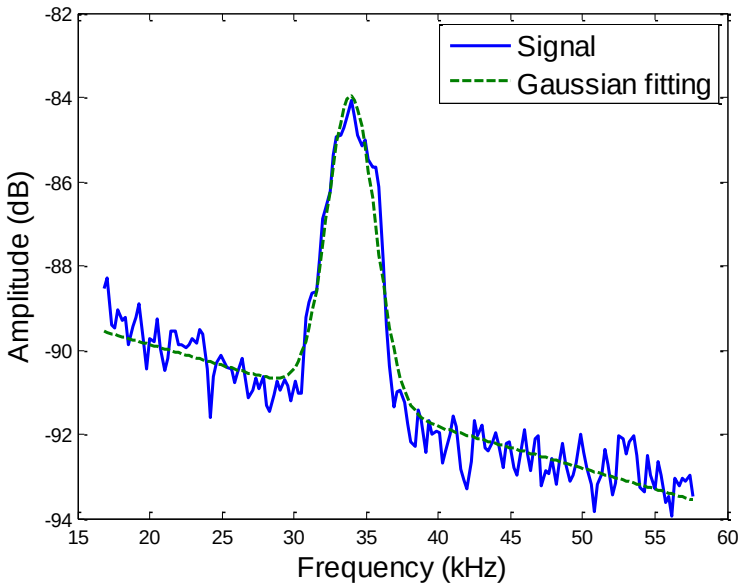

Fig. 2.14. Doppler peak in the spectrum fitted to equation 2.22. The spectrum corresponds to a current of 60 mA.

The evolution of the noise and the maximum of the Doppler peak for the blue-violet laser are represented in Fig. 2.14(a) and their difference, the signal-to-noise ratio (SNR) is plotted in Fig. 2.14(b).

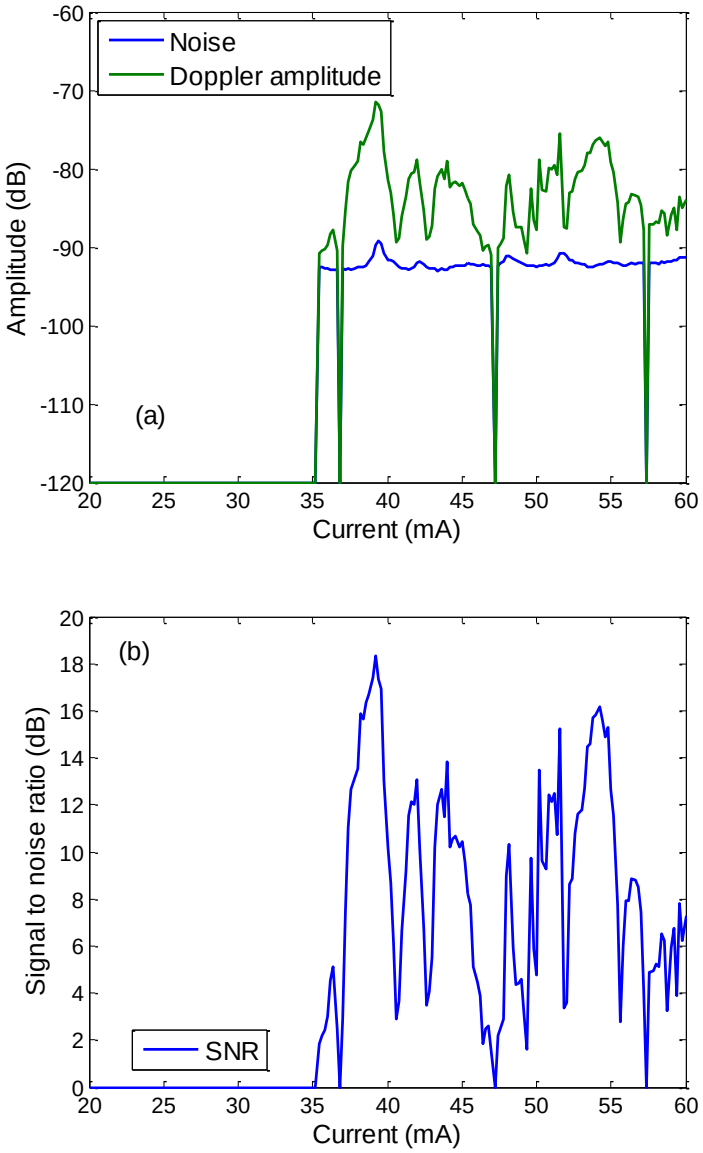

Fig. 2.15. Characteristic electrical behavior of the blue-violet laser for various values of input current.

As depicted in the Fig. 2.15(a) and 2.15(b), this laser has several current intervals where no signal-to-noise ratio is appreciated. In the best case scenario, the maximum SNR (around 18 dB) is reached when the injection current is slightly below 40 mA.

The electronic circuitry driving this laser was designed to operate in this range to achieve the best performance during the measurements. During the experimental series conducted with this laser, it was configured to generate an optical output power of 5 mW.

Chapter 3

Optical feedback interferometry in fluid flow sensing

Optical feedback interferometry (OFI) based flowmetry allows for the design of simple, robust, self-aligned and low cost systems to measure the fluid flow. In OFI based velocimetry (flowmetry), the OFI signal spectrum is the most usual tool to obtain information regarding the velocity of moving objects (particles). In the case of most solid target, the OFI signal spectrum exhibit a narrow peak at the unique Doppler frequency induced by the target displacement. In the case of measurement in liquids, the spectrum is strongly affected by the key elements of the flow. The velocity distribution in the probe volume has a direct impact in the Doppler frequency shift observed in the OFI spectrum. In addition, the spectrum morphology is influenced by the density of scattering particles embedded in the fluid. Depending on the particle concentration in the fluid, single scattering or multiple scattering may occur in the sensing point causing to a significant change in the shape of the power spectrum of the OFI sensor and thus in the methodology for the measurement of the flow parameters.

Since the work presented in this thesis corresponds to laminar flows with Newtonian behavior, we will focus our attention on the impact of the number of scatterers in the sensing volume contributing to the feedback that affects the laser's power spectrum. We will explore the reliability of the different signal processing methods to extract the velocity information from the OFI signals in cases of single and multiple scattering regimes.

The chapter is structured as follows. We present an analysis of the processing methods for flow velocity measurements using an OFI sensor in the case of multiple particles detection. A demonstration of the reliability of the signal processing is presented for each scattering regime and two applications in the different scattering regime are presented. First, an ex-vivo demonstration of flow mapping using an automatic processing in the single scattering regime is presented. Then, we present a real-time OFI system for non-steady flow measurements in the multiple scattering regime. The chapter presents in its last section a system for single micro-particle detection in microfluidic devices.

3.1 Reliability of optical feedback flowmetry: implications of the scattering regime.

Under flow-controlled conditions where a laminar behavior at low Reynold number is guaranteed, the challenge of measuring the flow rate or a local velocity with the OFI sensing technique lies in dealing with a robust processing to extract the quantitative velocity value. The scattering regime, because it induces various Doppler shifts to the back-scattered waves, imposes particular power spectrum morphologies as will be depicted lower. Thereby, different signal processing methods have been proposed to accurately extract the Doppler frequency from the power spectrum corresponding to the fluid velocity at the measurement volume. In this section, the reliability of the commonly used methods for various particle concentrations and at different flow rates is evaluated. To highlight the performances of the signal processing approaches, velocity profile measurements of flowing fluids in a circular microchannel by OFI for different particle concentrations are performed.

3.1.1 Processing Methods

As described above, the particle concentration in the sensing volume of the OFI sensor determines the power spectrum shape. In the case of very low concentration where only one particle crosses the sensing volume at the time, the signal spectrum exhibits a clear Doppler frequency peak. This case does not require a very complex signal processing approach and will be developed later in this chapter. For low particle concentrations and a small sensing volume as compared to the channel dimension, a well-defined Doppler frequency peak appears in the power spectrum [Rovati, 2011; Campagnolo, 2013a]. When the dimension of the sensing volume is larger than the channel diameter, the Doppler frequency peak becomes broader and may reach to an extent that no peak will be observed and the spectrum exhibits a flat distribution [Riva, 1972]. As the particle density increases, the signal spectrum is the sum of all contributions of each particles inside the sensing volume and the spectrum shows a slow decay from low to higher frequencies [Bonner, 1981]. Examples of this phenomenon are depicted in Fig. 3.1 for a highly diluted solution of polystyrene spheres (0.1 % in destilled water) and for blood flowing in a 200 µm diameter tube. The dashed

lines represent the maximum frequency corresponding to the maximum velocity in the duct.

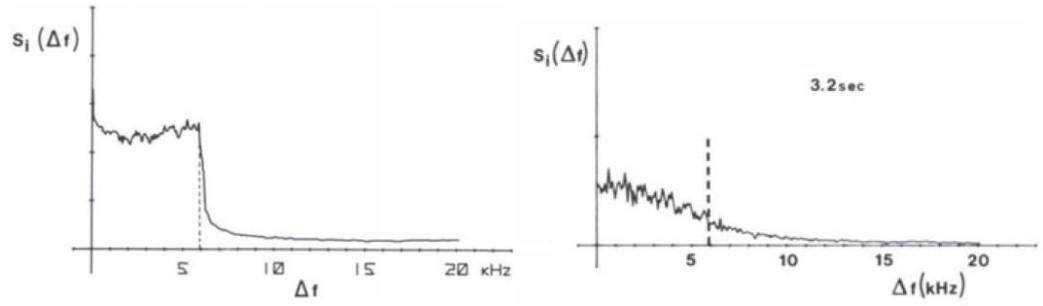

(a) **(b)**

Fig. 3.1. Power spectrum corresponding to the signal of a flow obtained by a collimated beam of an He-Ne laser. The flow moves in both cases at 1.44 cm/s inside a 200 μm diameter duct. (a) Power spectrum for 0.1 % of polystyrene spheres in water. (b) Power spectrum for blood. Images are taken from [Goldman, 1981].

In the case of a well pronounced frequency peak, obtaining the velocity information may require the use of different fitting functions to determine the frequency corresponding to the fluid velocity. In her thesis dissertation, Campagnolo [Campagnolo, 2013b] extensively addressed this issue and tested different functions to fit the spectrum for OFI sensors incorporating vertical cavity surface emitting lasers (VCSELs) and Fabry-Perot cavity semiconductor lasers. A Gaussian-like equation was successfully used by Campagnolo [Campagnolo, 2013b] to determine the Doppler frequency shift produced by a highly diluted liquid in a cylindrical microchannel with diameter of 320 μm, where single scattering characterized the feedback detection.

In the case where a flat frequency distribution is observed in the OFI spectrum, a cutoff frequency approximation may be used to obtain the Doppler frequency corresponding to the maximum fluid velocity [Riva, 1972; Nikolić, 2013]. In this method the frequency at which the flat spectrum falls below a certain threshold (cutoff level) is considered as the Doppler frequency corresponding to the maximum velocity. In fact there is no robust criterion to determine accurately the cutoff frequency. It was shown by Nikolić *et al*. [Nikolić, 2015] that depending on the particle concentration the cutoff level varies significantly. However, when calculating the Fast Fourier Transformation (FFT) of a raw OFI signal, it is usually accepted that the maximum velocity is determined using a threshold of -3 dB below the flat frequency distribution of the spectrum. The cutoff level is not only related to the concentration but also the sensing volume dimensions that may have an influence.

For a very high particle concentration, the multiple scattering regime induces the power spectrum to have a slow decay that contains a statistical distribution of Doppler shifts. In this case, the average particle velocity in the sensing volume can be obtained by calculating the weighted moment of the power spectrum as first proposed by de Mul *et al*. [de Mul, 1993]:

$$\bar{f} = \frac{M^1}{M^0} = \frac{\int_0^\infty f.p(f).df}{\int_0^\infty p(f).df} \tag{3.1}$$

where $\bar{f}$ is described by de Mul *et al.* as the average Doppler frequency, M^1 is the first order moment which is proportional to the average velocity times the number of particles generating Doppler shifts in the sensing volume, M^0 is the zero order moment which is related to both the number of particles generating Doppler shifts in the sensing volume as well as the Doppler shift values, and $p(f)$ is the power spectrum of the OFI signal obtained as the square module of the FFT of the signal. The interpretation of the average Doppler frequency is possible by linking the expression 3.1 with the center of mass of a frequency distribution. The frequency corresponding to the center of mass varies depending on the velocity of the fluid, thus it can be used as a measure of the velocity of particles merged in the fluid as long as the number of particles in the flow remains homogeneously distributed. To the best of our knowledge, the particle concentration range for which this method is valid to obtain the average Doppler frequency has not been investigated. In the next section, this issue will be verified.

In order to have various concentrations of particles in the fluid flowing inside the channel, different dilutions of bovine full cream milk were used (2, 4, 6, 8, 10, 12.5, 25, 100% w/w). Milk particles have several interests in the field of microfluidics experiments:

- first, it is a cheap and easy way to obtain particles that have a good density as compared to the carrying fluid (water). So diluted milk offers very uniform particle densities;

- second, milk when compared to other biological liquids, has a very reproducible composition thanks to the agro-industrial production methods;

- third, it is considered a good optical phantom for blood [Binzoni, 2014, Lohwasser, 1999].

3.1.2 Sensor description

A schematic representation of the system is depicted in Fig. 3.2. The laser diode (LD, Thorlabs L785P090), emitting at 785 nm an optical power of 90 mW is located at twice the focal distance of the focalization lens (Thorlabs C240TME-B, focal length *f* = 8 mm). The lens itself is positioned at twice its focal length from the center of the microchannel so that the beam waist is located exactly in the middle of the cylindrical duct where the flow velocity is the highest.

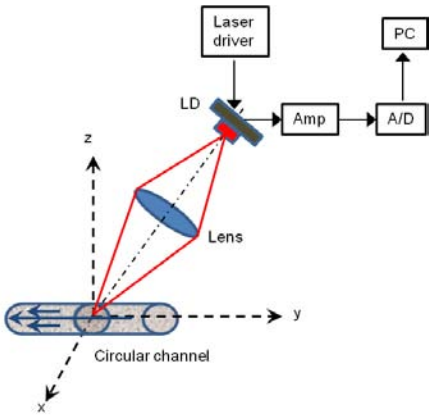

Fig. 3.2. Schematic representation of the sensing system. The laser is located at twice the focal distance from the lens and focalized in the center of the cylindrical channel.

The output optical power is monitored by the photodiode integrated in the laser package. The signal of the photodiode is then amplified by a custom built transimpedance amplifier. The assembly is tilted by 80º with respect to the flow direction. The photodiode signal was acquired using a National Instruments data acquisition card (BNC-2110). Acquired signals contain 8192 samples recorded at a sampling frequency of 250 kHz.

3.1.3 Channel description

The fluidic channel consist of a unique circular-cross section polydimethylsiloxane (PDMS) channel with a diameter of 320 µm. The PDMS chip was made of silicon elastomer (Sylgard 184) which is a two component elastomer: a silicon elastomer and the curring agent that was mixed in a ratio of 10 to 1, curable in ambient temperature if left for 24 hour. To manufacture the channel inside the PDMS, a fiber optic with a diameter of 320µm was placed inside the silicon elastomer before curing, then the wire was pulled out after it cured completely.

3.1.4 Velocity measurements at the channel center

The OFI signal acquired represent the sum of all contributions in the sensing volume. Each milk concentration was pumped at ten different flow rates (10, 20 ... 100 µl/min). At the maximum fluid flow rate (100 µl/min), the Reynold number Re for the used cylindrical channel was about 12, which is well within the laminar regime (Re <2100).

Figures 3.3 and 3.4 depict the power spectral density calculated from the square Fast Fourier Transform (FFT) of the signal for flow rates varying from 10 to 100 µl/min for milk concentrations of 2%, and undiluted milk (100% concentrated) respectively. As can be appreciated, even when using a small concentration (2%) a sharp Doppler peak does not appear in the signal power spectrum.

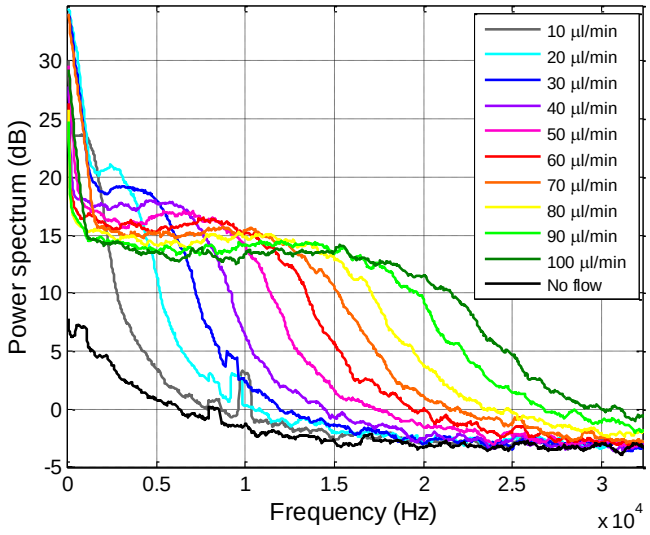

Fig. 3.3. FFT of the signal for flow rates from 10 to 100 µl/min for 2% milk concentration.

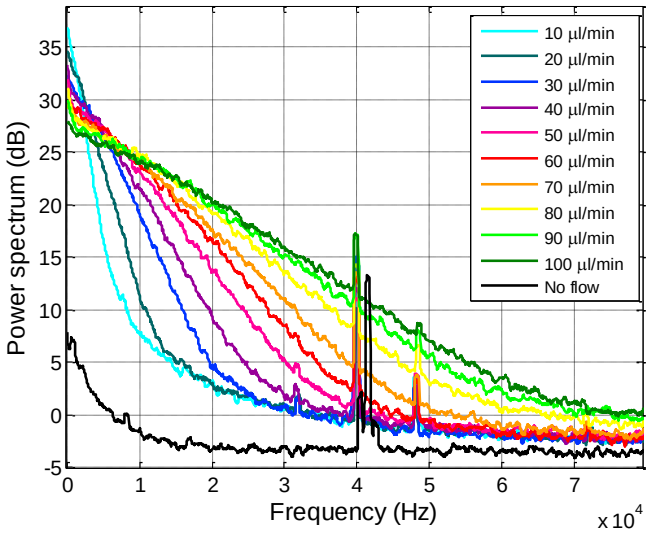

Fig. 3.4. FFT of the signal for flow rates from 10 to 100 µl/min for 100% milk concentration.

By increasing the flow rates at 2% concentration, the power spectrum gets broader but remains with a flat distribution. With 100% milk concentration, a slow decay is obtained at all flow rates.

Fig. 3.5 presents the evolution of the signal spectrum when increasing the milk concentration for a flow rate of 50 µl/min.

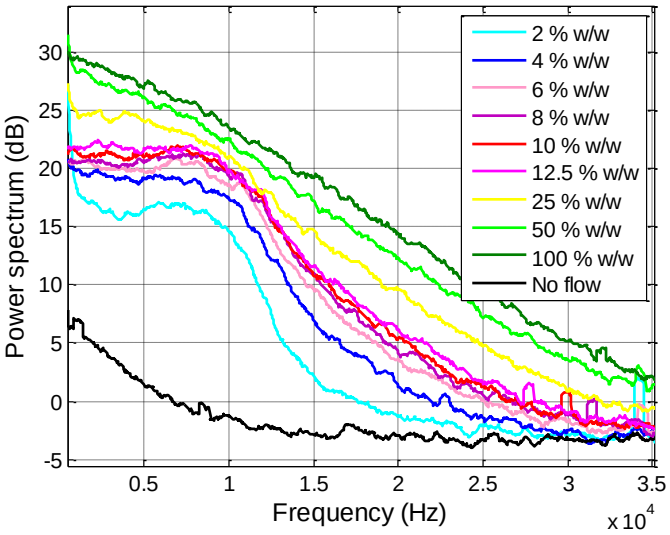

Fig. 3.5. FFT of the signal of varying milk concentrations from 2% to 100% w/w for 50 µl/min flow rate.

To find the milk concentration range within which the weighted moment approximation is valid for the determination of the average velocity, the average Doppler frequency (equation 3.1) has been calculated for flow rates from 10 µl/min to 100 µl/min. Figs. 3.6 to 3.10 show the obtained results for 2, 4, 6 10, 100 % w/w concentrations. Error bars show the standard deviation calculated from 10 measurements and the green line represents the theoretical Doppler frequency shift corresponding to the average velocity, which is equivalent to the flow rate and is determined from expression 1.6. This average velocity is calculated from the ratio of the flow rate and the area of the channel cross-section.

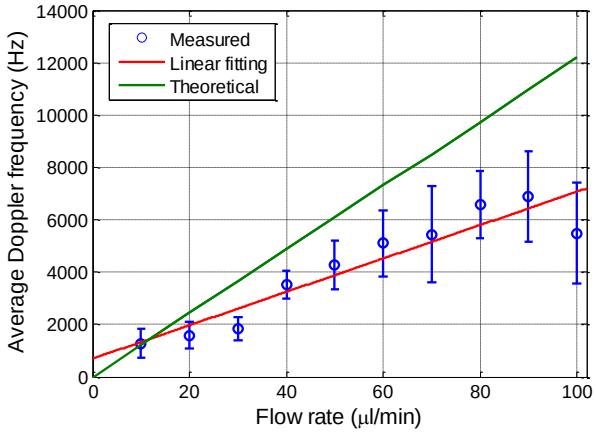

Fig. 3.6. Average Doppler frequency (obtained from weighted moment approximation) versus flow rates for milk concentrated at 2 %. Error bars indicate the standard deviations calculated from 10 measurements.

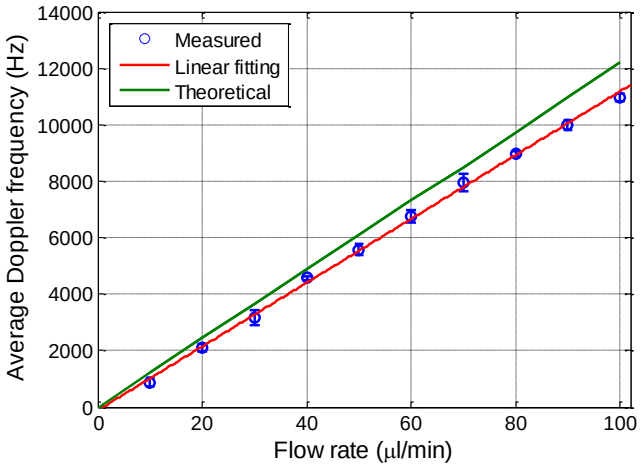

Fig. 3.7. Average Doppler frequency (obtained from weighted moment approximation) versus flow rates for milk concentrated at 4 %. Error bars indicate the standard deviations calculated from 10 measurements.

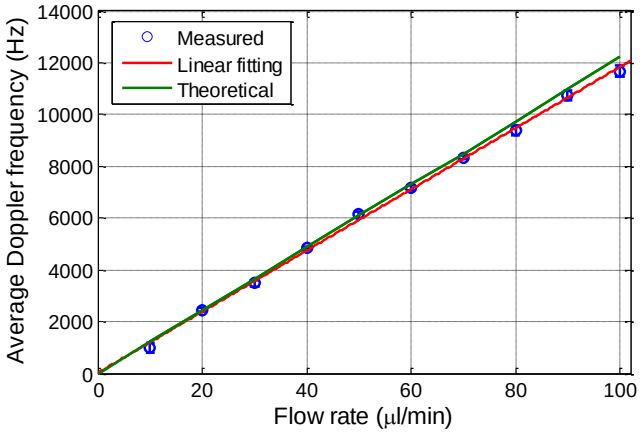

Fig. 3.8. Average Doppler frequency (obtained from weighted moment approximation) versus flow rates for milk concentrated at 6 %. Error bars indicate the standard deviations calculated from 10 measurements.

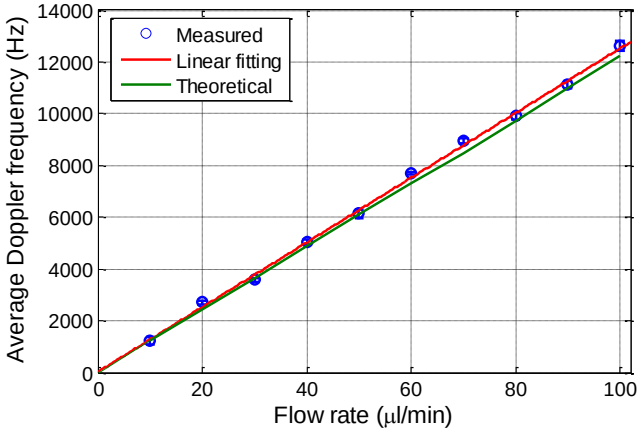

Fig. 3.9. Average Doppler frequency (obtained from weighted moment approximation) versus flow rates for milk concentrated at 10 %. Error bars indicate the standard deviations calculated from 10 measurements.

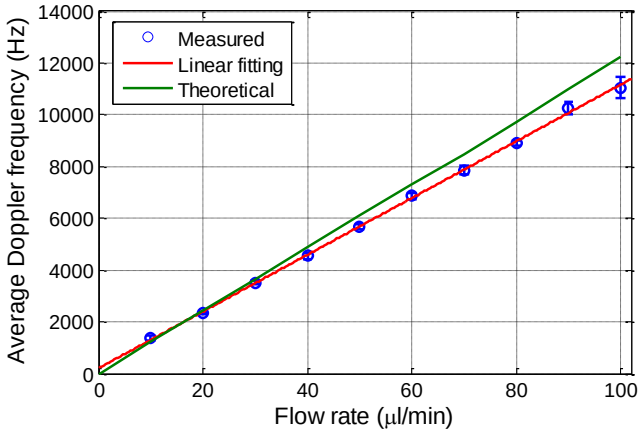

Fig. 3.10. Average Doppler frequency (obtained from weighted moment approximation) versus flow rates for undiluted milk. Error bars indicate the standard deviations calculated from 10 measurements.

As can be seen, the average Doppler frequency measurement for 2% milk concentration is not reliable not only due to the significant deviations from linearity (as evidenced in the red line within the figure) but also due to the large variations at each flow rate. The red solid line in Figs 3.6 to 3.10 show the best linear fit of average Doppler frequency obtained by equation 3.1. For the concentrations ranging from 4 % to 100 %, the measurement results show very small deviations from the expected values.

In Fig. 3.11, the relative error of the measured average Doppler frequency for all concentrations at a flow rate of 50 µl/min is calculated. As can be seen in these figures (3.6 – 3.10), the weighted moment method used to calculate the average Doppler shift is quite efficient as long as the dilution of milk in water is higher than 4 % w/w. In these cases the relative error is lower than 8 %. This result highlights the robustness of the method considering that at dilutions of 4 % and up to 25 %, the signal spectrum keeps a well-defined plateau which seems to say that the multiple scattering effects remain negligible.

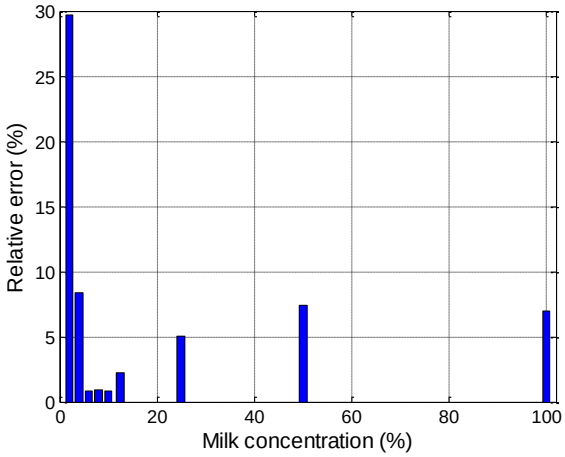

Fig. 3.11. Relative error of the measured average Doppler frequency (when using the weighted moment method) with respect to the theoretical value for all concentrations at 50 µl/min flow rate.

Another important aspect to ensure the weighted moment method validity is to evaluate its robustness over the flow rates range. Figure 3.12 shows the relative error calculated for various concentrations in the range 4% to 100 %. The frequencies measured are averaged and compared to the theoretical value corresponding to the flow rate imposed. The maximum error is around 6 %.

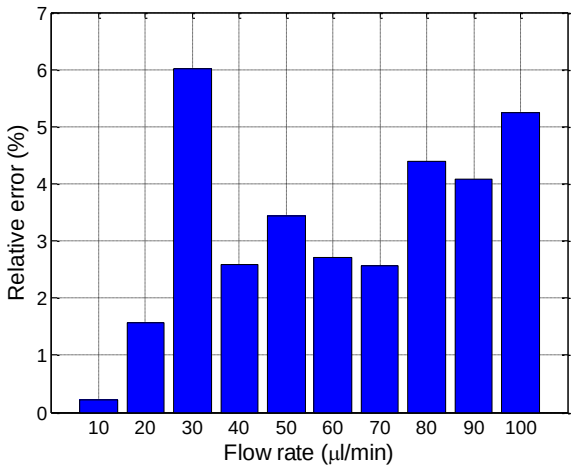

Fig. 3.12. Relative error calculated when using the weighted moment method for milk concentrations in the range 4% to 100% (w/w).

Figure 3.13 shows the relative standard deviations of the measured average Doppler frequency at each flow rate. The relative standard deviation is defined as the ratio between the standard deviation of the measured average frequencies and the mean frequency of the ensemble. As for Fig. 3.12, this deviation is calculated for the measurement at milk concentrations from 4% to 100%. For flow rates higher than 20 µl/min, the deviations are around 7% or lower.

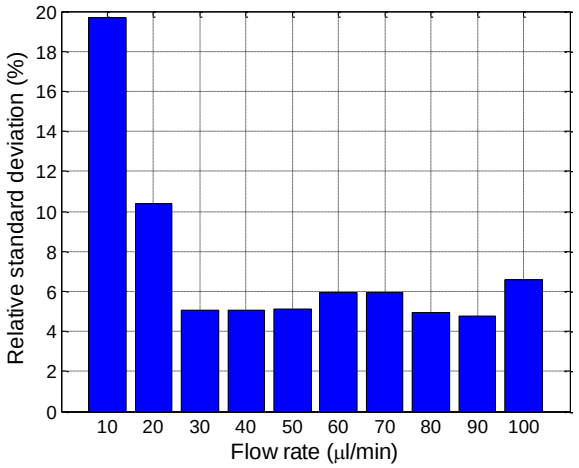

Fig. 3.13. Relative standard deviation of the measured average Doppler frequency (obtained by weighted moment approximation) at different flow rates when measuring different milk concentrations (4, 6, 8, 10, 12.5, 25, 50, 100% w/w).

At lower flow rates, higher deviations observed may be due to the noise that is very visible in the signal spectrum even in the no flow case. The noise in the OFI

sensing scheme includes electrical Flicker noise of the amplification and of the laser diode, mechanical noise induced by small vibrations between the micro-reactor and the sensor and the speckle effect induced by the particles [Atashkhooei, 2013]. The noise has a non-negligible impact on the calculation of the zero order moment and first order moment values. Another explanation could be that at lower flow rates, the power spectrum distribution is relatively narrower and the moments are then closer to zero, so any pertubation in the signal spectrum can have a significant impact in their values. However it shall be noted that this limitation is not directly linked to the flow rate but rather to the Doppler frequency shift. For a given flow rate, reducing the laser wavelength (using a blue laser diode for example) or changing the angle between the flow direction and the optical axis could solve this issue.

Then, for a 2% milk concentration, the weighted moment approximation technique is not a very accurate and robust method to calculate the average Doppler frequency. Under such conditions the cutoff frequency approximation method seems to represent a valid alternative. Campagnolo [Campagnolo, 2013b] tested this method to obtain the cutoff frequency proportional to the flow velocity in a microchannel, and a linear regression was obtained with the flow rate imposed into the duct for a cutoff of -3 dB. However, the cutoff level determination is ambiguous and may vary, as stated earlier in this chapter, depending on the optical configuration and the nature of the scattering particles [Nikolić, 2013]. To get over this issue, we characterized the frequency distributions depicted in Fig. 3.3 and compared the results obtained for a cutoff of -3 dB and for a cutoff with arbitrary threshold, which after empirical estimation corresponds to the Doppler shift induced at the maximum velocity in the spectrum. This threshold was found with our setup to be equal to -6 dB.

Figure 3.14 depicts the average Doppler frequency obtained using cutoff method for 2% milk concentration. Setting a fixed cutoff level at -3 dB (error bars with circles) from the plateau in the power spectrum yields a linear regression is found with respect to the flow rate. The measured points represented by the error bar with diamonds correspond to the frequency calculated using a cutoff level at -6 dB against flow rates. The average frequency is calculated from the maximum frequency obtained at the end of the spectrum. For a duct with circular cross-section the maximum velocity is twice the average velocity of the flow. In this figure, both error bars represent the standard deviations calculated from 8 measurements.

So, choosing a typically accepted threshold for the spectrums obtained with different configurations may lead to disagreement between the theoretical and the measured frequency correlated to the fluid velocity. The mismatch between the measured frequencies at different thresholds is more evident as the flow rates increase due to the broadening of the spectrum. With these results, we emphasize that a rigorous calibration of the OFI sensor should be performed to find the

proper cutoff frequency before measuring the flow speed in real sensing applications.

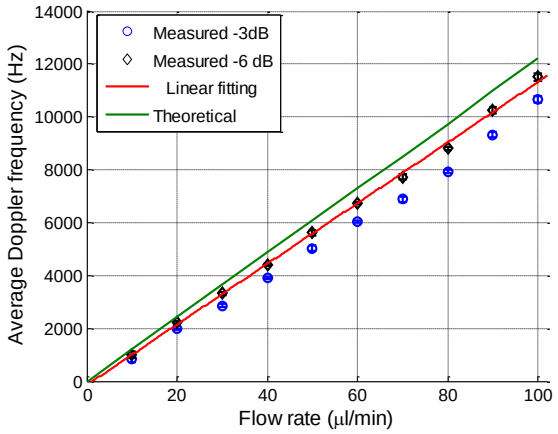

Fig. 3.14. Average Doppler frequency (obtained by cut-off method) versus flow rates for milk concentration of 2% w/w. The red line shows the linear fitting and the green line the theoretical relation of flow rate and velocity. Error bars represent standard deviations calculated from 8 measurements.

The location in the spectrum of the cutoff frequencies at -3 dB and -6 dB below the flat frequency distribution that corresponds to 40 µl/min are depicted in Fig. 3.15.

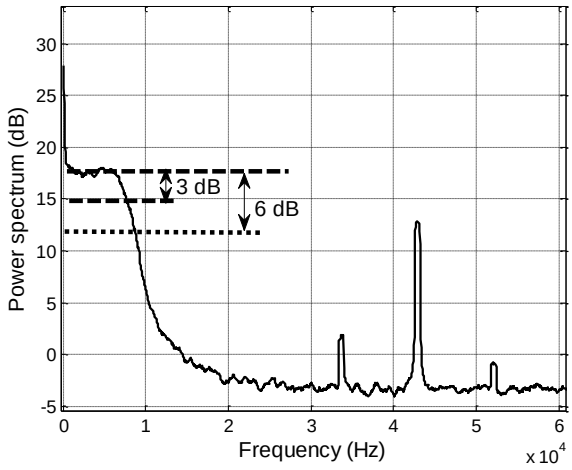

Fig. 3.15. Power spectrum of the OFI signal corresponding to a flow rate of 40 µl/min. The threshold levels below the plateau represent the cutoff frequencies used to generate the Fig. 3.14.

Although the relation of the frequency (and therefore the velocity) is always linear with respect to the flow rate, the calibration of the system is of utmost importance when implementing OFI for flow velocity measurements.

To find the milk concentration range within which the cutoff method is able to accurately estimate the average Doppler frequency, the relative error on the measured Doppler frequency with the theoretical values against milk concentrations at 50 µl/min have been calculated. The results are presented in Fig.

3.16. It is seen that except for 2 %, 4 % and 6 % concentrations, the errors are higher than 10 %. As can be seen directly in Fig. 3.4, the cutoff frequency varies depending on the concentration, therefore the -cutoff method results in a significant inaccuracy in Doppler frequency measurements for milk concentration higher than 4% regardless the cutoff level chosen.

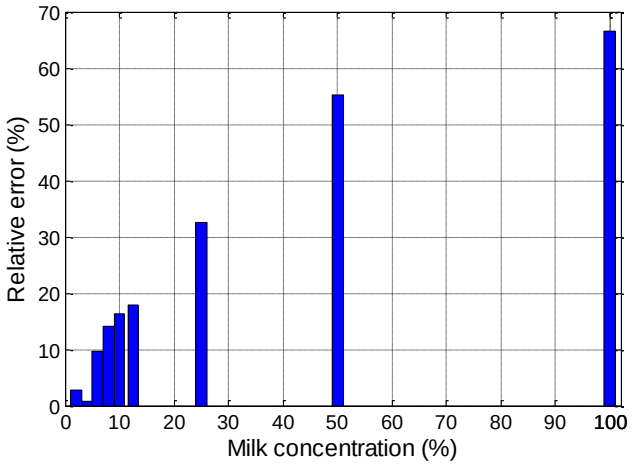

Fig. 3.16. Relative error of the measured average Doppler frequency when using the cutoff method for all milk concentrations at 50 µl/min flow rate. The cutoff level is set to -8 dB.

3.1.5 Zero order moment for various moving particles concentrations

The zero order moment is related to both the number of particles generating Doppler shifts in the sensing volume and to the Doppler shift values, which are proportional to the perfusion. For a given fluid with constant particle density, one could think that the zero order moment can be used to characterize the flow rate. This section aims at evaluating the pertinence the zero order moment for such tasks.

As shown earlier in Fig. 3.5, when the milk concentration increases, the number of Doppler shifts generated by the particles increases proportionally, thus changing the morphology of the spectrums. Therefore, because of multiple scattering, the Doppler frequency distribution, which corresponds to an image of the particle velocity distribution inside the sensing volume, shows a flat profile up to approximately 10 kHz for concentrations from 2 % to 12.5 %. Then, at higher concentrations, it shows a continuous decay from low to higher frequencies.

To evaluate the zero order moment relationship against milk concentration, zero order moment has been calculated for all milk concentrations for various flow rates. It was expected to have linear relationship between zero order moment and the Doppler generating particles concentration [de Mul, 1992].

Figures 3.17 and 3.18 show the zero order moment versus milk concentration for flow rates of 10 µl/min and 30 µl/min. The error bars demonstrate the standard deviation calculated from 10 measurements. The error bars depict the variations due to the opto-electro-mechanical noise of the OFI sensor and the instability of

fluid flow in the channel at the measurement point. We observed the same behavior for zero order moment against the milk concentration for all flow rates from 10 µl/min to 100 µl/min.

As can be appreciated, at higher concentrations (starting from 25 %), multiple scattering effects and/or absorption induce a lower increase of optical feedback power against the concentration. This results in the divergence of the zero order moment against concentration relationship from the linearity. It is noticeable that also at 2 % concentration, zero order moment deviates from the linearity and the error bar shows a large variation. This deviation at low concentration is due to the noise variation in power spectrum. As the zero order moment value is small at low concentration and especially at low flow rates, the impact of noise variation is significant. Thereby, zero order moment relationship against milk concentration is linear for the concentrations between 4 % and 25 %.

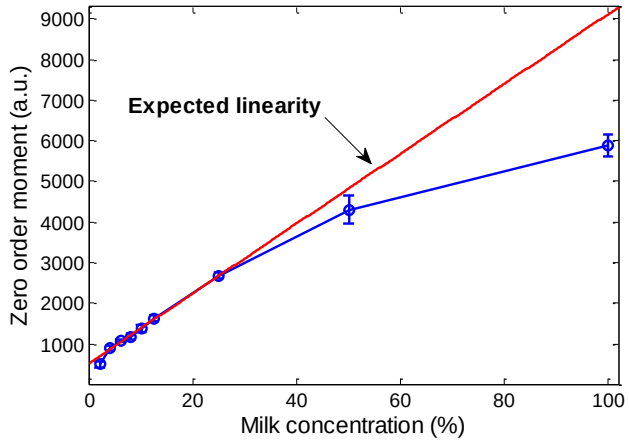

Fig. 3.17. Zero order moment versus milk concentration at 10 µl/min. The red line shows the expected linearity for zero order moment. Error bars demonstrate the standard deviation for 10 measurements.

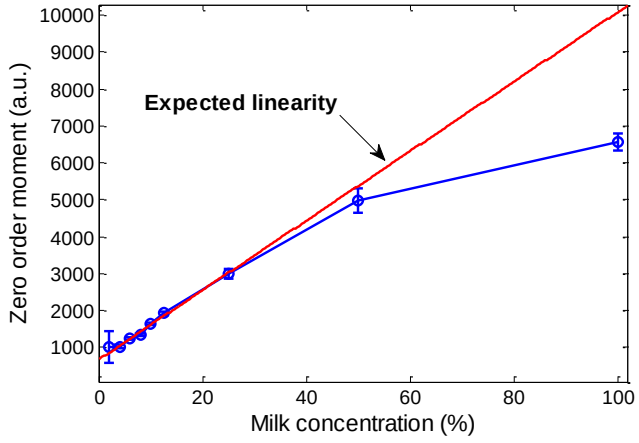

Fig. 3.18. Zero order moment versus milk concentration at 30 µl/min. The red line shows the expected linearity for zero order moment. Error bars demonstrate the standard deviation for 10 measurements.

3.1.6 Velocity profile measurement

Velocity profile measurement of a micro-channel has been demonstrated by Campagnolo [Campagnolo, 2013a] in the case of the single scattering regime. It is a very efficient solution to visualize the validity of the signal processing method because it displays with the same optical system, the same fluid and the same flow rate a large range of particle velocity distributions.

To measure the velocity profile, the sensor is moved along a line perpendicular to the flow direction. Thus, the velocity of the flowing fluid is measured at different locations along the channel section.

In a laminar fluid flow, the velocity profile of a circular cross section channel is described by the Poiseuille equation:

$$v(r) = v_{\max}\left(1 - \left[\frac{r}{R}\right]^2\right) \tag{3.2}$$

where R is the radius of the circular cross section of the flowchannel, r is the variable distance from the center to the wall of the cylinder and $v_{\max} = Q/A_S$ is the velocity in the center of the channel, Q is the volumetric flow rate and A_S is the area of the cross section.

The velocity profile inside the cylinder complies with the no-slip condition, thus it increases from zero at the channel's walls and reaches a maximum at the center.

In this section, the flow velocity profile of the circular channel will be measured using three different milk concentrations, a high dilution (2% w/w) and medium dilution (10% w/w). At high dilution, the cut-off frequency approximation with a cutoff level of -6 dB is used to determine the maximum frequency and at low dilution, weighted moment approximation (equation 3.1) is employed to calculate the average Doppler frequency. Then, equation 1.6 is used to calculate the velocity values of the flow at the sensing volume.

For profile determination the OFI sensor scanned the channel with 10 µm displacement steps. A micrometric stage device (Zaber-LSM 50A) is used as an XYZ displacement system to scan the channel from wall to wall.

Figures 3.19 and 3.20 show the velocity profile for 2% and 10% milk concentrations respectively. The solid line in the figures shows the theoretical estimation of the velocity profile plotted from equation 3.2 [Rovati, 2011; Campagnolo, 2013b] and the circle plots are the measured values at different local points of the scan.

As can be seen, at 2% milk concentration, measured profile is in good agreement with the theoretical estimation. At 10% milk concentration, similar agreement can be observed when measuring away from the walls. However a deviation from theoretical profile mostly at the positions close to the walls of the channel is

obviously observed. This degradation is probably the consequence of the poor accuracy of the weighted moment method at low velocity as has been discussed in section 3.1.4.

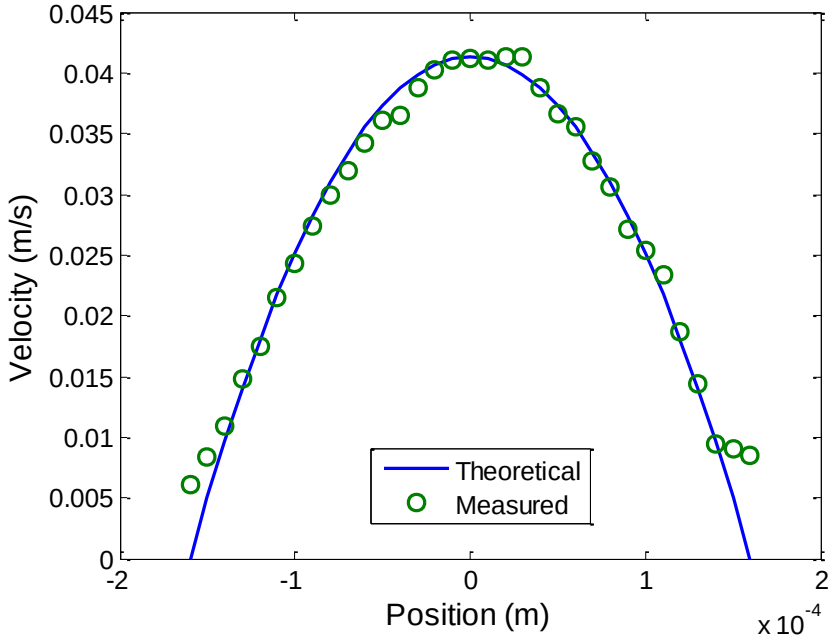

Fig. 3.19. Experimental (circles) and theoretical (solid line) fluid velocity profile for the circular channel with diameter of 320 µm obtained by the cut-off frequency method. Fluid was 2% w/w diluted milk pumped at 100 µl/min.

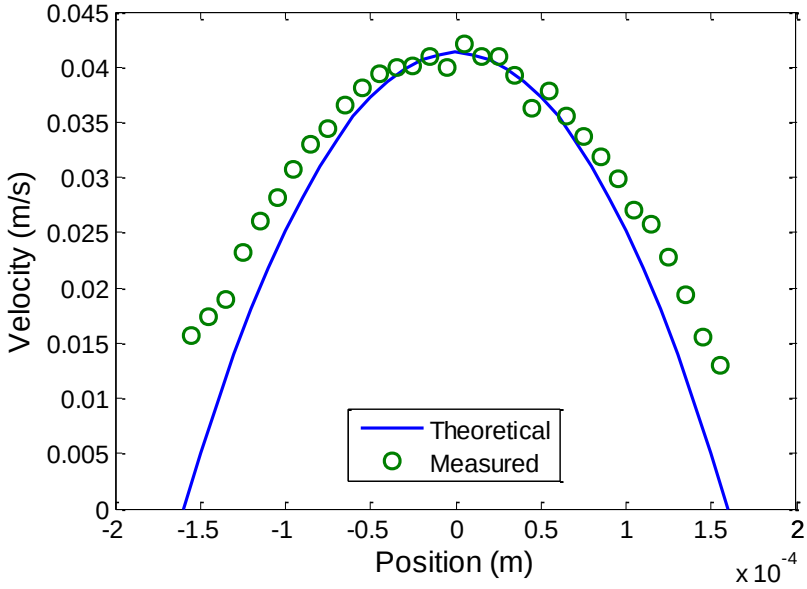

Fig. 3.20. Experimental (circles) and theoretical (solid line) fluid velocity profile for the circular channel with diameter of 320 µm obtained by weighted moment method. Fluid is milk concentrated at 10% and pumped at 100 µl/min.

3.2 Ex-vivo velocity profile measurements

The good agreement of the measured and theoretical profiles of fluids in the single scattering regime in cylindrical channels, demonstrates the possible implementation of optical feedback interferometry sensors in measurement of flow distribution in small vessels and arteries.

In-vivo flow velocity measurements can be used to quantify vital parameters associated to the circulatory system and angiography, and many systems are available to measure such flows. Some of them were reviewed in chapter 1. The need to accurately measure physiological functions and properties of small arteries, veins and other vessels is well established [Kamishima, 2012]. Vascular smooth muscle cells, located inside vessel wall play a key role in contraction and relaxation of arteries [Lu, 2011]. These vasoconstriction and conversely vasodilatation effects are driven, in normal conditions by the central nervous system or, in the case of disease, by vasodilative or vasoconstrictive drugs. In the perspective of vessel characterization, two kinds of measurement systems exist:

- The isometric method, which measures changes in force from dissected resistance arteries while the length (diameter) remains constant.
- The isobaric method, which measures changes in diameter while transmural pressure across the artery wall is kept constant.

We will be focused on isobaric or pressure myograph systems. In these sensors, a single vessel is isolated on two glass cannulas, pressurized and flushed by a liquid to simulate blood flow [Clifford, 2011]. Then, the artery is imaged on a video monitor and diameter is assessed by contrast detection of the arterial wall in the dimension analyzer. Investigation on myogenic response, vasodilatative effect and endothelium behavior can be done with this kind of system [McCarron, 1997]. In our sensor, the vessel cannulation set up is inspired from myograph systems. OFI is hereby proposed as an alternative method for flow mapping.

A new pressure myograph system based upon an OFI sensor gives information about local velocity in fluids and enables reconstruction of a velocity profile inside a vessel. We intend, thereby, to test the capabilities of the OFI sensing technique in ex-vivo measurements of local flow velocity of fluids in the single scattering regime. For biomedical sensing, OFI sensors are ideally suited for measurements of blood flow, local flow in rat brain [Figueiras, 2013] or extra corporal circulation [Donati, 2014; Norgia, 2012].

3.2.1 OFI pressure myograph sensor

Figure 3.21 shows an overview of OFI sensor used for this study. It is composed by three main parts:

- XYZ displacement system. Three miniature motorized linear stages (Zaber-LSM 50A) move the laser with a resolution of 0.1905 µm and are controlled by a computer.
- One plano-convex optical lens (Thorlabs LA1951-B).
- A compact electronic system that realizes both laser driving and signal amplification functions. The prototype fits on a 5x5 cm PCB.

The optical setup consists on a laser diode (Hitachi HL7851G) emitting at 785 nm while being driven at an injection current of 50 mA. The laser is coupled to a single lens with a focal length f = 25.4 mm and the collimated radiation is pointed to the vessel with angle of 86°.

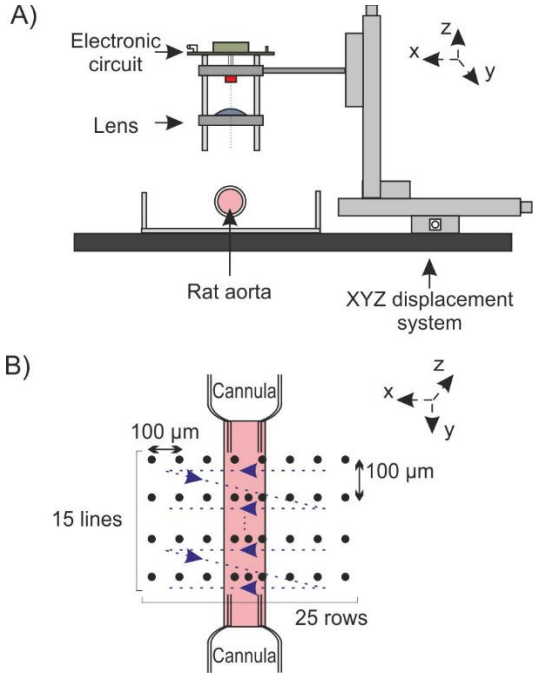

Fig. 3.21. OFI sensor coupled to an XYZ stage device for micrometric scanning: A) Lateral view, B) Top view of the aorta scanning

The amplified photodiode signal is digitized by a National Instruments card (NI USB 6251) connected via a USB interface to a computer. For each measurement point 4096 samples are recorded at 1 MHz.

The 2D automatic scanning protocol is presented in Fig. 3.21. For each position, 10 successive series of 4096 samples are recorded and processed off-line using a Matlab script. At the end of the recording process, each position data are stored in a text file with 40960 samples (4096 samples x 10 records). For an aorta scanning area of 3.75 mm^2, 10 minutes are required.

The flow velocity is directly measured inside an *ex vivo* rat vessel with a raster pitch of 100 µm. The size of a rat aorta is between 500 µm and 1 mm. An image of the cannulated aorta is presented in Fig. 3.22.

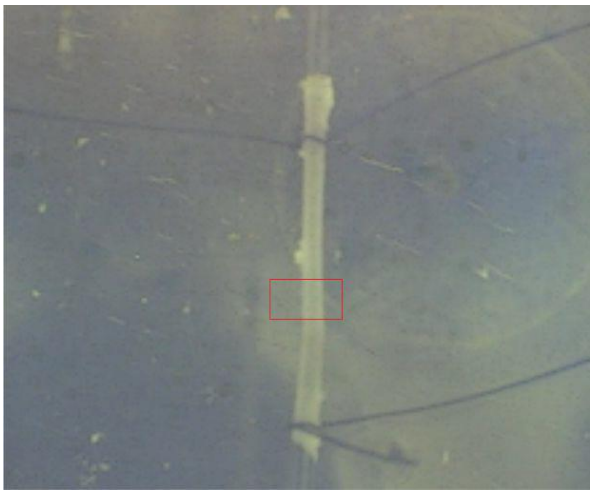

Fig. 3.22. Cannulated rat aorta: Red rectangle corresponds to the scanned area measured with OFI.

3.2.2 Experiment

Before scanning, the laser beam is focused on the center of the aorta. Then it is moved towards the x axis through the scan start point. As soon as the fluid velocity is stabilized the complete 2D laser scan is performed on a surface of 3.75 mm^2. In Fig. 3.22, the red rectangle represents the scan zone with a width of 2.5 mm (x axis) and a height of 1.5 mm (y axis). For each scan line (along x axis), a velocity profile is computed from the maximum Doppler frequency extracted from spectra using a signal processing method derived from the cut-off frequency method.

3.2.3 Signal processing

In the work presented by Campagnolo [Campagnolo, 2013a], the calculation of the maximal Doppler shift consisted in fitting the OFI signal spectrum with a complex Gaussian expression. This method, despite the excellent results obtained for the estimation of the fluid velocity, was requiring a rough calibration of several coefficients in the fitting function before running the fitting algorithm itself. Thus it was not possible to run the signal processing for the full scan in an automatized way.

The threshold cutoff method explained in section 3.1.1 and demonstrated in sections 3.1.4 and 3.1.6 was the starting point of the processing approach developed in this application. Since the determination of the cut-off requires a proper determination of the plateau level, an arbitrary threshold level of 17 dB was determined empirically and applied here to determine the flow velocity in an automatic way. The proposed method takes advantage of the fact that the decay of the spectrum is very strong after the cut-off frequency. The power spectral density of the signal obtained with the laser is shown in Fig. 3.23. The spectrum is similar to those presented in section 3.1.4 where a flat profile was evident in the OFI spectrum.

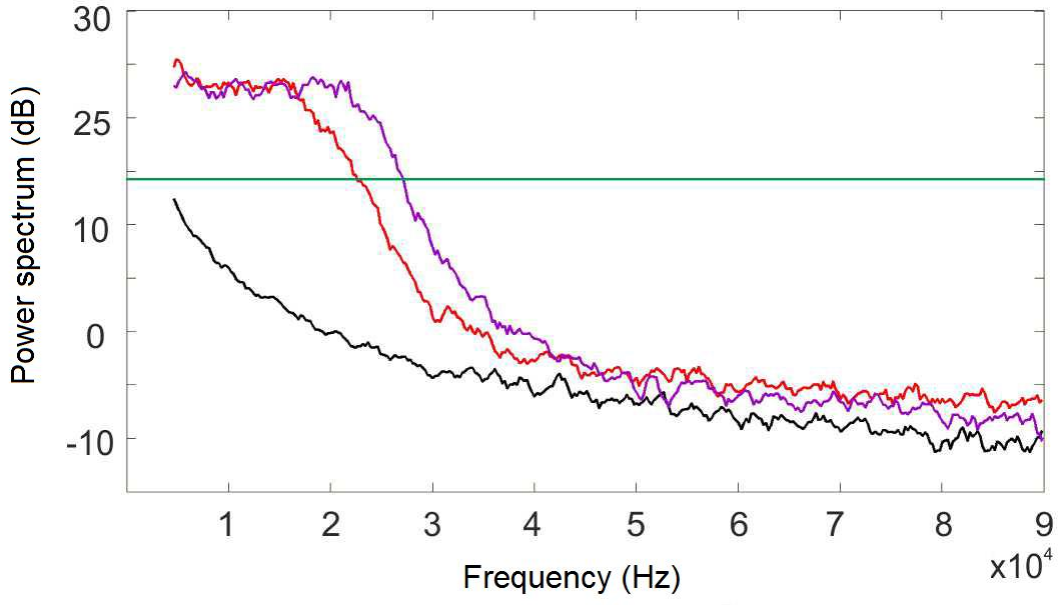

Fig. 3.23. One line scan on rat aorta by OFI: Three FFT spectra: outside the aorta (black), 300 µm from the scan start position (red) and 500 µm from the scan start position (purple) inside the aorta.

The fully automatic algorithm is represented in Fig. 3.24.

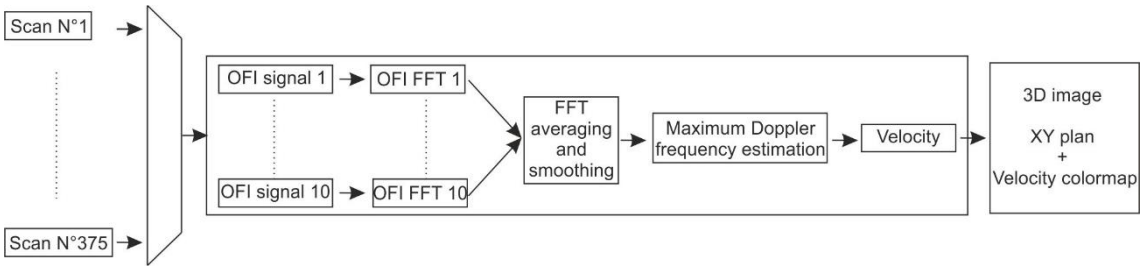

Fig. 3.24. Overview of the computational process, from OFI signal to 2D velocity mapping.

3.2.4 OFI flow mapping

The fluid velocity profile is composed by 25 measurements points and from the base profile width, an aorta diameter of 850 µm is measured. Even without any fitting, a parabolic shape is observed from the experimentally measured flow velocity profile plotted in Fig. 3.25 as expected from Poiseuille's law.

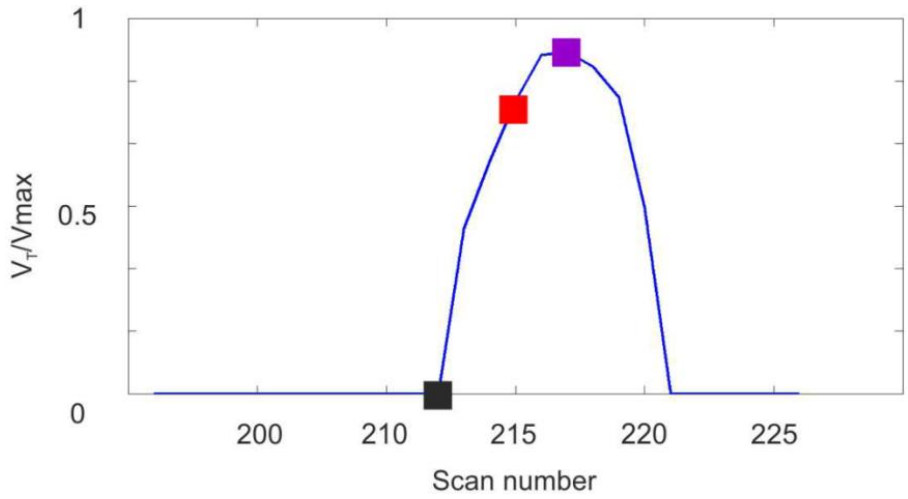

Fig. 3.25. Velocity profile measured with the OFI sensor. Normalized velocity represented by color squares are extracted from the spectrums in Fig. 3.23.

The complete 2D aorta scan and the comparison with the raw image is presented in Fig. 3.26. From the OFI sensor image, the aorta is clearly visible and the fluid velocity distribution can be analyzed. High speed flow (between 0.7 and 1 normalized speed) is observed on 300 µm in the middle of the aorta. Near aorta walls, velocity decreases drastically due to the absence of particles. The OFI sensor can provide with high precision the localization of the aorta outer bounds.

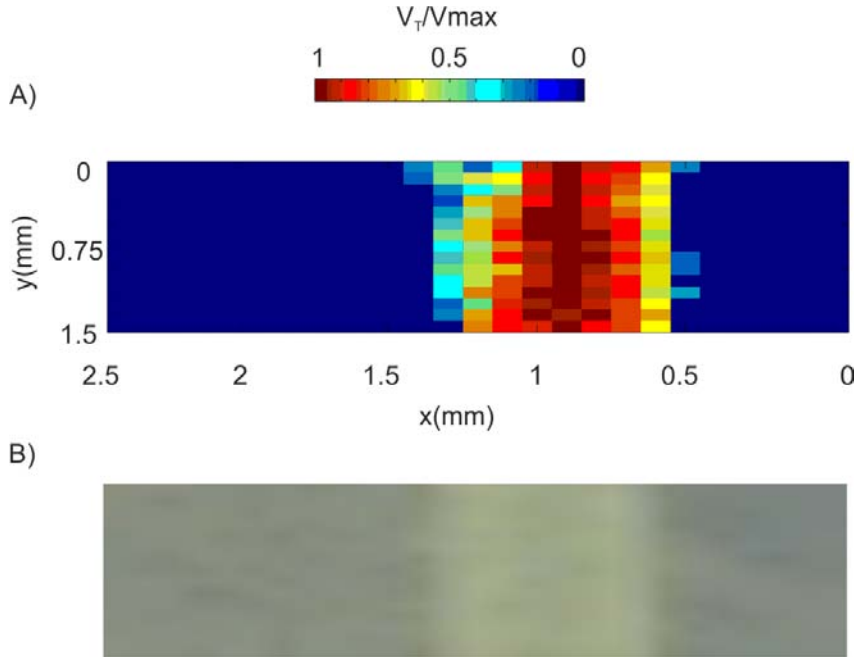

Fig. 3.26. Rat aorta imaging: A) 2D rat aorta fluid velocity imaging obtained by OFI and B) Raw image of the scanning zone captured by the camera.

3.3 Non-steady flow assessment

Most OFI flowmeters reported so far were tested for the assessment of steady and laminar flows [Campagnolo, 2013a; Kliese, 2010; Nikolić, 2013]. However, extending their possible implementation in the analysis of non-steady flows is still to be demonstrated.

In this section, we propose an OFI sensor for the interrogation of unsteady flows. We propose an *in-situ* calculation of a quantitative parameter allowing to easily evaluating the periodicity of non-steady flows without associated post-processing and with straightforward calibration. This approach is targeted to interrogate closed liquid-filled circuits during operation and it is also directly linked to the possibility of characterizing flows even if the technical features of the pumping device are unknown [Ramírez-Miquet, 2015; Perchoux, 2016].

3.3.1 Signal processing

The parameter calculated in this application is the zero order moment of the subtraction of the spectrum of two different measurements. It can be expressed as:

$$M_f = \sum_{f_{min}=0}^{f_{max}=F_s/2} \left| OFI_{flow} - OFI_{no\ flow} \right| \tag{3.3}$$

The quantitative value M_f is thus calculated in a continuous manner by subtracting the above-mentioned spectrums as represented in Fig. 3.27. The calculation of $OFI_{no\ flow}$ consists on a calibration step accounting for the local inherent noise added to OFI signals during a measurement.

In order to provide a reliable reference we performed three acquisitions at different times, thus allowing to discard isolated noise conditions. To further increase the repeatability of calibration step, this spectrum is smoothed with a Savitzky-Golay filter. The filter is dimensioned to preserve the main spectral features while reducing the spikes denoting noise conditions.

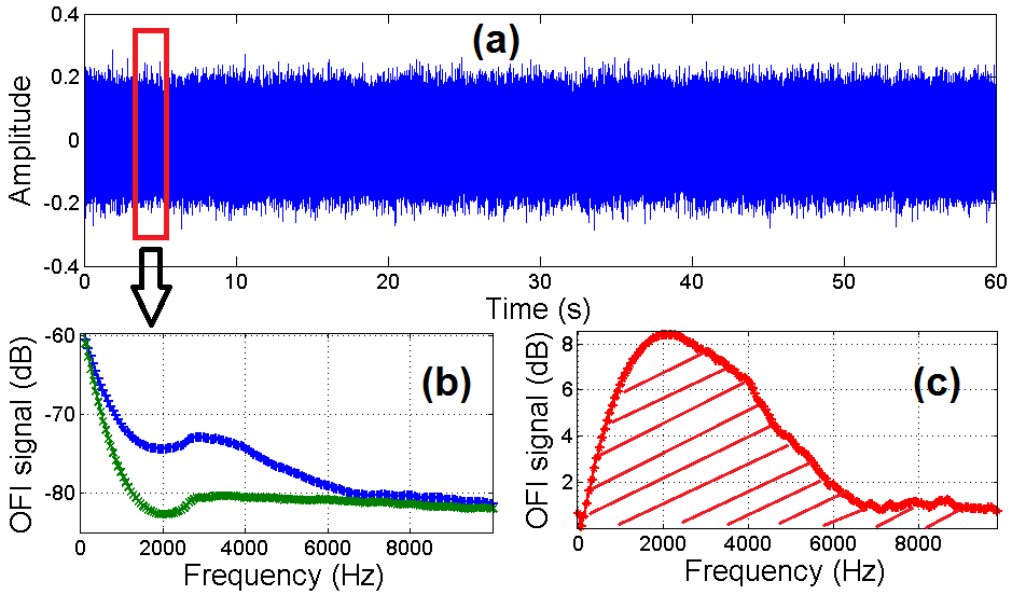

Fig. 3.27. (a) Overview of proposed method performing over a continuously acquired time domain OFI signal. (b) Spectrums of OFI_{flow} (blue) and $OFI_{no\ flow}$ (green). (c) absolute difference of spectrums.

The calculation of OFI_{flow} can be established as a set of FFTs of predefined size calculated along the signal acquired at a given sampling rate. For example, for 40960 samples acquired at 500 kHz (corresponding to around 82 ms), ten windows of 4096 samples are averaged, thus producing one M_f outcome. According to the noise conditions in a setup, performing an averaging of a set of FFTs reduces the influence of the extraneous noise. However, this trade-off between calculation time and noise reduction needs to be considered while attempting on-site calculation.

The flow speed induces a Doppler shift that is contained in a close range of frequencies. It is convenient to truncate a representative bandwidth from the spectrum to reduce computation resources. Cut-off frequency limits can be determined by inspecting the power spectral densities acquired for a minimum and maximum flow rate of a particular application. (e.g. for the experiment described in following section, we selected f_{min}= 100 Hz and f_{max}=50 kHz).

3.3.2 Real time implementation

The proposed method can be performed by a processing hardware as represented in Fig. 3.28. From the basic OFI configuration, an analog signal containing the information relative to the particle's flow speed is digitized with an analog-to-digital converter (ADC) and fed within a circular buffer to the processing hardware. The FFT calculation plus the spectrum truncation operation provide then a continuous M_f calculation. Referring back to the temporal OFI signal represented in Fig. 3.27(a), M_f is performed by block segments. The compromise between block size (N) and the acquisition sampling rate establishes the frequency

bin resolution (F_{bin}) as $F_{bin} = F_s/N$, thus imposing a hard real-time constraint to be inferior to $1/F_{bin}$.

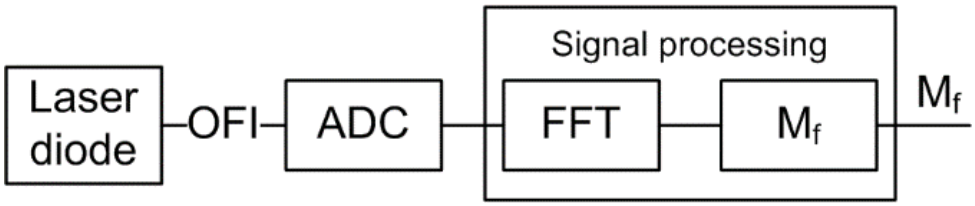

Fig. 3.28. Block diagram of the proposed real-time system's implementation.

3.3.3 Experimental setup

The optical setup is shown in Fig. 3.29. It consists on a laser diode (Thorlabs L785P090) emitting at 785 nm and driven by an injection current of 60 mA. The laser is coupled to a single lens of 8 mm focal length and the collimated radiation is pointed to a transparent tube with an angle of 80° between the optical and flow direction axes. With this configuration we found an optimal signal to noise ratio (SNR) in the spectrum. For the fluid, we tested a dilution of full cream milk (20.2 % w/w) in water.

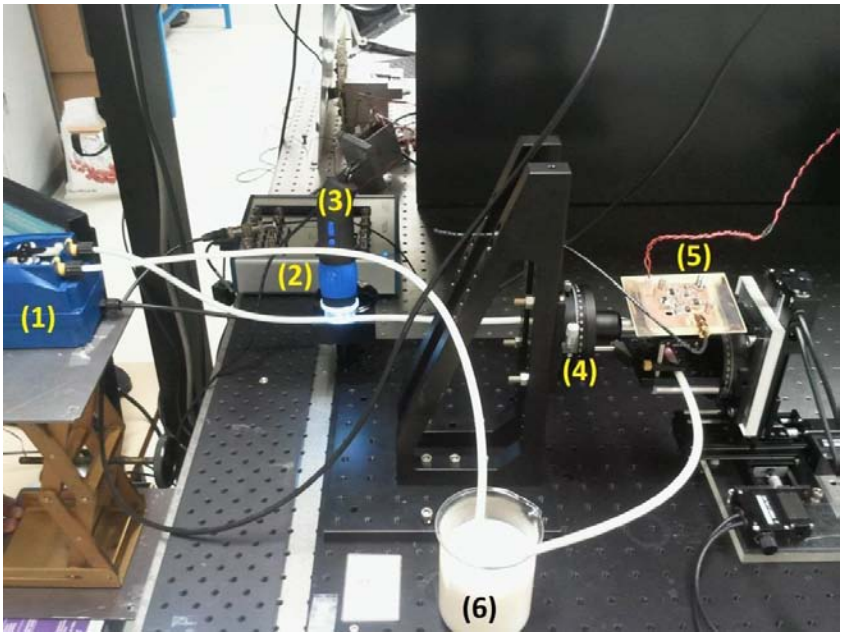

Fig. 3.29. Experimental setup: (1) peristaltic pump, (2) acquisition card, (3) camera, (4) goniometer, (5) laser and associated electronics, (6) fluid.

A two-squeezer peristaltic pump (Seko PR1) designed for warewashing in catering industry was used during the experiments. It includes an analog potentiometer with drawn marks to regulate the flow rate. The pump flow rate has been previously characterized to obtain a counter measurement for the experiment. During 1 min we measured the volume of fluid drained by the pump in a beaker for every position of the potentiometer. A USB camera is used to trail a single fluid bubble while one of the pressing part of the pump is squeezing the

tube to force the flowing. A simple processing of a sequence of images allowed the determination of the distance (S) traveled by the milk in the intermittent flow regime, which yielded 34.2 mm as shown in Fig. 3.30.

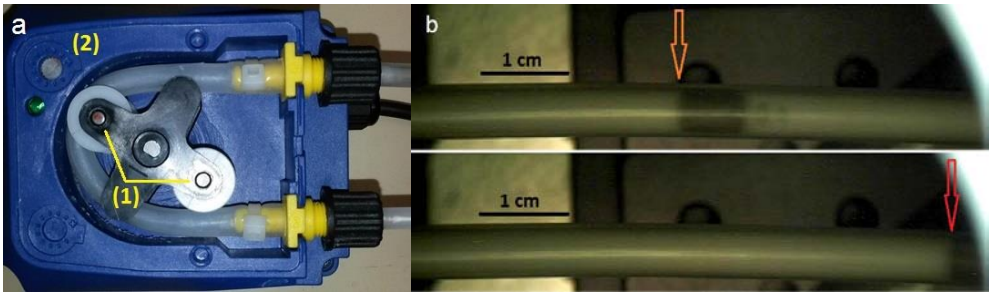

Fig. 3.30. a) Peristaltic pump generating unsteady flows; (1) Pump squeezers; (2) Potentiometer. b) Procedure to determine a counter measurement for fluid's displacement.

3.3.4 Unsteady flows interrogation

As a first step, we assess the flows using post-processing in order to have a comparative reference. Then, we performed the real-time analysis. The analysis of signals acquired during 1 min to reconstruct the periodicity of the pump is shown in Fig. 3.31 to 3.34. Four plots of M_f vs. time are represented, corresponding to four flow rates, from the minimum value in the potentiometer to higher values. It can be observed how the changes in the pump rate lead to an increment of the periodicity. Let us highlight the fact that this period-reconstruction algorithm allows to observe those instants where the non-steady regime produces a rapid suction and the flow is pulled back, as confirmed by the spikes in the vicinity of the minimal values in the figure.

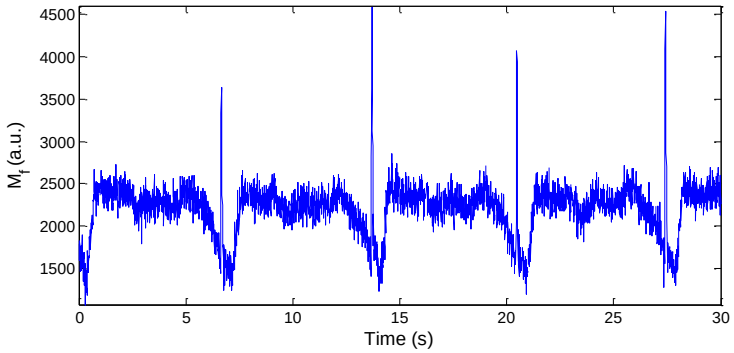

Fig. 3.31. Parameter M_f vs. time. Position of the potentiometer is 1.

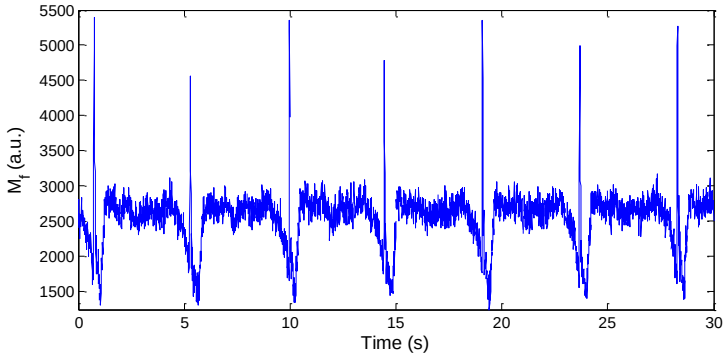

Fig. 3.32. Parameter M_f vs. time.: Position of the potentiometer is 4.

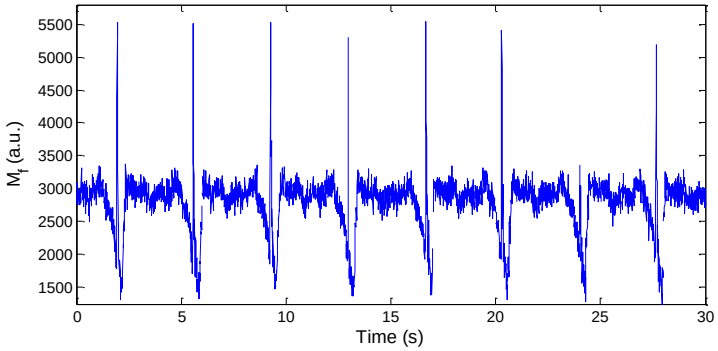

Fig. 3.33. Parameter M_f vs. time. Position of the potentiometer is 6.

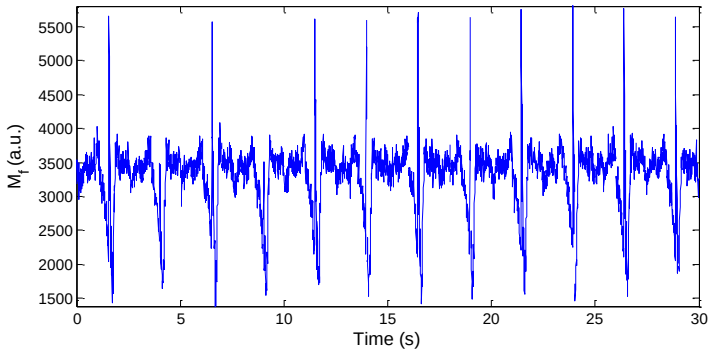

Fig. 3.34. Parameter M_f vs. time. Position of the potentiometer is 8.

Using the reconstruction of the periodicity of the pump, we proceeded to validate the linear relation between flow rate and parameter M_f. These last values were averaged in the intervals where the pressing squeezers were forcing the fluid to flow. Fig. 3.35 shows the errorbars of flow rate vs. M_f determined by the two methods for eight positions of the pump's potentiometer, depicting a good agreement of both measurements. A fitting of these experimental values shows a linear regression, the M_f axis crossing the 0 value for a flow of -7.76 ml/min, which is consistent with previous reports where this linear regression was also obtained [Campagnolo, 2013a; Norgia, 2010], and correlation coefficient R^2=0.99.

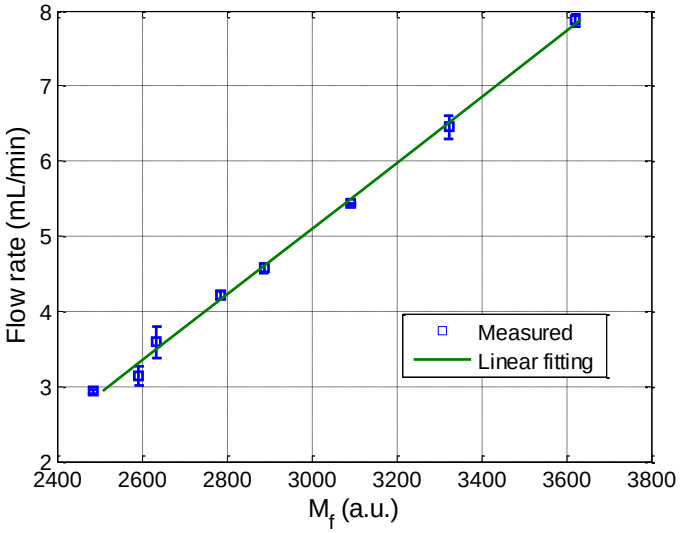

Fig. 3.35. Linear relationship of flow rate and parameter M_f.

For the real-time validation, the algorithm has been implemented in Matlab® using the data acquisition toolbox. We have relaxed the real-time constraint by averaging an increased number of FFTs and thus increasing the acquisition time before a new arrival of samples. Thus, the experimental imposed constraint of 8.19 ms (for Fs=500 kHz and N=4096 points) has been extended to 81.92 ms by averaging 10 FFTs for each point. As can be appreciated in the developed front panel of the instrument (Fig. 3.36), the pump's period reconstruction agrees with the off-line characterization. The added value of this approach is the possibility to assess and interrogate fluidic systems independently of the scattering regime imposed by the number of scatterers in the flow.

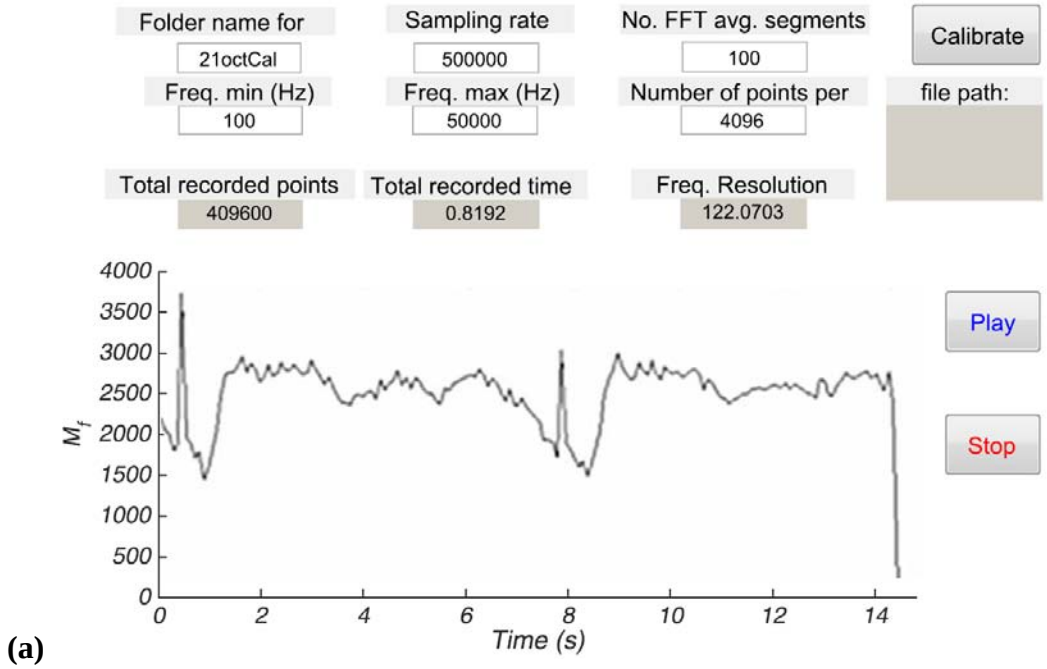

(a)

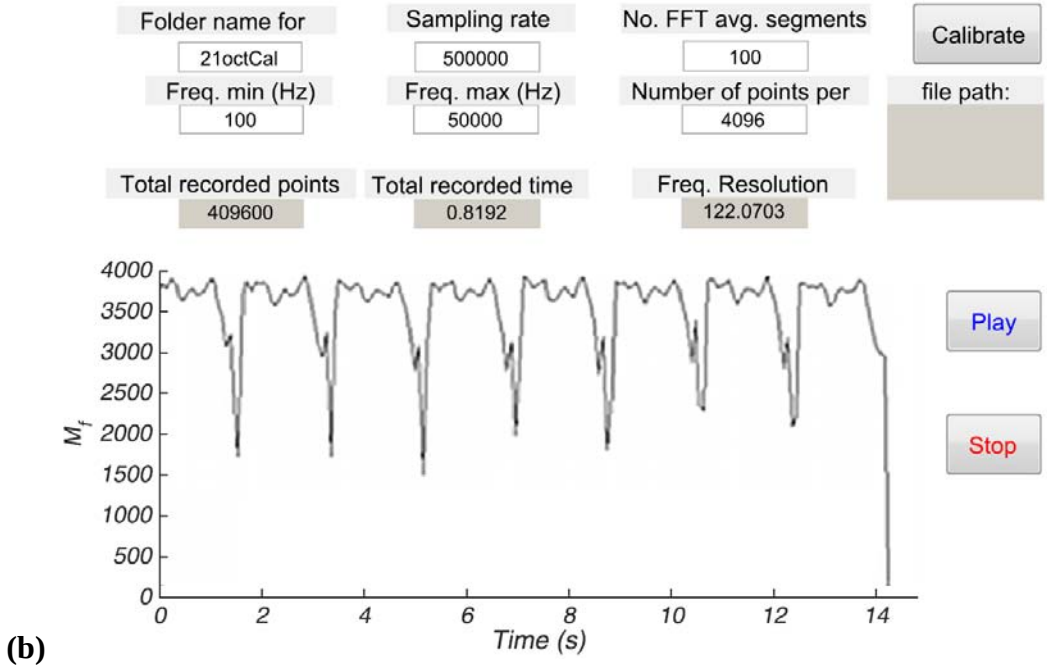

(b)

Fig. 3.36. Real time implementation for calculating the parameter M_f in time. Periodicity reconstruction for 1st and final position of the potentiometer.

3.3.5 Non-steady flow velocity measurement

The analysis presented in the previous sections is simple and can be applied whenever the geometry of the channel or the technical characteristics of the pump are unknown. For the purpose of flow interrogation it is sufficient to monitor the periodicity of the unsteady regime of the flow. This methodology can be applied

in either the scattering regime and the outcome of the calculations will enable an online assessment of the flow.

However, in most cases, the local velocity of the flow is a major interest. For the case of multiple scattering, the weighted momentum provides the quantitative information of the mean frequency to further determine the average velocity of a particular flow. Equation 3.1 is here used to re-process the data generated during the measurement performed and presented all over the present section.

The weighted momentum is calculated to extract the information of the kinetics of unsteady flows in the multiple scattering regime. Using the same optoelectronic configuration, the average velocity is determined in time for several positions of the pump's potentiometer.

Figures 3.37 and 3.38 show the time evolution of the average velocity for the two extreme position of the pump's potentiometer.

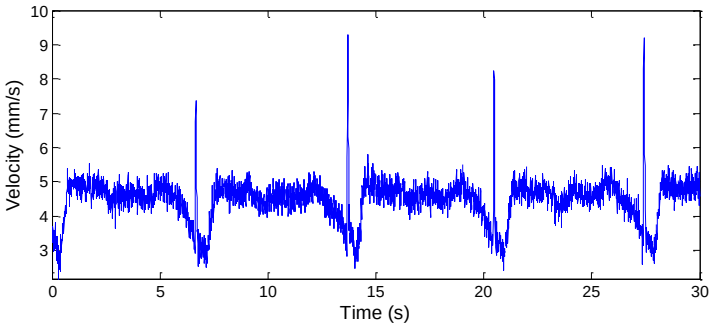

Fig. 3.37. Unsteady flow velocity measured during 30 seconds. Position of the potentiometer is 1.

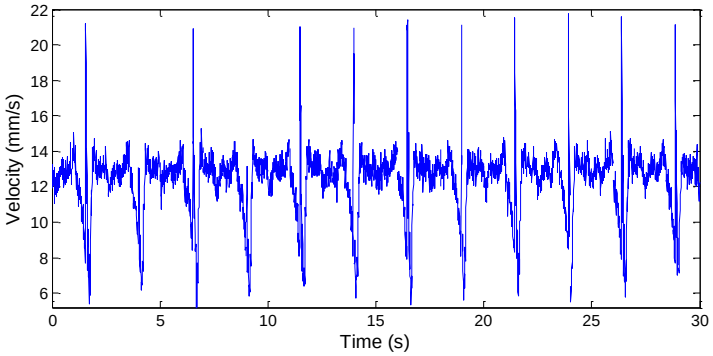

Fig. 3.38. Unsteady flow velocity measured during 30 seconds. Position of the potentiometer is 8.

As discussed throughout this chapter, the calculation of the average velocity of the fluid using Eq. 3.1 requires that the fluid has at least a number of particles corresponding to 4% concentration of full cream milk. If the concentration of scattering particles is lower than this quantity, then the only useful information that can be obtained is its periodicity.

3.4 Single particle characterization

In this section, a semi-automated method for particle detection in microfluidic devices is presented and demonstrated. Detection of single suspended particles in

a microchannel are a direct application of OFI sensing systems in the single scattering regime produced by the interaction of a laser beam with isolated particles.

We propose in what follows using the self-mixing signal in the laser to characterize the flowing particles in a microchannel. The objective behind the proposed methodology is the development of a new optical tool to the service of quality control in chemical, pharmaceutical and biomedical engineering that may be implemented for online inspection of fluids that should supposedly be free of particles, so this approach is not affected by the effect of feedback of several particles affecting the laser simultaneously. The OFI signal of the laser is used to trigger an online processing allowing the characterization of a particle flowing across the sensing volume.

3.4.1 Signal detection and processing

The detection mechanism is described as follows. Light emitted by a laser is focalized in a cylindrical transparent microchannel where a flow of water seeded with particles is pumped at a constant flow rate. The beam traverses the channel and the light scattering is produced as particles cross through the volume illuminated by the laser. A small portion of the scattered light propagates in the direction of the laser and enters inside it, so a modulation of laser power occurs which the photodiode detects as a burst of intensity.

A typical signal showing the perturbation in the laser due to the optical feedback produced by a particle crossing the sensing volume is represented in Fig. 3.39. As a result of the perturbation, the signal is modulated in amplitude.

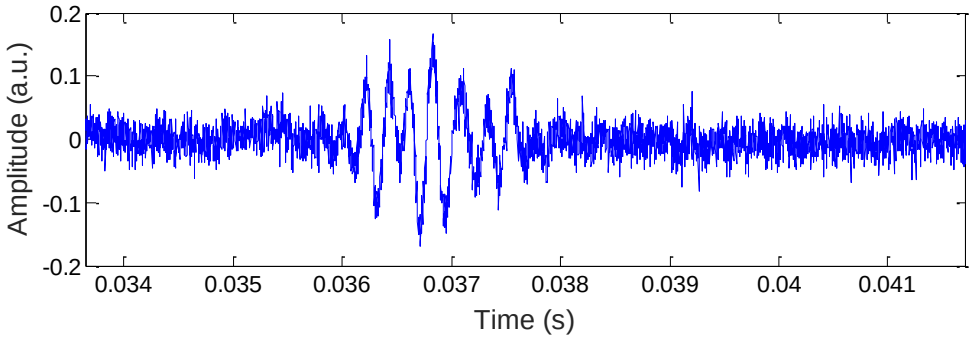

Fig. 3.39. Optical feedback signal showing the characteristic noise of the signal and the burst produced by a particle while it passes through the sensing volume.

The detection mechanism sets a pre-defined threshold empirically determined from a simple inspection of the segments of the raw signal without modulation due to the particles. Thereby, once the threshold condition is achieved, the system triggers the signal analysis to obtain information enabling the characterization of the burst.

The signal burst shows a modulation of the laser where fringes can be easily identified. A Hilbert transform is performed in the selected interval, normalized

by –10 π to 10 π, which allows a robust and automated detection of fringes as depicted in Fig. 3.40 [Arriaga, 2014b]. Fully developed fringes are used to determine the interval where the burst is confined.

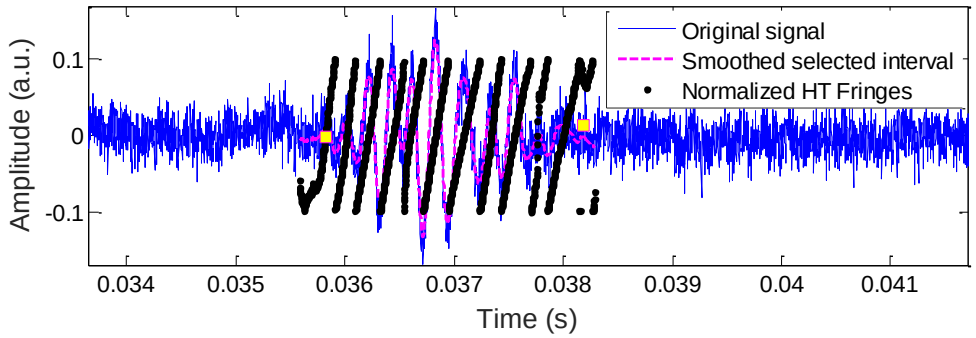

Fig. 3.40. Signal processed to confirm fringes in the burst. White squares indicate the selected beginning and the end of the burst. Hilbert transform representation is normalized by 10 π to fit the size of the amplitude.

An autocorrelation is processed on the signal and its power spectral density (PSD) is calculated from its fast Fourier transform. The PSD exhibits a maximum that is correlated to the velocity of the particle, and that may be used to determine the particle's location if the geometry/flow profile in the channel is known. Fig. 3.41 shows the power spectrums corresponding to the segment of the burst in between the two squares depicted in Fig. 3.40 and to its autocorrelation.

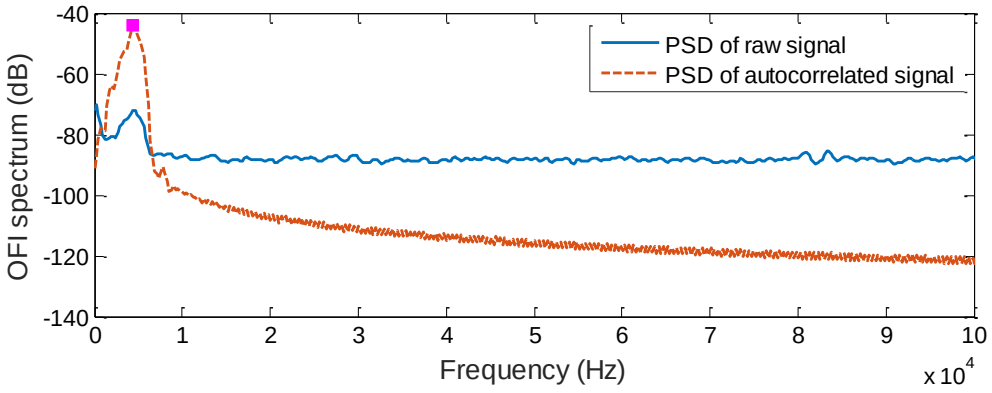

Fig. 3.41. Signal spectrum calculated from the fast Fourier transform of the raw signal and of the autocorrelation of the signal. Both maximums hold the same Doppler frequency. The square marker represents the maximum location in the power spectral density of autocorrelation.

Using the frequency corresponding to the maximum in the spectrum the velocity of the particle can be easily determined using the expression 1.9.

3.4.2 Particles, flow channel and experiment

Three different microparticles are used in this experimental work: iM30K and S22 glass particles from 3M^{TM} and PS-R-4.9 from Microparticles GmbH. Particle's sizes are available from the manufacturer's websites and were selected for their perfect spherical shape and their mass density allowing uniform suspension in the

fluid. According to the provided data, iM30K particles have 26.6 µm in diameter, S22 have 75 µm and finally, PS-R-4.9 have 4.89±0.08 µm.

The setup used in these experiments is similar to the experimental arrangement presented in section 3.1.2. The cylindrical PDMS channel described in previous section 3.1.3 was used as the microfluidic device and particles were detected as they passed through the laser illumination volume that crosses the channel through its center.

100 mL of demineralized water are prepared and 0.001 % by mass of particles of each kind are suspended in the water. Every suspension is prepared with one type of particles at the time. A flow-controlled syringe pump (Harvard Apparatus Pico 11 Plus) is used to introduce the flow with particles in the channel.

Diluted suspended particles are pumped inside the microfluidic cylindrical channel at 20 µL/min. For this flow rate, the analytical flow profile can be easily determined with the simple expression for Poiseuille presented in equation 3.2.

3.4.3 Theoretical sensing volume

The sensing volume is considered in first approximation as the illuminated region. This one is estimated through a simulation of the beam propagation through the lens and the PDMS material in Zemax®. The simulated beam distribution inside the 320 µm channel is represented in Fig. 3.42.

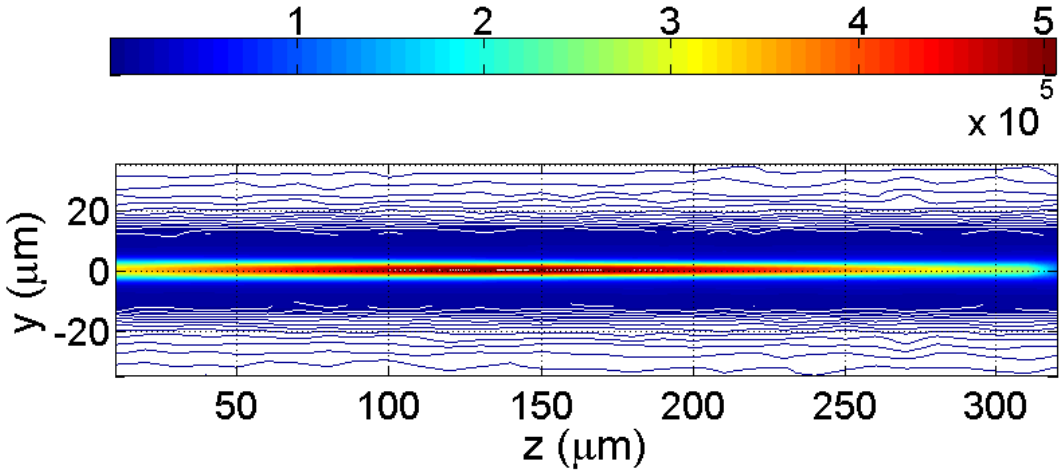

Fig. 3.42. Simulated beam propagating through the channel. The microfluidic channel diameter is represented in *z* direction, and the laser beam diameter is represented in *y* direction. Intensity scale is given in arbitrary units.

Simulated results yielded a beam diameter in the sensing volume of 20.89 µm following the $1/e^2$ criterion.

3.4.4 Detected particles

Measurements were performed with different suspended particles over 10 minutes. During this time, 27 particles iM30K, 10 particles S22 and 11 particles PS-R-4.9 were detected.

According to the frequency estimation of the Doppler peak for each detected burst, and based on the flow profile calculation, the location of those particles is represented in Fig. 3.43.

As can be observed in this figure, particles move at different velocities depending in their position in the channel.

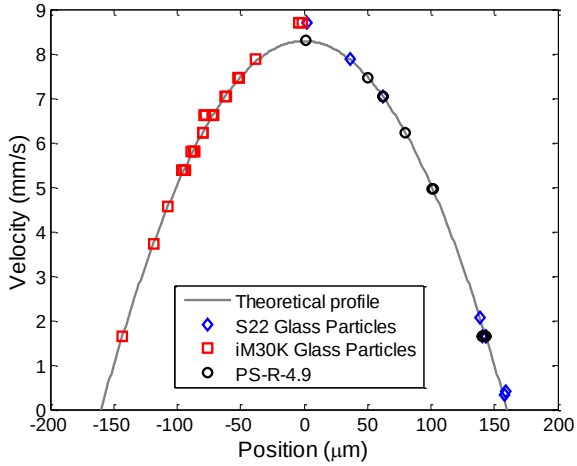

Fig. 3.43. Particles localization inside the microchannel. Position are given with respect to the center of the channel. Theoretical profile is calculated from the flow rate and the cross-section of the cylindrical channel.

In order to ensure the validity of the detection, the burst width measured is compared to the expected burst time (taking into account the particle velocity and the beam diameter). Results are displayed in Fig. 3.44 and they evidence fairly good agreement between the calculated and the expected burst time

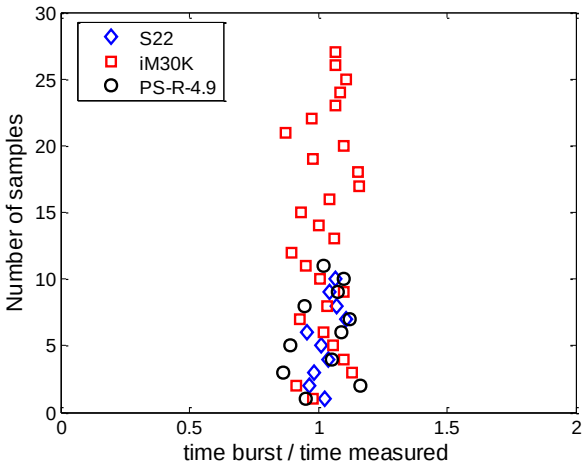

Fig. 3.44. Validation of the burst detection by comparison of the expected and measured burst time.

The results presented in this section are the first obtained of the work on single particle detection and characterization in microfluidic devices. This work is currently part of the research activities being developed by our group at LAAS-CNRS in the frame of the potential applications of optical feedback interferometry.

3.5 Conclusions

Throughout this chapter, we have performed an extensive analysis of the reliability of the optical feedback interferometry sensing technique. The experimental demonstrations show that OFI can be applied with reasonable accuracy to fluid flow sensing. The processing method based upon the weighted moment allows the quantification of the Doppler frequency shift as long as the concentration of scatterers equivalent to at least 4 % of full-cream milk is used. For highly diluted fluids, the cutoff frequency method may be a viable solution, but it is recommended that a calibration of the system is performed to find the proper cutoff level in the signals spectrum. We have demonstrated the potential used of optical feedback interferometry for the interrogation of fluid flows, the measurement of velocity profiles at the microscale and ex-vivo flow mapping in the single scattering regime.

An OFI real time system was presented to interrogate unsteady flows. This system allows reconstructing the periodicity of the flow, which may be applied independently of the number of scattering particles merged in the fluid. In addition, the proposed methodology enables to obtain information of non-steady flows even if the pumping device features are unknown.

In the previous section, we presented an OFI sensor allowing the detection of single particles in microfluidic devices. The system on which this sensor is based, enables the processing of a signal burst that is caused by the particles crossing the volume illuminated by the laser. In this way, we processed the burst to obtain the Doppler frequency shift that is related to the particle's velocity. Once this velocity is calculated, it is possible to locate the particle in a flow profile. The results presented are part of the ongoing research on particle detection and characterization in microfluidic devices. Future work will be focused on automatizing the processing method and extending the methodology to discriminate particles by size.

Chapter 4

Application of optical feedback interferometry to the analysis of multiphase flows

4.1 General context

Multiphase flows refer to flows carrying matter in different states. As per definition, these flows are not restricted to a combination of substances comprising different states of matter, so they are found in both gas-liquid solutions and in liquid-liquid solutions [Brennen, 2005]. For the latter, it is understood that the liquids hold different hydrodynamic properties.

Multiphase flows are present everywhere. The most obvious cases are seen every day in clouds, snow and smoke, but also in food products of daily consumption such as mayonnaise and salad dressing. Likewise, in water supply in domestic services and in some type of drinking water, bubbly and sparkling flows are notable. As early as 1950, it was found that adding up to 12 % of air into domestic water would allow saving billions of liters of water a year, and would make the water supply equally efficient, especially for cleaning purposes. Two-phase flows intervene in multiple chemical and biochemical processes including mixing, diffusion, cavitation and synthesis [Rudyak, 2014; Gordon, 2014; Rooze, 2012]. Still, multiphase flows are not limited to only two-phase flows. The oil extraction

industry deals continuously with water, oil and gas in pipes transporting the organic material [Taitel, 1995]. Three-phase flows have been subject of study since many years, in both large scale and microscale engineering [Vinegar, 1987; Oddie, 2003; Yue, 2014]. Also, solutions of detergent, soap and other foam-forming substances are good examples of multiphase flows present in daily life.

Microfluidics continues to be an active area in research, covering a wide range of applications in chemical, biological and medical engineering. The characterization of fluid flows in microchannels has been particularly interesting for the scientific community dedicated to microreactor technology. In this regard, the measurement of physical parameters related to motion is still of great interest for the interrogation of fluids at the micro-scale, with consequent impact on quality control of industrial processes and on diagnostic purposes in biomedical field. Additionally, microfluidics offers a complete platform to control and assess chemical and biomedical processes that are too complex to be addressed at larger scales. Typical microscale devices allow for flow assessment in laminar regime, where experimentation and processes can be controlled. Moreover, interactions between two laminar fluids at the microscale can be easily monitored and interrogated. Just to mention a simple example, oil and water behave different in large scale reservoir as compared to small pipes. These fluids are immiscible, and normally at the macroscale oil floats in water due to its lower density. However, when confined in a microchannel of a microfluidic chemical reactor, an oil-water interface is created with such a surface tension that it remains vertical and fluids develop parallel rather than stratified, where the gravity effect is not predominant. So, using microfluidic chips to study immiscible fluids interactions is a suitable tool for an easy inspection of motion related parameters in the hydrodynamics of particular liquid-liquid interaction.

The configuration where two immiscible substances are flowing in the same microchannel is subject of much current research [Raimondi, 2014]. In this regard, the formation of droplets in microfluidic devices and the hydrodynamics of slug flows have received extensive attention [Kashid, 2008]. In particular, the scientific community devoted to microreactor engineering has projected great efforts towards the study the dynamics of two phase liquid-liquid interactions. The gold standard to characterize the interaction of two liquid flows at the microscale is the analysis of flow patterns, but still there remains a large variety of liquid-liquid interactions to be properly characterized [Foroughi, 2011].

To understand the liquid-liquid interactions (two-phase flow structure, mixing, mass transfer, etc.), hydrodynamics parameters have to be determined. However, measuring velocities in small dimension channels with acceptable accuracy is challenging. Particle Image Velocimetry and Laser Doppler Velocimetry (LDV) are currently used to measure velocity fields in large scale pipes [Kumara, 2010]. At present, the conventional technique to measure velocity fields at the microscale

is the Micro Particle Image Velocimetry (μ-PIV). However, currently available μ-PIV systems in their minimal configuration [Wereley, 2010] include a bulky high-power pulsed Nd:YAG laser, a fast acquisition camera and a microscope system. The tracers in the fluid have to be fluorescent particles. The optical arrangement in μ-PIV requires that the vision field of the camera and the laser focus to be in perfect correspondence and then implies a robust and precise alignment of all the opto-mechanical assembly. Thus, μ-PIV are then heavy and expensive systems. PIV requires the use of heavy equipment as a laser and a microscope that are needed for flow quantification. In addition, is expensive and necessitates advanced post-processing of images generated as flows are visualized. On the other hand, LDV uses an interferometer with several optical components that make its assembly unpractical for microchannel flow measurements. Imaging systems are largely used in the study of multiphase flows. They allow tracking and following the hydrodynamic system behavior under many possible configurations. However, the assessment is usually subjective as a single-side view of the channel is typically used. Imaging systems such as PIV and dual-slit have been used as a powerful tool in assessing and quantifying flow behavior and interactions. In a recent paper [Campagnolo, 2012], OFI technique was compared to dual slit and both techniques successfully experimentally reproduced the flow profile of a laminar flow in a rectangular microchannel. We will use the optical visualization as a reference tool to confirm our experimental results obtained with OFI in this chapter.

In previous chapters we have proven how Optical Feedback Interferometry (OFI) can be used as a sensing method for velocity measurements. In addition, OFI sensors for flows assessment were presented for those cases when the channel contained only one fluid [Campagnolo, 2013a; Lim, 2010; Norgia, 2016]. However, OFI's possible implementation in the analysis of multiphase flows is still to be demonstrated. In this chapter we intend to fill the gap in the utilization if OFI for the study of multiphase parallel liquid-liquid flows.

Pohar *et al*. [2012] demonstrated that when two parallel immiscible fluids interact in a microchannel, they occupy a fraction of volume that depends directly on their viscosity and the volume filled by every fluid is defined by the interface between the flows. In the case of parallel oil-water flows, each phase develops its own velocity profile and the interface can be displaced by changing the flow rate at the inlets. The demonstration of the effect of viscosity on the hydrodynamics of parallel flows relies on a visualization of the transparent channel, thus the information provided by images is sufficient to determine the volume occupied by each fluid in the channel.

As a first approach, we drove our attention towards velocity measurements of oil-water parallel flows in a Y-shaped microreactor and tested the OFI sensing technique as a tool to characterize two-phase parallel flows and to estimate the

location of the interface separating immiscible fluids in a microchannel. Parallel flows are the simplest case of liquid-liquid immiscible interactions. In this chapter, we will demonstrate the potential of OFI in the analysis of oil-water flows departing from a characterization of motion-related parameters allowing velocity profiles measurements. Since velocity is related to flow distribution, it can be used as a parameter to estimate and localize the interface of oil-water immiscible flows in a microchannel. We present experimental results of velocity profile measurements and explore the impact of changes in the water flow rate. Indeed the latter provides valuable quantitative information on the spatial repartition of the fluids. In addition, we use the OFI sensing scheme to interrogate the flow profiles while maintaining constant the ratio of flow rates imposed at the inlets. Under such conditions, the interface position is expected to remain unchanged.

Experimentally obtained velocity profiles can be fitted to a theoretical approximation considering oil and water as viscous fluids. In this approximation, the interaction of both immiscible fluids is characterized by the influence of a pressure gradient and viscosity in the kinetics of each parallel flow. As a consequence, a theoretical model that considers oil and water as viscous fluids is proposed to describe the the possible influence of one phase on the other. It is based on the Couette flows approximation and is compared to the experimental results.

4.2 Theoretical model of parallel liquid-liquid flows

As mentioned in the previous section of this chapter, the hydrodynamics of two immiscible fluids in a microchannel can be described by modeling the possible influence of one fluid on the other. As both fluids move under a pressure gradient, the kinetics is influenced by the pressure drop imposed by the pumps at the inlets. In such a case, fluids occupy a portion of volume in the channel that is highly dependent on the intrinsic properties of the fluids, particularly their viscosity.

In an attempt to address the influence of one liquid on the other and the role of the interface separating them, we first present a basic theory on the type of flows considered in the theoretical approach presented in this section. Thereby, we introduce the concept of Couette flows and its suitability to describe the oil-water system hydrodynamics.

Couette flows are considered as confined fluids into two parallel plates subject to the relative movement of one of the plates respect to the other. In such a case, the velocity of the flow in one of its spatial boundaries is different from zero. Figure 4.1 present a schematic representation of the situation that will help understand the general concept. If a fluid at rest is pushed by the action of one of the wall that confined it, then a dragging effect will affect the velocity distribution of the flow with a maximum velocity in the moving plate.

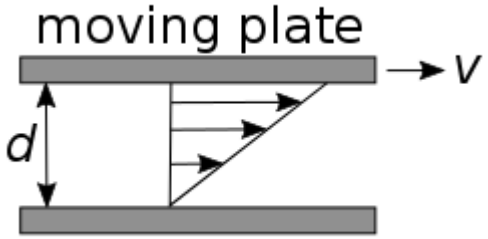

Fig. 4.1. Representation of Couette flows. The plate induces the velocity distribution of the fluid as it moves with velocity *v*. The velocity distribution is represented by the arrows in between the two plates.

A more general case is given when in addition to the situation explained in Fig. 4.1 the flow is subject to a pressure gradient. The new situation there implies that the velocity distribution is now dependent on several conditions and that the maximum velocity may be in the moving plat or not. Figure 4.2 shows a simplified representation of a fluid flow directly affected by a pressure drop and the movement of one of the plates confining it.

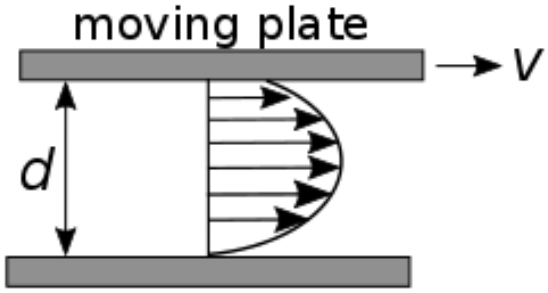

Fig. 4.2. Representation of Couette flows under a pressure gradient. The moving plat induces a non-null velocity of the fluid at the boundary. Arrows represent the flow distribution.

We propose to describe the interactions occurring between oil and water when flowing in parallel flow by considering that each fluid can be modeled as a laminar viscous flow [Langlois, 2014]. Parallel immiscible liquid-liquid flows pumped by a flow-controlled device, would follow the model represented in Fig. 4.2. Due to the immiscibility, the interaction of those fluids generates an interface that acts as one of the plates. In the theoretical flow approximation, the model considers two Couette flows under a pressure gradient along a conduct. If, there the interface behaves as a wall, then the non-slip condition is used for both confined flows. If, on the contrary, there is slipping at the interface, then the fluids behave following a combination of the situations represented in Figures 4.2 and 4.3.

Let’s consider that each fluid can be described as a laminar viscous Couette flow. In this case, the Navier-Stokes equations can be reduced to the following equation [Wilkes, 2006]

$$\frac{\mathrm{d}^2 v}{\mathrm{d}x^2} = \frac{1}{\eta}\frac{\mathrm{d}P}{\mathrm{d}y} \tag{4.1}$$

where v is the axial velocity component of the fluid, $\frac{\mathrm{d}P}{\mathrm{d}y}$ is the pressure gradient parallel to the walls and to the interface and η is the viscosity of the fluid.

The liquid-liquid interaction of immiscible flows was studied here experimentally for oil and water. Let's consider the schema represented in Fig. 4.3, denoting liquid 1 as water and liquid 2 as oil. The microchannel of width $w = l_2 + l_1$ contains both immiscible fluids and the interface between them is located at a transverse position *x=0* along the channel. Considering a constant pressure gradient, solving Equation 4.1 for each phase leads to the following formulation for water and oil respectively:

$$\frac{\mathrm{d}^2 v_1}{\mathrm{d}x^2} = \frac{1}{\eta_1}\frac{\mathrm{d}P}{\mathrm{d}y} = A_1, \tag{4.2}$$

$$\frac{\mathrm{d}^2 v_2}{\mathrm{d}x^2} = \frac{1}{\eta_2}\frac{\mathrm{d}P}{\mathrm{d}y} = A_2. \tag{4.3}$$

Equations (4.2) and (4.3) lead to the following solutions:

$$v_1(x) = \frac{A_1 x^2}{2} + B_1 x + C_1 \tag{4.4}$$

$$v_2(x) = \frac{A_2 x^2}{2} + B_2 x + C_2 \tag{4.5}$$

where B_i, C_i are constants that are extracted by taking in consideration that both fluids comply with the no-slip condition in the walls. So, null velocity in the walls serve as boundary conditions leading to solutions of Equations 4.4 and 4.5. Considering the water-wall as $-l_1$ and the oil-wall as $l_2 = w - l_1$ the boundary conditions would be: $v_1(-l_1) = v_2(l_2) = 0$. The velocity distribution in the microchannel is then given by:

$$v_1(x) = \frac{A_1 x^2}{2} + \left[\frac{v_{i1}}{l_1} + \frac{A_1}{2} l_1\right] x + v_{i1} \qquad \text{for } -l_1 < x < 0 \tag{4.6}$$

$$v_2(x) = \frac{A_2 x^2}{2} - \left[\frac{v_{i2}}{l_2} + \frac{A_2}{2} l_2\right] x + v_{i2} \qquad \text{for } 0 < x < l_2 \tag{4.7}$$

where v_1 and v_2 are the axial velocities of water and oil at a given transverse location x respectively and v_{i1} and v_{i2} are the axial velocity component of water and oil at each side of the interface.

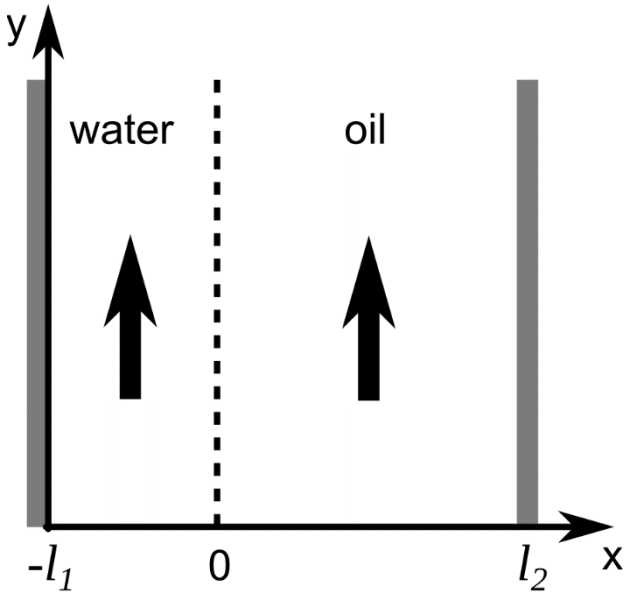

Fig. 4.3. Oil and water in a rectangular microchannel. The interface is represented at position *x=0.*

4.3 Experiments

The basic idea of experiments is to pump oil and water in a Y-shaped microreactor. Once both immiscible liquids are inside the channel, their interaction produces parallel flows characterized by a continuous interface defining the volume occupied by each fluid. Then, OFI is used as the sensing technique to obtain the velocity distribution over a scanned line in the channel containing oil and water.

4.3.1 Microfluidic chip

A custom made Y-shaped microreactor is built in SU8 over a glass substrate using optical lithography. Previously designed photo-masks are employed to create the lithographic geometries on the material. SU8 is a standard negative polymeric photoresist capable of being inert to almost every substance flowing inside it once polymerized. In many works dealing with microstructures it is used for building robust microdevices for chemical and biomedical applications [Nemani, 2013; Liu, 2004]. The optical properties of SU8 have been described elsewhere [Parida, 2009; Salazar-Miranda, 2010]. The constructed microreactor has a refractive index of 1.59 and null extinction coefficient.

The fabrication consists of building the microstructure in three progressive steps. The glass wafer (AF32) is chemically treated with sulfuric acid diluted 50 % with hydrogen peroxide. The glass wafer is rinsed and dried, then exposed to oxygenic plasma during 15 minutes at 1.5 mbar. A first layer of 5 µm of SU8 is deposed on the glass surface and mechanically turned to distribute the resist all over the glass and heated at 95 ºC during three minutes. Then, the material is exposed to UV radiation using the mask corresponding to this layer and developed during approximately 5 minutes until it polymerizes completely.

A second layer of SU8 (100 µm high) is added to the polymerized layer and the same procedure explained for the first layer is applied, this time using the appropriate mask with printed 300 µm wide grooves. The microgrooves avoid polymerization of a small part of the material that once developed becomes a channel.

Finally, a third layer (25 µm high) is prepared over a polyester layered wafer and aligned with the rest of the microstructure.

The final microreactor is presented in Fig. 4.4. The main channel is 11 mm long and the other two channels containing the inlets are 7 mm long. The angle between the inlets is 60º. All the channels in the microfluidic chip have a 100 µm x 300 µm rectangular cross section (aspect ratio $\alpha^* = h/w = 1/3$, where h represents the channel's height and w is the channel's width).

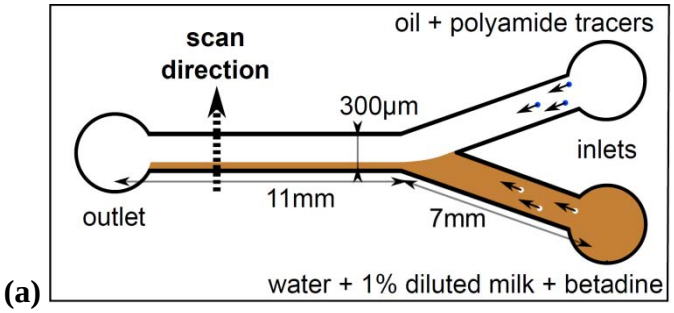

(a)

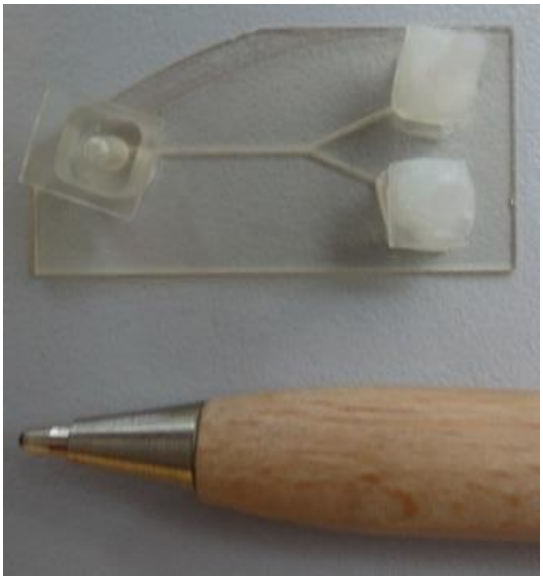

(b)

Fig. 4.4. (a) Simplified representation of the Y-shaped microreactor. (b) Real SU8 microrector.

4.3.2 Fluids

Oil (Polydimethylsiloxane, Sigma Aldrich 481939) and demineralized water are used. Oil's viscosity and density were determined experimentally to be 28 mPa·s and 0.982 g·cm^{-3} respectively at 25°C. Water's viscosity and density are 1 mPa·s

and 1 g·cm^{-3} respectively. A small concentration (0.4 % by mass) of 5 µm tracer polyamide particles (Dantec Dynamics 9080A3011) is merged in the oil which density is 1.02 g·cm^{-3} and 1% of full-cream milk (determined by mass) is embedded in the water. During the experiments a small percentage of betadine (0.2 % by mass) was added to water to enhance contrast between both liquids.

Oil and demineralized water are pumped using two independent flow rate-controlled pumps (Harvard Apparatus Syringe Pump 11 Pico Plus).

4.3.3 Signal processing

Time domain signals acquired from the internal photodiode are processed and the power spectral density (PSD) is calculated using the Welch's averaged periodogram method. To enhance the signal-to-noise ratio (SNR) and thus increase the reliability of the Doppler frequency calculation, the spectrum is calculated on the autocorrelation of the OFI signal. The autocorrelation is calculated and normalized so that it is equal to unity at zero lag. We found that the SNR in the PSD of autocorrelated signals is higher by 13 dB as compared to the PSD of raw signals.

Since the signal is related to the velocity vector of each particle in the flow, its frequency domain representation shows a distribution of power in the low frequency range. The low concentration of particles in the fluids induces a typical signal's spectrum with a frequency distribution corresponding to the single scattering regime with a plateau that ends at the maximum Doppler frequency. In the case of single scattering, it is then usually accepted to calculate the maximum velocity at the the maximum velocity from a cutoff frequency determined at a threshold of -3 dB below the plateau of the power spectrum [Campagnolo, 2012]. Because our signal's spectrum is calculated from the autocorrelation of the signal, then the maximum velocity is found at a cutoff frequency that corresponds to a thresold of -6 dB, which corresponds to the square of the standard threshold. Figure 4.5 depicts a power spectrum calculated from an OFI signal obtained during the calibration OFI setup.

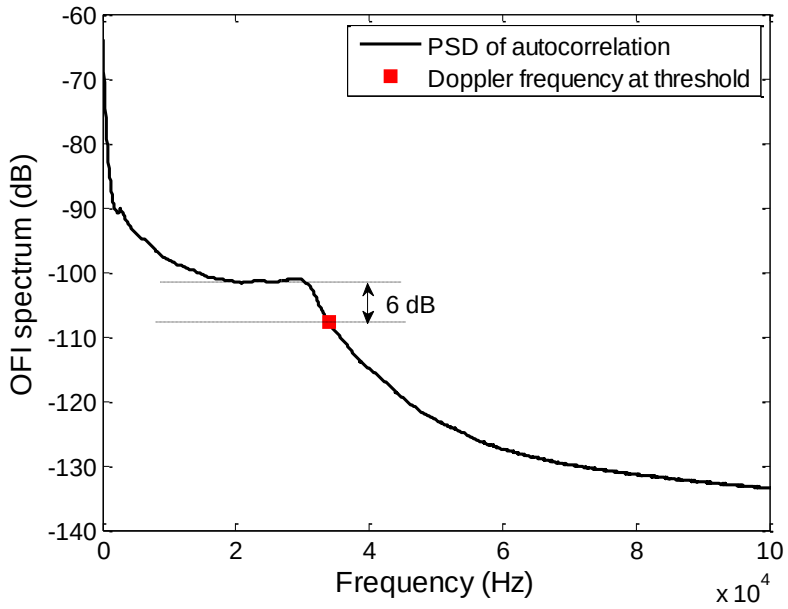

Fig. 4.5. Power spectrum of the autocorrelated OFI signal. The red square represents the cutoff frequency corresponding to the maximum velocity of the flow.

4.3.4 Optoelectronic configurations

The flows of both fluids are visualized using a Digital Microscope Camera (Oowl Tech Ltd., MZ 902). These images are used to determine the location of the interface by quantifying in terms of pixels the area occupied by oil and water using the upper view of the channel as a reference.

4.3.4.1 Single lens configuration

The simplest configuration of an optical feedback flowmeter implemented in microfluidics consists upon using a laser and its electronic circuitry (laser driver and transimpedance amplifier) coupled with a single lens. The electronic circuitry is presented in detail in Annex 1. This set-up was initially used in preliminary experiments performed to measure velocity of parallel oil-water flows at the microscale [Ramírez-Miquet., 2016a]. A simplified scheme of the set-up is shown in Fig. 4.6. Light emitted by a semiconductor laser (Thorlabs L785P090) lasing at 785 nm and driven by an injection current of 60 mA is focused with a single lens (Thorlabs C240TME-B, focal distance f = 8 mm) and pointed with an angle of 80º with respect to the propagation of the flow in the channel. The piece supporting the laser and the lens is connected to a 3D-stage computer-driven device that allows scanning the microchannel to reconstruct the velocity profile along the width of 300 µm. Using a single lens reduces the optical setup and system costs. However, due to the beam collimation, the sensing volume might be large enough to detect a signal in the very low frequency range even if the laser spot is pointing the channel wall.

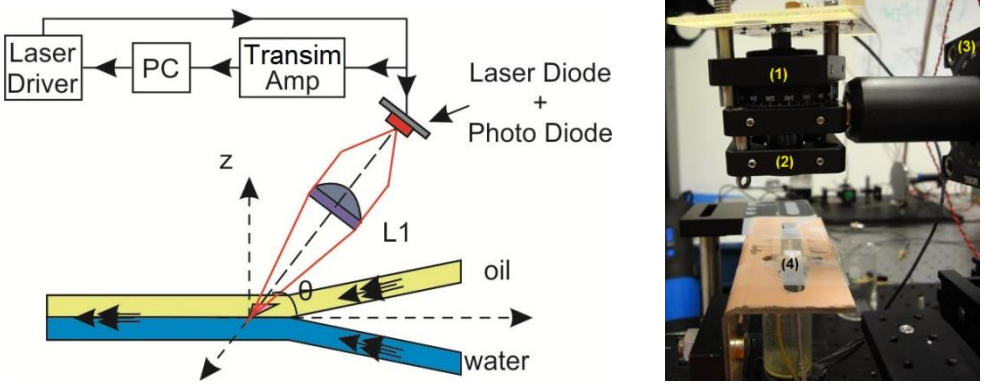

(a) (b)

Fig. 4.6. Simplified set-up configuration using single lens optics for optical feedback velocity measurement of parallel oil-water flows (a). Real set-up used during the measurements (b): (1) Laser, (2) Lens, (3) Goniometer and (4) SU8 Y-shaped microreactor.

4.3.4.2 Measured profile with single lens configuration

The velocity profile measured from the spectrum of the signals from the laser are represented in Fig. 4.7 and 4.8. The blue and green lines represented in Fig. 4.7(a) and 4.8(a) show plotted squares with errorbars and theoretical profiles fitted from equations 4.6 and 4.7 for water and oil respectively. Images in Fig. 4.6b and 4.7b are taken as a reference to plot the beginning and end of each fluid in the inner volume of the channel. Arrows indicate the direction and location of the scan performed to measure points separated by 10 µm each. Errorbars in the measured points correspond to three measurements performed in consecutive scans. The scanned line is at 5 mm from the junction in the Y-shaped microreactor.

The parameters of the fitting used in the theoretical curves depicted in the graphs are represented in Table 4.1.

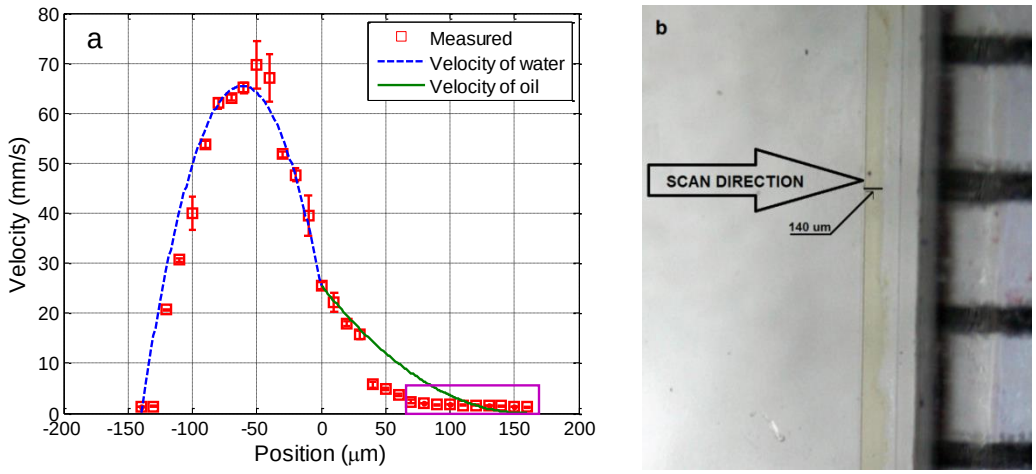

Fig. 4.7. Measured maximum velocity profile and theoretical fitting for water pumped at 35 µL/min and oil pumped at 1.5 µL/min (a). Reference image indicating the scan (b).

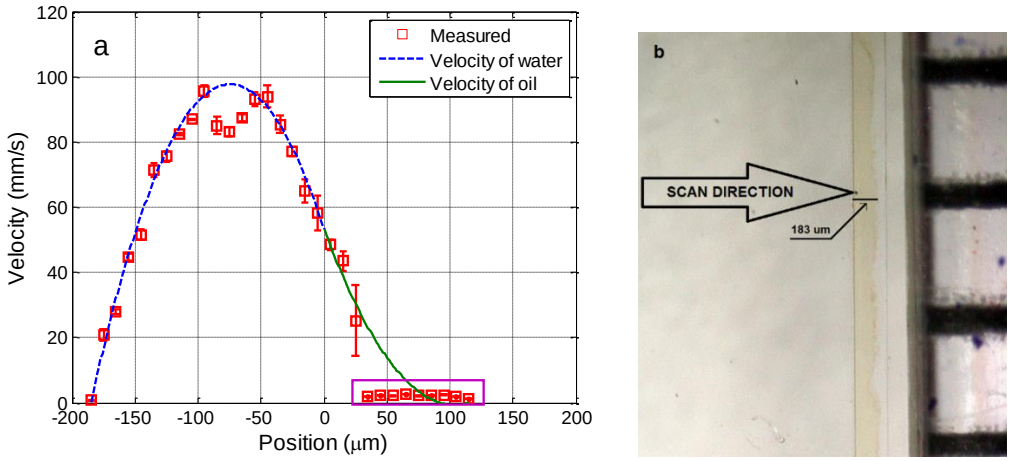

Fig. 4.8. Measured maximum velocity profile and theoretical fitting for water pumped at 65 μL/min and oil pumped at 1.5 μL/min (a). Reference image indicating the scan (b).

Table 4.1 Fitting parameters used in theoretical profiles plotted in Figs. 4.6 and 4.7				
Flow rate water	**Flow rate oil**	**A_1**	**A_2**	**v_i**
35 μL/min	1.5 μL/min	$-2.12 \cdot 10^7$ $m^{-1}s^{-1}$	$2.05 \cdot 10^6$ $m^{-1}s^{-1}$	25.54 mm/s
65 μL/min		$-1.60 \cdot 10^7$ $m^{-1}s^{-1}$	$1.02 \cdot 10^7$ $m^{-1}s^{-1}$	53.31 mm/s

From these preliminary measurements it can be concluded that OFI technique is sensitive enough to reconstruct a profile and measure locally the velocity of oil and water. However, only a few points were measured close to the interface in the oil side. Due to its higher viscosity, oil shows a much lower velocity as compared to water in the parallel flow. Consequently, a part of the profile on the oil side cannot be measured due to the lack of sensitivity of the sensor in the very low velocity range obtained with only 1.5 μL/min. The points marked in the purple squares represent those scan point where the sensor could not perform valid velocity measurements.

Also, the model fits fairly good with the experimental results. However, both fluids were pumped using a pressure gradient imposing higher pressure values at the inlets. Therefore, parameters A_1 and A_2 should be negative because flows move under a negative (or favorable) pressure gradient.

In addition, the measurements performed with only one lens made difficult the identification of one fluid from the other due to a relatively large sensing volume. The optoelectronic system was then modified to explore in detail other features of oil water flows interactions.

4.3.4.3 Dual-lens configuration

A slightly simple modification was made to the optoelectronic setup described in the previous section. A second lens (Thorlabs C240TME-B) was added and the same laser and associated circuitry was maintained as described in section 4.3.4.1. The new system is depicted in Fig. 4.9 and a real image is presented in the same figure. Lens L1 is positioned at its focal distance from the laser for collimation and lens L2 is used to focus the laser spot in the channel. The new laser spot is calculated to be around 10 µm.

Using the dual-lens configuration, we explored the capabilities of OFI for reconstruction of oil-water velocity profiles. The idea of modifying the original setup presented in section 4.3.4.1 is to obtain a smaller sensing volume to further being able to discern between one fluid and the other, and then estimate more accurately the localization of the interface. Many configurations of flow rates imposed at the inlets were tested, which will be detailed in the next section.

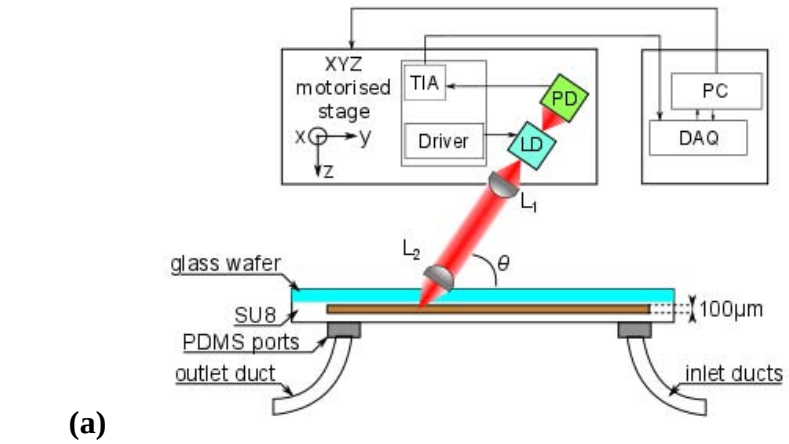

(a)

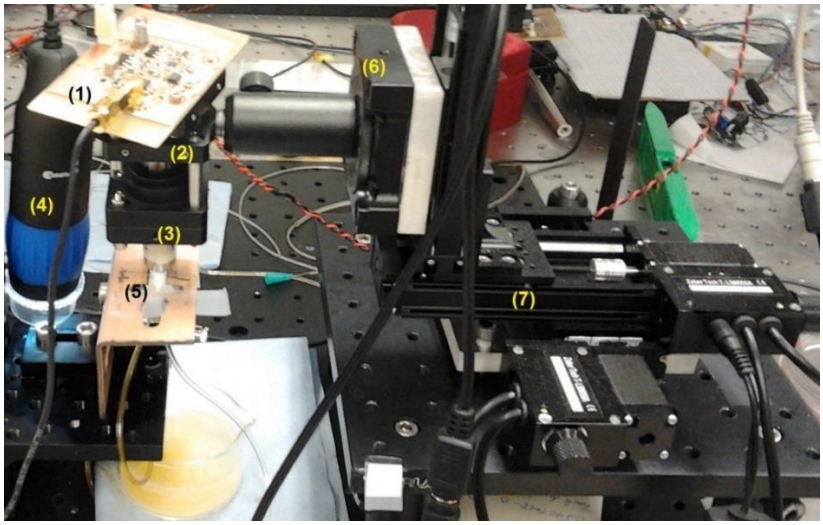

(b)

Fig. 4.9. Schematic representation of the two-lens infrared laser setup (above). Real image of the setup (below): (1) Electronic circuitry driving the laser, (2) Collimation lens, (3) Focalization lens, (4) Camera, (5) Y-shaped microreactor, (6) Goniometer and (7) Micrometric stage device for scanning.

4.3.4.4 Measured profile with dual lens configuration and infrared laser

The velocity profiles for the dual lens configuration with the infrared laser are presented in Figs 4.10 and 4.13 for several flow rates provided at the microreactor's inlets.

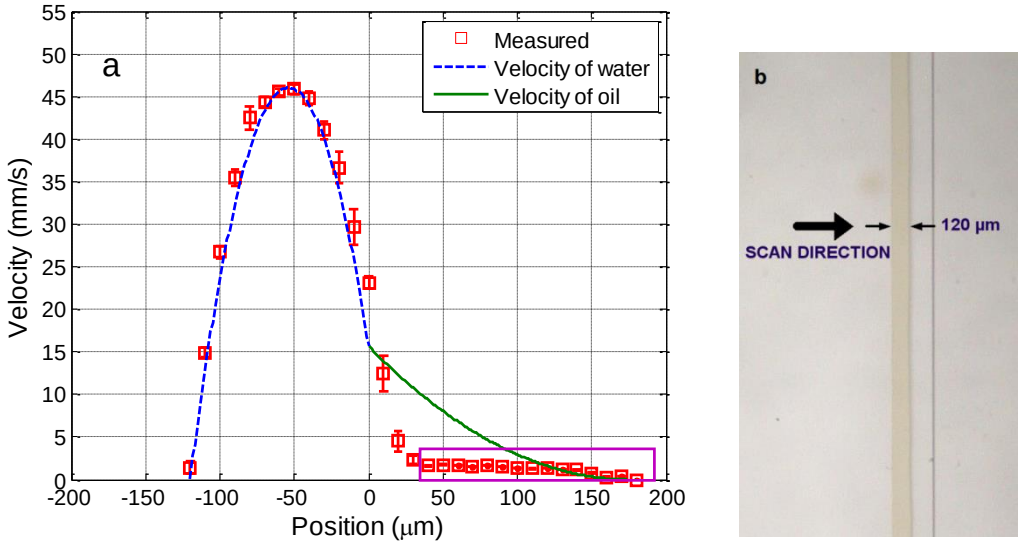

Fig. 4.10. Measured maximum velocity profile with the dual lens configuration and theoretical fitting for water pumped at 20 µL/min and oil pumped at 1.5 µL/min (a). Reference image indicating the scan (b).

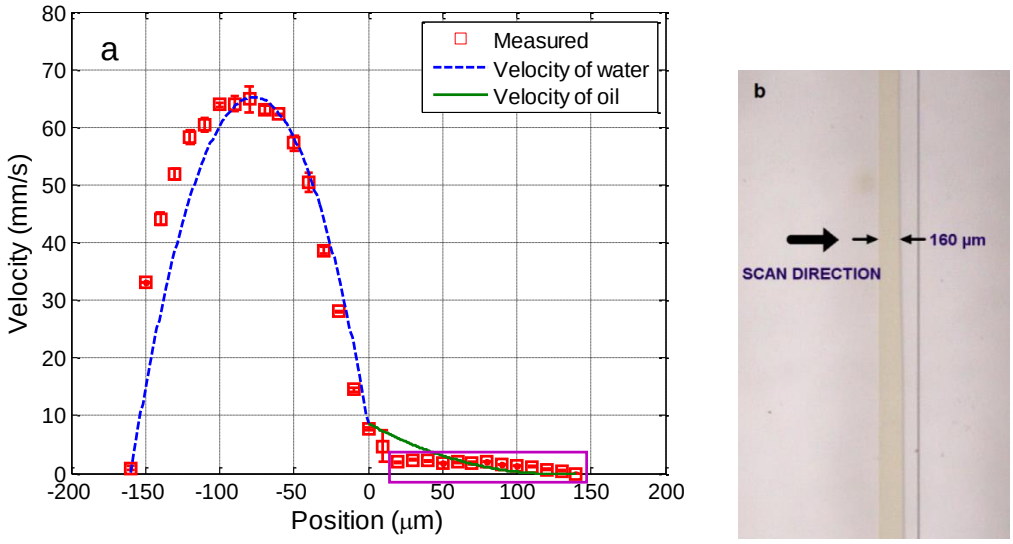

Fig. 4.11. Measured maximum velocity profile with the dual lens configuration and theoretical fitting for water pumped at 35 µL/min and oil pumped at 1.5 µL/min (a). Reference image indicating the scan (b).

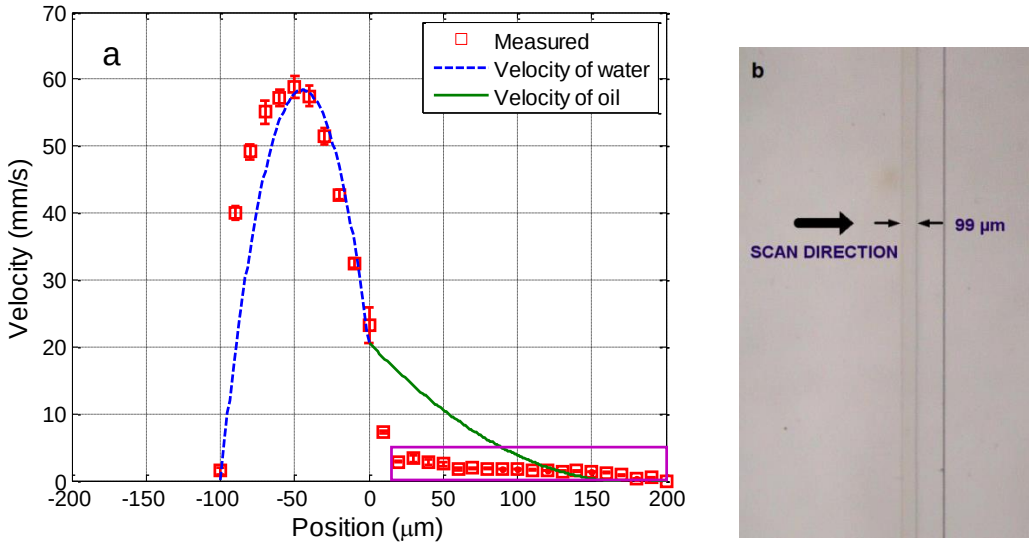

Fig. 4.12. Measured maximum velocity profile with the dual lens configuration and theoretical fitting for water pumped at 20 μL/min and oil pumped at 3 μL/min (a). Reference image indicating the scan (b).

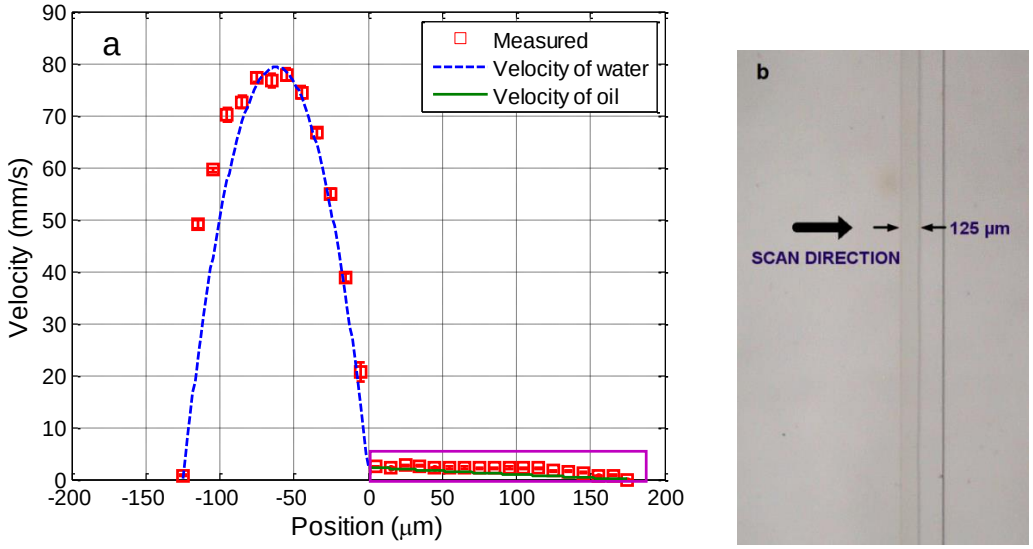

Fig. 4.13. Measured maximum velocity profile with the dual lens configuration and theoretical fitting for water pumped at 35 μL/min and oil pumped at 3 μL/min (a). Reference image indicating the scan (b).

The information of the fitting with the theoretical curves is presented in Table 4.2.

Table 4.2 Fitting parameters used in theoretical profiles plotted in Figs. 4.3 to 4.5

Flow rate $_{water}$	**Flow rate $_{oil}$**	A_1	A_2	v_i
20 μL/min	1.5 μL/min	$-2.1\cdot10^{7}$ $m^{-1}s^{-1}$	$1.05\cdot10^{6}$ $m^{-1}s^{-1}$	15.64 mm/s
35 μL/min		$-3.8\cdot10^{7}$	$1.1\cdot10^{7}$	8.65 mm/s
20 μL/min	3 μL/min	$-2.05\cdot10^{7}$	$1.3\cdot10^{6}$	20.62 mm/s
35 μL/min		$-4.02\cdot10^{7}$	$1.9\cdot10^{4}$	2.32 mm/s

All profiles represented in all tested configurations show that OFI can be used with success in profiling water flow, but still the sensor lacks enough sensitivity to perform valid velocity measurements in the oil. Nevertheless, the two-lens configuration evidences more precisely the possible location of the interface. From this set of measurements can be concluded that the laser wavelength is probably too long to detect slow velocities as those corresponding to oil. The maximum flow rate used (3 µL/min) is too slow to generate a detectable signal with the infrared laser. In all figures, those points inside the purple rectangle could not be properly measured and velocities values are inaccurate. This situation imposes a redesign of the OFI sensor to make a new configuration capable of detecting useful signals all over the scanned line that may fit a theoretical profile for oil with negative pressure gradient contained in parameter A_2. Also, it will be important to have accurate measurements to have a better understanding of the velocities at each side of the interface. This will allows us to understand how the velocity profiles are developed and how their interaction may affect the behavior of both fluids.

4.3.4.5 Measured profile with dual-lens configuration and blue-violet laser

In previous sections we have shown how an OFI flowmeter based upon an infrared laser can perform accurate measurements of water flowing at several tens of uL/min in a chemical microreactor. However, in the study of oil-water flows in the same small channel, no valid velocity measurements could be done to fully reconstruct the profile of both parallel fluids.

The real experimental set-up is shown in Figure 4.14 and the simplified representation of the setup is consistent with the diagram shown in Fig. 4.6. It consists of a blue-violet laser diode (Panasonic DL-5146-101S) with a short wavelength λ=405 nm. Kliese [2010] demonstrated that OFI flow sensors incorporating lasers with shorter wavelength are capable to measure very slow velocities, out of the range that an infrared laser would detect. The OFI sensor is coupled to two lenses (Thorlabs C240TM-A). Lens L1 is used for collimation while the lens L2 is dedicated to the focalization at the microchannel's center in depth. The laser spot size obtained with this configuration has been calculated with a ray tracing software, and is expected to be around 9 µm in diameter according to the $1/e^2$ criterion. The electronic circuitry relative to this laser is presented in Annex 2.

At first, in order to vary the position of the interface between both fluids, the flow rate of water (Q_{water}) varies from 20 µL/min to 65 µL/min in steps of 15 µL/min while the flow rate of oil (Q_{oil}) was fixed at 3 µL/min.

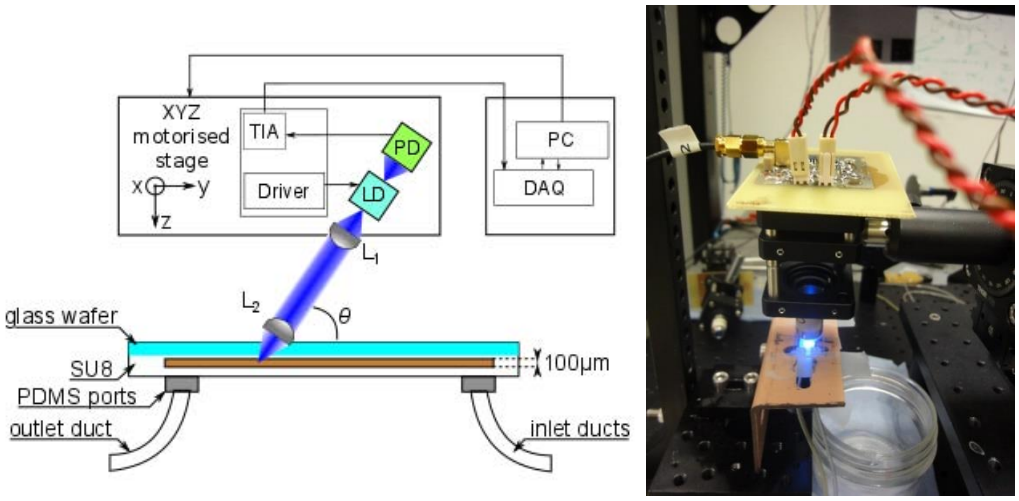

Fig. 4.14. Scheme of the experimental setup incorporating a blue-violet laser (left). Real OFI sensor (right).

First, some experiments designed to vary the position of the interface between both fluids are carried out. The flow rate of oil is fixed at 3 µL/min and the flow rate of water varies from 20 µL/min to 65 µL/min in steps of 15 µL/min.

Figures 4.15 to 4.18 show the measured velocity profiles associated with the oil-water parallel flows in the microchannel [Ramírez-Miquet, 2016b]. The square measurement points represent the averaging of the maximum velocity values measured over 8 consecutive scans and the errorbars represent the standard deviation of the maximum velocities at the same position. The locations of the interface, determined by image analysis, are reported on these profiles. Measured points near the interface are probably due to the effect of the sensing volume or the definition of the boundaries in the images, which have an intrinsic resolution of 8 µm.

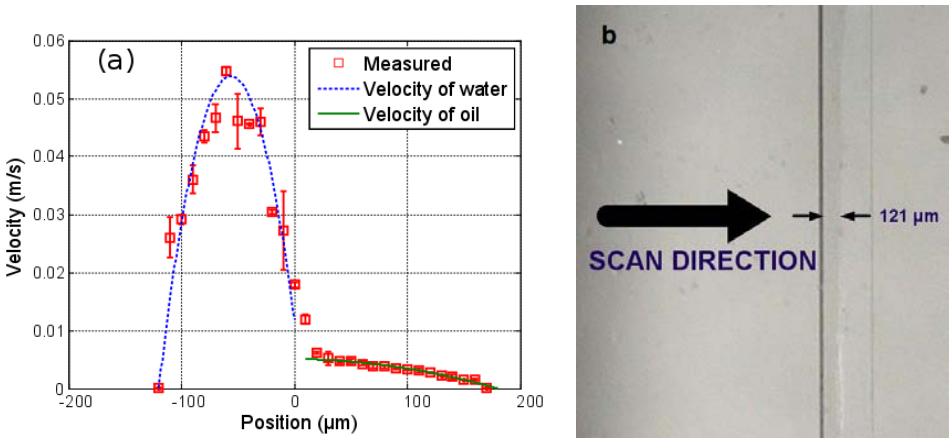

Fig. 4.15. Measured maximum velocity profile with the dual lens configuration and theoretical fitting for water pumped at 20 µL/min and oil pumped at 3 µL/min (a). Reference image indicating the scan (b).

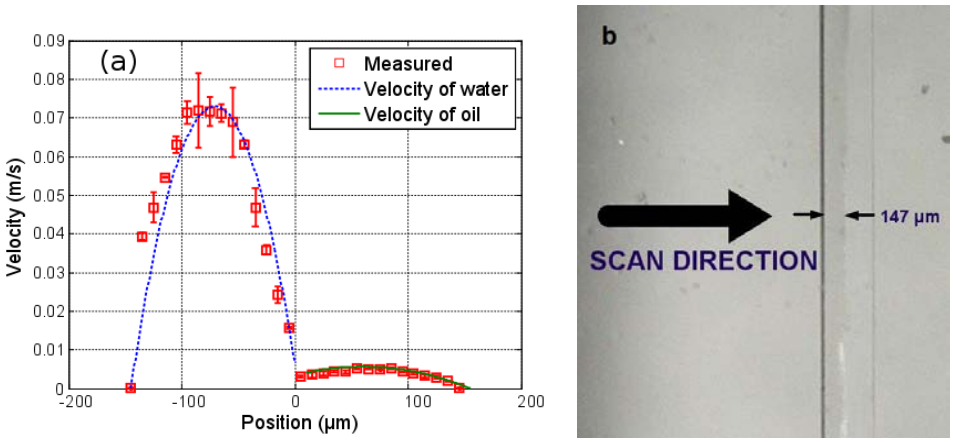

Fig. 4.16. Measured maximum velocity profile with the dual lens configuration and theoretical fitting for water pumped at 35 µL/min and oil pumped at 3 µL/min (a). Reference image indicating the scan (b).

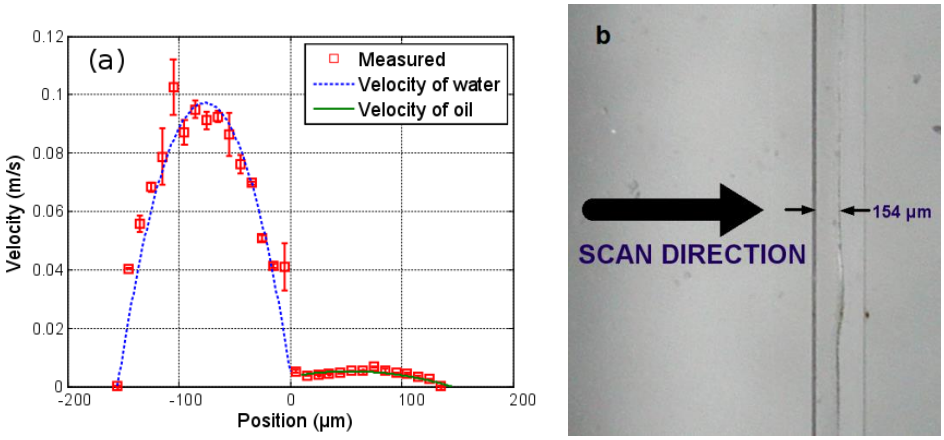

Fig. 4.17. Measured maximum velocity profile with the dual lens configuration and theoretical fitting for water pumped at 50 µL/min and oil pumped at 3 µL/min (a). Reference image indicating the scan (b).

The OFI sensor using a blue-violet semiconductor laser was capable of profiling the flow velocities all over the scanned line. Profiles are here represented with maximum velocity, which corresponds to the velocity in the center of the channel, at 50 µm below the upper glass.

The velocity profiles show that each fluid develops its own profile as stated by Pohar [Pohar, 2012]. Also, at Fig. 4.15 one can see that a slipping phenomenon exists at the interface while for higher flow rate ratios (Figures 4.16 to 4.17) the dragging effect is much less notable. In the case represented in Figure 4.15, the water flow affects the oil flow in a way that the oil reaches its maximum velocity in the vicinity of the interface. This behavior is typical of Couette flows, in which it is considered that each liquid is flowing in between two plates, one of which is moving – in this case, the fluids interface. So, the interface does not play a wall-like role between the two fluids. For the configurations represented in Figures

4.16 to 4.17, our measurements indicate a small slipping at the interface, as velocity values have a local minimum there.

Further, scan measurements are carried out aiming at profiling velocity fields of oil-water parallel flows for which the ratio of flow rates is kept constant. Measurements are performed with Q_{oil} varying from 1.5 µL/min to 4.5 µL/min in steps of 1.5 µL/min and proportionally Q_{water} varies as follows: 20, 40 and 60 µL/min.

Figures 4.18 to 4.20 show the measured velocity profiles for oil and water when the ratio of flows rates remains constant. Square points and errorbars are calculated from eight scans. Measurements enable to verify that the interface remains in the same location as the flows rates are varied proportionally and thus the fraction of volume occupied by each fluid in the microchannel is constant. These findings confirm the relevancy of the OFI technique when implementing in two-phase parallel flows.

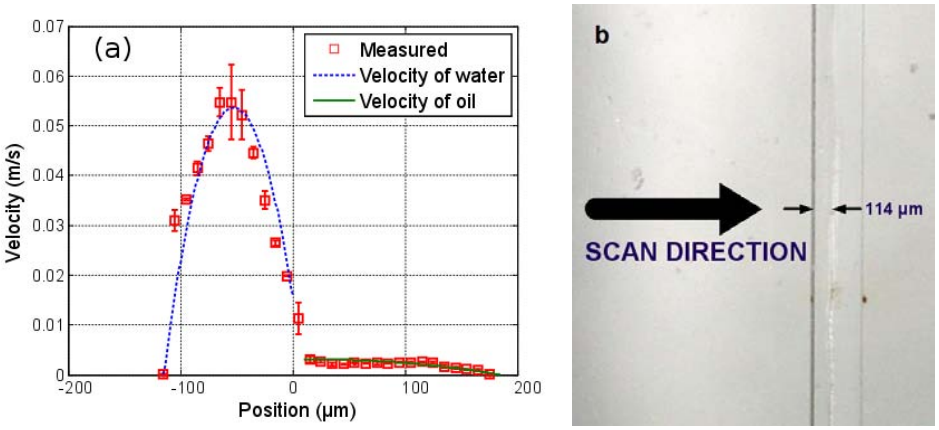

Fig. 4.18. Measured maximum velocity profile with the dual lens configuration and theoretical fitting for water pumped at 20 µL/min and oil pumped at 1.5 µL/min (a). Reference image indicating the scan (b).

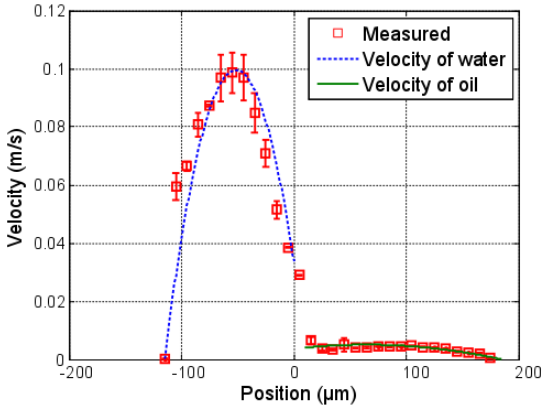

Fig. 4.19. Measured maximum velocity profile with the dual lens configuration and theoretical fitting for water pumped at 40 µL/min and oil pumped at 3 µL/min. Reference image is shown in Fig. 4.20(b).

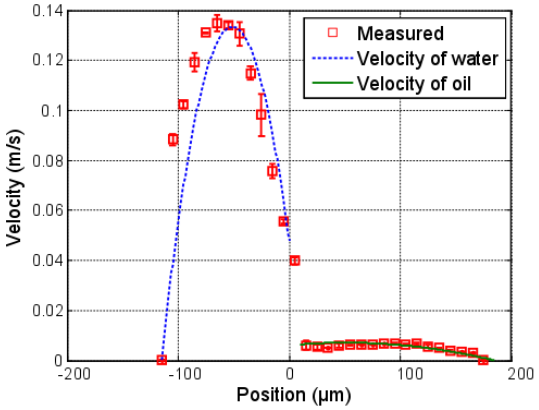

Fig. 4.20. Measured maximum velocity profile with the dual lens configuration and theoretical fitting for water pumped at 60 µL/min and oil pumped at 4.5 µL/min. Reference image is shown in Fig. 4.20(b).

The parameters of the model used to fit the experimentally obtained values plotted in Fig. 4.15 to 4.21 are shown in Table 4.3. As depicted in the graphs, fairly good agreement is found between theoretical profiles plotted after Equations 4.6 and 4.7, and experimentally measured profiles. Thus, the theoretical approximation considering two independent viscous fluids interacting in the microchannel is suitable to describe the system's hydrodynamics, even when this interaction makes the fluid behave as Couette flows. The negative values in parameters A_1 and A_2 denote the presence of profiles in which the pressure gradient is favorable.

In order to definitively validate the technique, an integration of the velocity distribution can serve to obtain the flow rates imposed in the inlets for every tested configuration. This calculation serves as confirmation of our measurements. Shah and London [Shah, 1978] proposed an expression in the case of rectangular microchannel to obtain the volumetric flow rate from the velocity distribution. Considering that the measured profile is scanned from one wall until the other and that our laser detects a maximum frequency in the center of the channel, the flow rates are calculated from the mean values represented in square points in the graphs using the following approximation for a channel with aspect ratio $\alpha^* = 1/3$:

$$Q = \int_{-h/2}^{h/2} v_{meas.} \left[1 - \left(\frac{z}{h} \right)^2 \right] dz \qquad (4.8)$$

where variable z represents the position in height inside the channel.

Table 4.3. Fitting parameters used in Eq. 4.6 and 4.7					
Flow rate$_{water}$ (μL/min)	Flow rate$_{oil}$ (μL/min)	A_1 ($m^{-1}\cdot s^{-1}$)	A_2 ($m^{-1}\cdot s^{-1}$)	v_{i1} (m/s)	v_{i2} (m/s)
20	3	$-2.65\cdot10^{-7}$	$-2.95\cdot10^{-5}$	$11.9\cdot10^{-3}$	$5.1\cdot10^{-3}$
35	3	$-2.65\cdot10^{-7}$	$-1.25\cdot10^{-6}$	$6.5\cdot10^{-3}$	$3.4\cdot10^{-3}$
50	3	$-3.15\cdot10^{-7}$	$-1.25\cdot10^{-6}$	$5.12\cdot10^{-3}$	$3.4\cdot10^{-3}$
20	1.5	$-2.75\cdot10^{-7}$	$-2.35\cdot10^{-6}$	$15.7\cdot10^{-3}$	$3.0\cdot10^{-3}$
40	3	$-4.95\cdot10^{-7}$	$-6.95\cdot10^{-6}$	$33.7\cdot10^{-3}$	$3.6\cdot10^{-3}$
60	4.5	$-6.60\cdot10^{-7}$	$-1.25\cdot10^{-6}$	$47.1\cdot10^{-3}$	$3.4\cdot10^{-3}$

Calculations obtained from the integration in Equation are represented in Table 4.4. Again, good agreement is found when compared to the flow rates imposed for each configuration.

Table 4.4. Flow rates calculated by integrating the experimental velocity profile				
Flow rate$_{water}$ (μL/min)	Flow rate$_{oil}$ (μL/min)	Flow rate$_{total}$ (μL/min)	Flow rate$_{measured}$ (μL/min)	Relative error (%)
20	3	23	23.4	1.79
35	3	38	36.4	4.08
50	3	53	51.8	2.19
20	1.5	21.5	22.3	4.02
40	3	43	42.1	1.86
60	4.5	64.5	59.9	7.5

It should be stressed that the combination of the theoretical model and the experimental results may be useful in determining fundamental properties of the fluids involved. The model contemplates constant *A* as the ratio of the pressure gradient and the viscosity. If one of those parameters is controlled during the experiment then the other can be easily determined. In case that a pressure-controlled pump is used instead of a flow-controlled pump, then the viscosity of the fluids could be calculated because the pressure gradient is known. With this in mind, optical feedback interferometry sensors are hereby proven to be well-suited not only as laser velocimeters, but equally as flowmeters and viscometers or rheometers.

4.4 Perspectives

The implementation of OFI sensors in the analysis of multiphase opens up new promising perspectives for studies of interfacial liquids. This new approach allows to measure accurately local velocity of two-phase parallel flows in microchannels and study flows even if the interface is not straight or becomes unstable. Furthermore, a natural extension of the present work would consist in applying this methodology as a new tool to assess fluid's velocity in the presence of stationary slug droplets of one phase compromising the cross section and causing an acceleration of the second phase in a microchannel. In this regards, OFI sensors offer a compact solution for interrogating flow distribution in the vicinity

of interfaces typically found in the studies of slug flows, transport of highly viscous fluids and organic-water mixtures.

Conclusions

The present thesis had the purpose of implementing the optical feedback interferometry technique for multiple sensing applications in fluidic systems with interest in biomedical and chemical engineering and with experimental projection mainly at the micrometric scale but also with larger channels.

In the first chapter, we reviewed the Doppler methods currently used for flow quantification. A direct comparison between all the methods highlighted the full potential of optical feedback interferometry (OFI) sensors in terms of spatial resolution, costs, ease of mounting and bulkiness. OFI presents a viable alternative to other Doppler techniques allowing flow measurements and is one of the few techniques that can address flow measurements at the micro-scale. A notable ongoing research in the potential of optical feedback systems is actively being developed in the field, thus pushing the new applications of the emerging field of optofluidics. The motivations of the present thesis are presented in the frame of the number of unexplored issues and applications related to OFI and its implementation for fluid flow assessment in both the single and multiple scattering regime.

Chapter 2 presents the fundaments of the optical feedback effect in the case of the interaction of the laser with a group of particles. A discussion on the scattering regimes that may be applied to the theoretical approaches governing the laser-

fluid interaction is presented. A derivation of the equations explaining the physics supporting the phenomenon is proposed. The derivation of the rate equations that constitute the core theory of the lasers subject to external feedback has been extended to generate a simple model that takes into account the impact of a plurality of particles contributing to the laser feedback. In addition, we provided a complete description of the OFI sensor principles that included a set of characterization measurements of the lasers involved in the experiments presented in this manuscript.

In Chapter 3, we present the processing methods that could be used to extract the quantitative values of velocity of flows in a microchannel and presented an analysis of their suitability to successfully retrieve the quantitative information of flows in both the single and the multiple scattering regime. We found that the weighted moment method is well-suited for Doppler frequency shift determination and velocity calculation as long as the fluid holds a concentration similar to 4 % of full-cream milk or higher, as demonstrated by the relative errors below 8 %. In addition, the relative errors obtained for weighted moment processing method are lower than 6 % for a wide range of flow rates. The second processing method tested, consisting in using a cutoff frequency method provides a reasonable accuracy in the measurements at flow rates below 20 ul/min and may provide an accurate measurement for concentrations up to 4 % of full-cream milk with relative errors associated below 5 %.

In addition, from the number of elements that we identified as potential research work in Chapter 1, we have addressed experimentally in Chapter 3 multiple applications of the optical feedback interferometry in fluid flow sensing. We have tested the OFI technique and its capabilities for flow measurements in microchannels, flow profiling, ex-vivo flow mapping, the analysis of non-steady flows and single particle detection. We demonstrate thereby that OFI is a suitable technique to be implemented at the microscale for flow sensing with reasonable accuracy. The demonstrations presented in the third chapter clearly emphasize the latent fertile ground of possibilities that OFI opens as a new simple optical technique for milli and microchannel flow sensing, flow steadiness characterization and particle detection and location in microfluidic devices. The experimental evidences presented in this chapter present OFI as powerful non-contact sensing method in the field of optical measurement techniques at the microscale.

Finally, in the fourth chapter, we present what we believe is the first implementation of optical feedback interferometry sensors for the analysis of multiphase flows. We combined the possibilities of flow profiling with an analytical model issue from the Couette flow approximation, to reconstruct the velocity profile of immiscible liquids at the microscale. This theoretical model was developed in this thesis for describing the hydrodynamics of the immiscible

fluids. The model fits fairly well with the experimental measurements and the methodology presented opens up new possibilities for understanding behavior of parallel flows and the influence of one flow on the other mostly evidenced by the slipping at the interface that is equivalent to consider moving plates of Couette flows under a pressure gradient. This behavior allows us to understand under which circumstances the velocity profile of the flows is developed independently and their interaction is minimal.

The work presented in this thesis paves the way to further developments in the field of optofluidic implementation, microchannel flows interrogation, particle characterization in microfluidic channels and multiphase flow analysis.

Our group at LAAS-CNRS is currently developing new automated OFI systems enabling flow profiling at the microscale, which incorporate a micromirror to guide the laser towards the flow. This avoids using micromechanical stepping devices to perform the scan during flow profiling and flow mapping measurements, thus simplifying the scanning scheme of the sensor. An extension of this system is being investigated for scan cancer detection in the European project Diagnoptics. The project consists in developing a set of photonic instrumentation tools including the design and development of an optical feedback interferometry sensor capable of quantifying the microcirculation associated to malignant tissue as an indicator of skin cancer, especially the melanomas.

In the field of particle detection in microfluidic devices new research work is being conducted to implement OFI for the characterization of particles in a flow beyond the detection and location in a profile. Further work will deal with the possible discrimination of particles by size and shape using different methodologies such as continuous signal burst scanning and its relation to the geometrical properties of the particles. Moreover, to the best of our knowledge, no OFI sensing has been tested for detecting particles significantly smaller than the laser wavelength, where Rayleigh scattering rules the interaction. Future theoretical and experimental work could be directed towards the detection and characterization of small particles producing extremely weak Rayleigh scattering.

A set of new perspectives are identified to further implement optical feedback interferometry sensors in other situations involving multiphase flows. In this regard, OFI can be potentially tested for the analysis of droplets in gas-liquid flows, by providing information on the velocity and sizes as they pass through the sensing volume. Other possibilities are found in the analysis of slug flows of different immiscible fluids in microreactors. Stationary slug flows of one fluidic phase can compromise the cross section of the channels, and then cause an acceleration of the second phase that can be quantified with OFI flow profiling and mapping.

List of publications

Conference papers

Quotb, A., Ramírez-Miquet, E. E., Tronche, C. and Perchoux, J. (**2014**). Optical feedback interferometry sensor for flow characterization inside ex-vivo vessel. *Proc. IEEE Sensors*, 313-316.

Ramírez-Miquet, E. E., Arriaga, A. L., Quotb, A., Sotolongo-Costa, O. and Perchoux, J. (**2015**). In-situ measurement of non-steady flows using optical feedback interferometry. *Proc. IEEE International Conference on Industrial Technology*, 1469-1473.

Ramírez-Miquet, E. E., Sotolongo-Costa, O., Quotb, A., Loubière, K., Plat, L. and Perchoux, J. (**2016**). Profiling oil-water flows in microchannel: preliminary results using optical feedback interferometry. *Optical Measurement Techniques for Systems and Structures III*, 251-258.

Journal papers

Perchoux, J., Quotb, A., Atashkhooei, R., Azcona, F. J., Ramírez-Miquet, E. E., Bernal, O., Jha, A., Luna-Arriaga, A., Yanez, C., Caum, J., Bosch, T. and Royo, S. (**2016**). Current developments on optical feedback interferometry as an all-optical sensor for biomedical applications. *Sensors* **16**, 694.

Ramírez-Miquet, E. E., Perchoux, J., Loubière, K., Tronche, C., Prat, L. and Sotolongo-Costa, O. (**2016**). Optical feedback interferometry for velocity measurement of parallel liquid-liquid flows in a microchannel. *Sensors* **16**, 1233.

References

Acket, G., Lenstra, D., Den Boef, A. and Verbeek, B. (1984). The influence of feedback intensity on longitudinal mode properties and optical noise in index-guided semiconductor lasers. IEEE J. Quantum Electron. 20(10), 1163-1169.

Açikgöz, M., França, F., Lahey Jr, R. T. (1992). An experimental study of three-phase flow regime. Int. J. Multiphase Flow 18(3), 327-336.

Ahn Y.C., Jung W. and Chen, Z. (2008). Optical sectioning for microfluidics: secondary flow and mixing in a meandering microchannel. Lab Chip. 8, 125-133.

Akamatsu, S., Kondo, Y. and Dohi, S. (1996). Velocity measurement with a new ultrasonic Doppler method independent of angle of incidence. J. Anesth. 10, 133-139.

Alexandrova, A. and Welsch, C.P. (2016). Laser diode self-mixing technique for liquid velocimetry. Nucl. Instrum. Meth. A, doi: 10.1016/j.nima.2015.12.042

Atashkhooei, R., Royo, S. and Azcona, F. J. (2013). Dealing with speckle effects in self-mixing interferometry measurements. IEEE Sensors J., 13(5), 1641-1647.

Atashkhooei, R., Urresty, J. C. Royo, S., Riba, J. R. and Romeral, L. (2014). Runout tracking in electric motors using self-mixing interferometry. IEEE/ASME Trans. Mechatron. 19, 184–190.

Attwell, D., Buchan, A.M., Charpak, S., Lauritzen, M., Macvicar, B.A. and Newman, E.A. (2010). Glial and neuronal control of brain blood flow. Nature 468, 232-243.

Arriaga, A. L., Bony, F. and Bosch, T. (2016). Real-time algorithm for versatile displacement sensors based on self-mixing interferometry. IEEE Sensors J. 16, 195-202.

Arriaga, A. L. (2014a). Analysis and implementation of algorithms for embedded self-mixing displacement sensors design. Thesis dissertation.

Arriaga, A. L., Bony, F. and Bosch, T. (2014b). Speckle-insensitive fringe detection method based on Hilbert transform for self-mixing interferometry. App. Opt. 53(30), 6954-6962.

Baker, D. W. (1970). Pulsed ultrasonic Doppler blood flow sensing. IEEE Trans. Sonic. Ultrasonics SU 17(3), 170-185.

Baldini, F. (2006). Optical, chemical, and biochemical sensors in medicine. SPIE Newsroom, doi: 10.1117/2.1200602.0061.

Ball, G. J. (1988). A stochstic model for laser transit velocimeter correlograms in flows with high vorticity. J. Mod. Opt. 35(5), 761-782.

Bernal, O., D., Zabit, U. and Bosch, T. M. (2015). Robust method of stabilization of optical feedback regime by using adaptive optics for a self-mixing micro-interferometer laser displacement sensor. IEEE J. Sel. Top. Quant. Electron., 21(4), 336-343.

Bes, C., Belloeil, V., Plantier, G., Gourinat, Y. and Bosch, T. (2007). A self-mixing laser sensor design with an extended Kalman filter for optimal online structural analysis and damping evaluation. IEEE/ASME Trans. Mechatronics 12(3), 387-394.

Binzoni, T., Torricelli, A., Giust, R., Sanguinetti, B., Bernhard, P. and Spinelli, L. (2014). Bone tissue phantoms for optical flowmeters at large interoptode spacing generated by 3D-stereolithography. Biomed. Opt. Express, 5(8), 2715-2725.

Bohren, C. F. and Huffman, D. R. (2004) Absorption and scattering of light by small particles. Wiley-VCH Verlag GmbH & Co.

Bonner, R. and Nossal, R. (1981). Model for laser Doppler measurements of blood flow in tissue. Appl. Opt. 20(12), 2097-2107.

Bosch, T., Servagent, N. and Donati, S. (2001) Optical feedback interferometry for sensing application. Opt. Eng. 40, 20–27.

Boppart, S. A., Luo, W., Marks, D. L. and Singletary, K. W. (2004). Optical coherence tomography: feasibility for basic research and image-guided surgery of breast cancer. Breast Cancer Res Treat 84, 85–97.

Brennen, C. E. (2005). Fundamentals of multiphase flows. Cambridge University Press.

Büttner, L., Skupsch, C., König, J., & Czarske, J. (2010). Optic simulation and optimization of a laser Doppler velocity profile sensor for microfluidic applications. Opt. Eng., 49(7), 073602.

Cadel, D. R. and Lowe, K. T. (2015). Cross-correlation Doppler global velocimetry (CC-DGV). Opt. Lasers Eng. 71, 51-61.

Campagnolo, L., Roman, S., Perchoux, J. and Lorthois, S. (2012). A new optical feedback interferometer for measuring red blood cell velocity distributions in individual capillaries: a feasibility study in microchannels. Comput. Methods Biomech. Biomed. Engin. 15(sup1), 104-105.

Campagnolo, L., Nikolić, M., Perchoux, J., Lim, Y. L., Bertling, K., Loubière, K., Prat, L., Rakić, A. D. and Bosch, T. (2013a). Flow profile measurement in microchannel using the optical feedback interferometry sensing technique. Microfluid. Nanofluid. 14, 113-119.

Campagnolo, L. (2013b). Optical feedback interferometry for flow measurements in microchannels. Doctoral dissertation.

Chen, Z., Milner, T.E., Srinivas, S., Wang, X., Malekafzali, A., van Gemert, M. J., Nelson, J.S. (1997). Noninvasive imaging of in vivo blood flow velocity using optical Doppler tomography. Opt. Lett. 22, 1119-1121.

Clancy, P. S. and Samimy, M. (1997). Two-component planar Doppler velocimetry in high-speed flows. AIAA J. 35(11), 1729–1738.

Clancy, P., Samimy, M. and Erskine, W. R. (1999). Planar Doppler Velocimetry: three-component velocimetry in supersonic jets. AIAA J. 37(6), 700–707.

Clifford, P. S., Ella, S. R., Stupica, A. J., Nourian, Z., Li, M., Martinez-Lemus, L. A., Dora, K. A., Yang Y., Davis M. J., Pohl U., Meininger, G. A. and Hill, M. A. (2011). Spatial Distribution and Mechanical Function of Elastin in Resistance Arteries A Role in Bearing Longitudinal Stress. Arteriosclerosis, thrombosis, and vascular biology, 31(12), 2889-2896.

Davis, M. A., Kazmi, S. M. S. and Dunn, A. K. (2014). Imaging depth and multiple scattering in laser speckle contrast imaging. J. Biomed. Opt. 19(8), 086001.

de Mul, F. F. M., van Spijker, J., van der Plas, D., Greve, J., Aarnoudse, J. G., Smits, T. M. (1984). Mini laser-Doppler (blood) flow monitor with diode laser source and detection integrated in the probe. Appl. Opt. 23(17), 2970-2973.

de Mul, F. F. M., Koelink, M. H., Weijers, A. L., Greve, J., Aarnoudse, J.G., Graaff, R. and Dassel, A. C. M. (1992). Self-mixing laser Doppler velocimetry of liquid flow and of blood perfusion in tissue. Appl. Opt. 31(27), 5844-5851.

de Mul, F. F. M., Koelink, M.H., Weijers, A.L., Greve, J., Aarnoudse, J.G., Graaff, R. and Dassel, A.C.M. (1993) A semiconductor laser used for direct measurement of the blood perfusion of tissue. IEEE Trans. Biomed. Eng. 40(2), 208-210.

Donati, S. (1978). Laser interferometry by induced modulation of cavity field. J. Appl. Phys. 49(2), 495-497.

Donati, S. (2000). Photodetectors, Devices, Circuits and Applications, Chapter 8, Prentice Hall, Upper Saddle River, NJ.

Donati, S. (2012). Developing self-mixing interferometry for instrumentation and measurements. Laser Photonics Rev. 6(3), 393-417.

Donati, S., and Norgia, M. (2014). Self-mixing interferometry for biomedical signals sensing. IEEE J. Sel. Top. Quant. 20(2), 104-111.

Doppler, C. (1843). Über das farbige Licht der Doppelsterne und eineger anderer Gestirne des Himmels. Abhandl Konigl Bohm Ges. Ser. 2, 465-482.

Drexel, W. (2004). Ultrahigh resolution optical coherence tomography. J. Biomed. Opt. 9(1), 47-74.

Elliott, G.S., Samimy, M. and Arnette, S. A. (1992). Study of compressible mixing layers using filtered Rayleigh scattering based visualizations," AIAA J. 30, 2567-2569.

Elliott, G. S., Samimy, M., and Arnette, S. A. (1994). A molecular filter based diagnostics in high-speed flows. Exp. Fluids 18, 107-118.

Elliott, G. S. and Beutner T. J. (1999). Molecular Filter based planar Doppler velocimetry. Prog. Aeros. Sci. 35, 799-845.

Fainman, Y., Lee, L., Psaltis, D., and Yang, C. (2009). Optofluidics: fundamentals, devices, and applications. McGraw-Hill, Inc.

Figueiras, E., Oliveira, R., Lourenço, C. F., Campos, R., Humeau-Heurtier, A., Barbosa, R. M., Laranjinha, J., Ferreira, L. F. R. and de Mul, F. F. M. (2013). Self-mixing microprobe for monitoring microvascular perfusion in rat brain. Med. Biol. Eng. Comput. 51(1-2), 103-112.

Fischer, A., Wilke, U., Schlüßler, R., Haufe, D., Sandner, T and Czarske, J. (2014). Extension of frequency modulated Doppler global velocimetry for the investigation of unsteady spray flows. Opt. Lasers Eng. 63, 1-10.

Foreman Jr., J. W. George, E. W. and Lewis, R. D. (1965). Measurement of localized velocities in gases with a laser Doppler flowmeter. Appl. Phys. Lett. 7(4), 77-78.

Foreman, J. W., George, E. W., Jetton, J. L., Lewis, R. D., Thornton, J. R. and Watson, H. J. (1966). 8C2-fluid flow measurements with a laser Doppler velocimeter. IEEE J. Quant. Electron. 2(8), 260-266.

Foroughi, H. and Kawaji, M. (2011). Viscous oil–water flows in a microchannel initially saturated with oil: flow patterns and pressure drop characteristics. Int. J. Multiphas. Flow, 37(9), 1147-1155.

Förster, W., Karpinsky, G., Krain, H., Röhle, I. and Schodl, R. (2002). 3-Component Doppler laser-two-focus velocimetry applied to a transonic centrifugal compressor. Laser Techniques for Fluid Mechanics, 55-74.

Franklin, D. L., Schelegel, W. and Rushmer, R. F. (1959). Blood flow measured by Doppler Frequency shift of back scattered ultrasound. Science 134, 564-565.

FritzGerard, D. E. and Drumm, J. E. (1977). Noninvasive measurement of the fetal circulation using ultrasound: a new method. Br. Med. J. 2, 637-641.

Giuliani, G., M. Norgia, M., S. Donati, S. and T. Bosch, T. (2002). Laser diode self-mixing technique for sensing applications. J. Opt. A: Pure Appl. Opt. 4, S283–S294.

Goldman, L. (1981). The biomedical laser: technology and clinical applications. Chapter 13.

Gordon, A., & Vynnycky, M. (2014). Analysis of Two-Phase Flow in the Gas Diffusion Layer of a Polymer Electrolyte Fuel Cell. In Progress in Industrial Mathematics at ECMI 2012. Springer International Publishing, 177-183.

Harris, S. J. and Maricq, M. M. (2001). Signature size distributions for diesel and gasoline engine exhaust particulate matter. J. Aerosol Sci., 32(6), 749-764.

Hilsum, C. and King, P. G. R. (1963). Some demonstrations of the properties of optical masers. Contemp. Phys. 4, 435-444.

Honeycutt, T. E. and Otto, W. (1972). FM-CW radar range measurement with a CO_2 laser. IEEE J. Quantum Electron. 8, 91-92.

Huang, D., Swanson, E. A., Lin, C. P., Schuman, J. S., Stinson, W. G., Chang, W., Hee, M. R., Flotte, T., Gregory, K., Puliafito, C. A. and Fujimoto, J. M. (1991). Optical coherence tomography. Science 254, 1178-1181.

Jones, T. B. (2001). Development and Testing of the Virginia Tech Doppler Global Velocimeter (DGV). MSc. Thesis, p. 104.

Kalkman, J., Bykov, A. V., Streekstra, G. J. and van Leeuwen, T. G. (2012). Multiple scattering effects in Doppler optical coherence tomography of flowing blood. Phys. Med. Biol. 57, 1907-1917.

Kamishima, T. and Quayle, J. M. (2013). Small Vessel Myography. In Essential Guide to Reading Biomedical Papers: Recognising and Interpreting Best Practice. Wiley-Blackwell, 39-48.

Kane, D. M. and Shore, K. A. (Eds.) “Unlocking Dynamical Diversity - Optical feedback effects on semiconductor lasers”, Wiley, 2005.

Kashid, M. N., Rivas, D. F., Agar, D. W. and Turek, S. (2008). On the hydrodynamics of liquid–liquid slug flow capillary microreactors. Asia-Pac. J. Chem. Eng. 3(2), 151-160.

Kim, G and Menon, R. (2014). An ultra-small 3D computational microscope. Appl. Phys. Lett. 105, 061114.

King, P. G. R. and Steward, G. J. (1963). Metrology with an optical maser. New Sci. 17, 180-182.

King, P. G. R. and Steward, G. J. (1968). Apparatus for measurement of lengths and of other physical parameters which are capable of altering an optical path length. U.S. patent 3409370.

Kliese, R., Taimre, T., Bakar, A. A. A., Lim, Y. L., Bertling, K., Nikolić, M., Perchoux, J., Bosch, T. and Rakić, A. D. (2014). Solving self-mixing equations for arbitrary feedback levels: a concise algorithm. Appl. Opt. 53(1), 3723-3736.

Kliese, R., Lim, Y. L., Bosch, T. and Rakić, A. D. (2010). GaN laser self-mixing velocimeter for measuring slow flows. Opt. Lett. 35(6), 814-816.

Koelink, M. H., Slot, M., de Mul, F. F. M., Greve, J., Graaff, R., Dassel, A. C. M. and Aarnoudse, J.G. (1992). Laser Doppler velocimeter based on the self-mixing effect in a fiber-coupled semiconductor laser: theory. Appl. Opt. 31(18), 3401-3408.

Komine, H. and Brosnan, S. (1991). Instantaneous, three-component, Doppler global velocimetry. Laser Anemom. 1, 273-277.

König, J., Voigt, A., Büttner L. and Czarske J. (2010). Precise micro flow rate measurements by a laser Doppler velocity profile sensor with time division multiplexing. Meas. Sci. Technol. 21, 074005.

Kost, F. and Kapteijn, C. (1997). Application of Laser-Two-Focus Velocimetry to Transonic Turbine Flows. 7th International Conference on Laser Anemometry - Advances and Applications, University of Karlsruhe, Germany, September 8-11.

Kumara, W. A. S., Elseth, G., Halvorsen, B. M. and Melaaen, M. C. (2010). Comparison of Particle Image Velocimetry and Laser Doppler Anemometry measurement methods applied to the oil-water flow in horizontal pipe. Flow Meas. Instrum. 21, 105-117.

Lang, R. and Kobayashi, K. (1980). External optical feedback effects on semiconductor injection laser properties. IEEE J. Quantum Electron. QE-16, 347-355.

Langlois, W. E. and Deville, M. O. (2014). Exact Solutions to the Equations of Viscous Flow. In *Slow Viscous Flow*, pp. 105-143.

Leitgeb, R. A., Werkmeister, R. M., Blatter, C. and Schmetterer, L. (2014). Doppler optical coherence tomography. Prog. Ret. Eye Res. 41, 26-43.

Liu, J., Cai, B., Zhu, J., Ding, G., Zhao, X., Yang, C. and Chen, D. (2004). Process research of high aspect ratio microstructure using SU-8 resist. Microsyst. Tech. 10, 265-268.

Lim, Y. L., Kliese, K., Bertling, K., Tanimizu, K., Jacobs, P. A. and Aleksandar D. Rakić, A. (2010) Self-mixing flow sensor using a monolithic VCSEL array with parallel readout. Opt. Express 18(11), 11720-11727.

Lohwasser, R. and Soelkner, G. (1999). Experimental and theoretical laser-Doppler frequency spectra of a tissuelike model of a human head with capillaries. Applied optics, 38(10), 2128-2137.

Lu, X. and Kassab, G. S. (2011). Assessment of endothelial function of large, medium, and small vessels: a unified myograph. Am. J. Physiol. Heart Circ. Physiol. 300(1), H94-H100.

Maret, G. and Wolf, P. E. (1987). multiple light scattering from disordered media. The effect of brownian motion of scatterers. Z. Phys. B Cond. Matter 65, 409-413.

Merlo, S. and Donati, S. (1997). IEEE J. Quantum Electron. 33(4), 527–531.

McCallum, W. D., Olson, R. F., Daigle, R. E. and Baker, D. W. (1977). Real time analysis of Doppler signals obtained from the fetoplacental circulation. Ultrasound. Med. 3B, 1361-1364.

McCarron, J. G., Crichton, C. A., Langton, P. D., MacKenzie, A. and Smith, G. L. (1997). Myogenic contraction by modulation of voltage-dependent calcium currents in isolated rat cerebral arteries. J. Physiol., 498(Pt 2), 371-379.

McKenzie, R. L. (1996). Measurement capabilities of planar Doppler velocimetry using pulsed lasers. Appl. Opt. 35(6), 948-964.

McKenzie, R.L. (1997). Planar Doppler velocimetry performance in low-speed flows. AIAA Paper 97-0498.

Menn, N. (2004). Practical Optics. Elsevier Academic Press.

Meyers, J. F. (1992). Doppler Global Velocimetry: The Next Generation? AIAA 17th Aerospace Ground Testing Conference.

Michalski, M. -C., Briarn, V. and Michel, F. (2001). Optical parameters of milk fat globules for laser light scattering measurements. Lait 81, 787-796.

Miles, R. and Lempert, W. (1990). Two-dimensional measurement of density, velocity, and temperature of turbulent air flows from UV Rayleigh scattering. Appl. Phys. B B51, 1-7.

Mishchenko, M. I., Hovenier, J. W. and Mackowski, D. W. (2004). Single scattering by a small volume element. J. Opt. Soc. Am. 21(1), 71-87.

Moger, J., Matcher, S. J., Winlove, C. P., & Shore, A. (2005). The effect of multiple scattering on velocity profiles measured using Doppler OCT. J. Phys.D: Appl. Phys. 38(15), 2597-2605.

Mowla, A., Nikolić, M., Taimre, T., Tucker, J. R., Lim, Y. L., Bertling, K. and Rakić, A. D. (2015). Effect of the optical system on the Doppler spectrum in laser-feedback interferometry. Appl. Opt. 54(1), 18-26.

Murakawa, H., Muramatsu, E., Sugimoto, K., Takenaka, N., & Furuichi, N. (2015). A dealiasing method for use with ultrasonic pulsed Doppler in measuring velocity profiles and flow rates in pipes. Meas. Sci. Technol. 26(8), 085301.

Nakamura, T., Hayashi, K., Taenaka, Y., Umezu, M., Nakatani, T. and Takano, H. (1986). Ultrasonic flowmeter with implentable miniature sensors. Med. Biol. Eng. Comput. 24, 235-242.

Nemani, K. V., Moodie, K. L., Brennick, J. B., Su, A. and Gimi, B. (2013). In vitro and in vivo evaluation of SU-8 biocompatibility. Mat. Sci. Eng. C 33, 4453-4459.

Nikolić, M., Hicks, E., Lim, Y. L., Bertling, K. and Rakić, A. D. (2013). Self-mixing laser Doppler flow sensor: an optofluidic implementation. Appl. Opt. 52(33), 8128-8133.

Nikolić, M., Taimre, T., Tucker, J. R., Lim, Y. L., Bertling, K. and Rakić (2014). Laser dynamics under frequency-shifted optical feedback with random phase. Electron. Lett. 50(19), 1380-1382.

Nikolić, M., Lim, Y. L., Bertling, K., Taimre, T. and Rakić, A. D. (2015). Multiple signal classification for self-mixing flowmetry. Appl. Opt. 54(9), 2193-2198

Nilsson, G. E. (1984). Signal processor for laser Doppler tissue flowmeters. Med. Biol. Eng. Comput. 22, 343-348.

Norgia, M., Pesatori, A. and Rovati, L. (2010). Low-cost optical flowmeter with analog front-end electronics for blood extracorporeal circulators. IEEE Trans. Instrum. Meas. 59(5), 1233-1239.

Norgia, M., Pesatori, A. and Rovati, L. (2012). Self-mixing laser Doppler spectra of extracorporeal blood flow: a theoretical and experimental study. IEEE Sensors J. 12(3), 552-557.

Norgia, M., Magnani, A., Melchionni, D. and Pesatori, A. (2015). Drop measurement system for biomedical application. IEEE Trans. Instrum. Meas. 64(9), 2113-2117.

Norgia, M., Pesatori, A. and Donati, S. (2016). Compact Laser-Diode Instrument for Flow Measurement. IEEE Trans. Instrum. Meas. 65(6), 1478-1483.

Oddie, G., Shi, H., Durlofsky, L. J., Aziz, K., Pfeffer, B., Holmes, J. A. (2003). Experimental study of two and three phase flows in large diameter inclined pipes. Int. J. Multiphase Flow 29, 527-558.

Ortalano, D. M., Picraux, L., Clapp, L., Merchak, P. A. and Schwarts, R. J. (2015). Pigment dispersion and printing inks with improved coloristic properties. Patent Application Publication US 2015/0252201 A1.

Osiac, E., Săftoiu, A., Gheonea, D. I., Mandrila, I. and Angelescu, R. (2011). Optical coherence tomography and Doppler optical coherence tomography in the gastrointestinal tract. World J. Gastroenterol. 17(1), 15-20.

Parida, O. P. and Bhat, N. (2009). Characterization of optical properties of SU-8 and fabrication of optical components. In *Proceedings of the ICOP 2009-International Conference on Optics and Photonics*, Chandigarh, India.

Penner, S. S., Davidor, W. and Bien F. (1970). Determination of Interference Patterns from Laser Produced Schlieren Interferometry. Am. J. Phys. 38(12), 1413-1415.

Perchoux, J., Quotb, A., Atashkhooei, R., Azcona, F. J., Ramírez-Miquet, E. E., Bernal, O., Jha, A., Luna-Arriaga, A., Yanez, C., Caum, J., Bosch, T. and Royo, S. (2016). Current developments on optical feedback interferometry as an all-optical sensor for biomedical applications. Sensors 16, 694.

Peronneau P. A. and Leger, F. (1969). Doppler ultrasonic pulsed blood flowmeter. Proc. of the 8th Conference on Medical and Biological Engineering, 10-11.

Petermann, K. (1991). Laser diode modulation and noise. Kluwer Academic Publishers. Tokyo.

Pohar, A., Lakner, M. and Plazl, I. (2012). Parallel flow of immiscible liquids in a microreactor: modeling and experimental study. Microfluid. Nanofluid. 12(1-4), 307-316.

Psaltis, D., Quake, S. R. and Yang, C. (2007). Developing optofluidic technology through the fusion of microfluidics and optics. Nature 442, 381-386.

Quirantes, A., Arroyo, F., & Quirantes-Ros, J. (2001). Multiple light scattering by spherical particle systems and its dependence on concentration: a T-matrix study. J. Colloid Interface Sci., 240(1), 78-82.

Quotb, A., Ramírez-Miquet, E. E., Tronche, C. and Perchoux, J. (2014). Optical feedback interferometry sensor for flow characterization inside ex-vivo vessel. In *IEEE Sensors*, 362-365.

Raghunathan, R., Singh, M., Mary E. Dickinson, M. E. and Larin, K. V. (2016). Optical coherence tomography for embryonic imaging: a review. J. Biomed. Opt. 21(5), 050902.

Raimondi, N. D. M., Prat, L., Gourdon, C. and Tasselli, J. (2014). Experiments of mass transfer with liquid–liquid slug flow in square microchannels. Chem. Eng. Sci. 105, 169-178.

Rajadhyaksha, M., Anderson, R. R. and Webb, R. H. (1999). Video-rate confocal scanning laser microscope for imaging human tissues in vivo. Appl. Opt. 38, 2105-2015.

Ramírez-Miquet, E. E., Arriaga, A. L., Quotb, A., Sotolongo-Costa, O. and Perchoux, J. (2015). In-situ measurement of non-steady flows using optical feedback interferometry. In *IEEE International Conference on Industrial Technology*, 1469-1473.

Ramírez-Miquet, E. E., Sotolongo-Costa, O., Quotb, A., Loubière, K., Prat. L. and Perchoux, J. (2016a). Profiling oil-water flows in microchannel: preliminary results using optical feedback interferometry. Optical measurement techniques for systems and structures III, 251-258. Shaker Publishing.

Ramírez-Miquet, E. E., Perchoux, J., Loubière, K., Tronche, C., Prat, L. and Sotolongo-Costa, O. (2016b). Optical feedback interferometry for velocity measurement of parallel liquid-liquid flows in a microchannel. Sensors 16, 1233.

Riva, C., Ross, B. and Benedek, G. B. (1972). Laser Doppler measurements of blood flow in capillary tubes and retinal arteries. Invest. Ophthalmol. Vis. Sci. 11(11), 936-944.

Roehle, I. (1998). Method for measuring flow vectors in gas flows US Patent 5751410 A.

Roehle, I, Karpinski, G. and Schodl, R. (1999). 3-Component-Doppler-Laser-2-Focus: A new kind of three component velocimeter. 18th International Congress on Instrumentation in Aerospace Simulation Facilities ICIASF99, Toulouse, 13/1-13/9.

Roman, S., Lorthois, S., Duru, P. and Risso, F. (2012). Velocimetry of red blood cells in microvessels by the dual-slit method: Effect of velocity gradients. Microvasc. Res. 84, 249-261.

Rooze, J., André, M., van der Gulik, G. J. S., Fernández-Rivas, D., Gardeniers, J. G., Rebrov, E. V., Schouten, J. C. and Keurentjes, J. T. (2012). Hydrodynamic cavitation in micro channels with channel sizes of 100 and 750 micrometers. Microfluid. Nanofluid. 12(1-4), 499-508.

Rovati, L., Cattini, S. and Palanisamy, N. (2011). Measurement of the fluid velocity profile using a self-mixing superluminescent diode. Meas. Sci. Tech. 22(2), 025402.

Rudd, M. (1968). A laser Doppler velocimeter employing the laser as a mixer-oscillator. J. Sci. Instrum. 1, 723-726.

Rudd, M. J. (1969). A new theoretical model for the laser dopplermeter. J. Phys. E Scient. Instrum. 2(1), 55-58.

Rudyak, V and Minakov, A. (2014). Modeling and optimization of Y-type micromixers. Micromachines, 5(4), 886-912.

Salazar-Miranda, D., Castillón, F. F., Sánchez-Sánchez, J. J., Angel-Valenzuela, J. L., Márquez, H. (2010). Refractive index modulation of su-8 polymer optical waveguides by means of hybrid photothermal process. Rev. Mex. Ing. Quim. 9(1), 85-90.

Samimy, M. and Wernet, M. P. (2000). Review of planar multiple-component velocimetry in high-speed flows. AIAA J. 38(4), 553-574.

Satomura, S., (1957). Ultrasonic Doppler method for the inspection of cardiac functions. J. Acoust. Soc. Am. 29, 1181-1183.

Satomura, S. and Kaneko, Z. (1960). Ultrasonic blood rheograph. Proc. of the 3rd International Conference on Medical Electronics. London, 254-258.

Schodl, R. (1980). A Laser-Iwo-Focus (L2F) velocimeter for automatic flow vector measurements in the rotating components of turbomachines. J. Fluid Eng.-T. ASME, 102(4), 412-419.

Seko, A., Mitsuhashi, Y., Morikawa, T., Shimada, J. and Sakurai, K. (1975). Self-quenching in semiconductor lasers and its applications in optical memory readout. Appl. Phys. Lett. 27(3), 140-141.

Servagent, N., Mourat, G., Gouaux, F. and Bosch, T. (1998). Analysis of some intrinsic limitations of a laser range finder using self-mixing interference. Proc. of 3479, 76-83.

Shah, R. K. and London, A. L. (1978). Laminar flow forced convection in ducts: a source book for compact heat exchanger analytical data (vol. 1). Academic Press.

Shet, A. S. (2008). Characterizing blood microparticles: technical aspects and challenges. Vasc Health Risk Manag 2008:4(4) 769–774.

Shinohara, S., Mochizuki, A., Yoshida, H. and Sumi, M. (1986). Laser Doppler velocimeter using the self-mixing effect of a semiconductor laser diode," Appl. Opt. 25(9), 1417-1419.

Soares, R. R., Barbosa, H. C., Braga, R. A., Botega J. V. L. and Horgan, G. W. (2013). Biospeckle PIV (Particle Image Velocimetry) for analyzing fluid flow. Flow Meas. Instrum. 30, 90–98.

Stern, L., Bakal, A., Tzur, M., Veinguer, M., Mazurski, N., Cohen, N. and Levy, U. (2014). Doppler-Based Flow Rate Sensing in Microfluidic Channels. Sensors, 14(9), 16799-16807.

Strandness, D. E., Schultz, R. D., Sumner, D. S., Rushmer, R. F. (1967). Ultrasonic flow detection – a useful technique in the evaluation of peripheral vascular disease. Am. J. Surg. 113, 311-314.

Sudo, S. Miyasaka, Y., Nemoto, K. Kamikariya, K. and Otsuka, K. (2007). Detection of small particles in fluid flow using a self-mixing laser. Opt. Express 15(13), 8135-8145.

Sun, J. G., Adie, S. G., Chaney, E. J., Boppart, S. A. (2013). Segmentation and correlation of optical coherence tomography and x-ray images for breast cancer diagnostics. J. Innov. Opt. Health Sci. 6(2), 1350015.

Swanson, E. A., Izatt, J. A., Hee, M. R., Huang, D., Lin, C. P. Schuman, J. S., Puliafito, C. A. and Fujimoto, J. G. (1993). In-vivo retinal imaging by optical coherence tomography. Opt. Lett. 18, 1864-1866.

Taimre, T., Nikolić, M., Bertling, K., Lim, Y. L., Bosch, T., Rakić, A. D. (2015). Adv Opt. Photonics 7, 570-631.

Taitel, Y., Barnea, D. and Brill, J. P. (1995). Stratified three-phase flows in pipes. Int. J. Multiphase Flow. 21(1), 53-60.

Takeda, Y. (1986). Velocity profile measurement by ultrasound Doppler shift method. Velocity profile measurement by ultrasound Doppler shift method. Int. J. Heat Fluid Flow 7(4), 313-318

Takeda, Y. (1999). Ultrasonic Doppler method for velocity profile measurement in fluid dynamics and fluid engineering. Exp. Fluids 26, 177-178.

Tamura, T. and Fronek, A. (1988). New method for Doppler probe angle determination. J. Biomed. Eng. 10, 271-274.

Tamura, T., Yoganathan, A and Sahn, D. J. (1987). In vitro methods for studying the accuracy of velocity determination and spatial resolution of a color Doppler flow mapping system. Am. Heart J. 114, 152-158.

Tamura, T. and Johnston, K. W. (1990). Determination of 2-D velocity vectors using color Doppler ultrasound. IEEE Ultrasonics 1537-1540.

Thompson, D.H. (1968). A tracer particle fluid velocity meter incorporating a laser. J. Phys. E 1, 929–932.

Turgeon, M. L. (2004). Clinical Hematology: Theory and Procedures. Chapter 6. Lippincott Williams & Wilkins.

Vinegar, H. J. and Wellington, S. L. (1987). Tomographic imaging of three-phase flow experiments. Rev. Scientif. Instrum. 58(1), 96-107.

Voigt, A., Bayer, C., Shirai, K., Büttner L. and Jürgen C. (2008). Laser Doppler field sensor for high resolution flow velocity imaging without camera. Appl. Opt. 47(27), 5028-5040.

Wang, C. P. (1974). Doppler velocimeter using diffraction grating and white light. Appl. Opt. 13(5), 1193-1195.

Wang, C. P. (1988). Laser Doppler velocimetry. J. Quant. Spectrosc. Radiat. Transfer 40(3), 309-319.

Wang, Y., Fawzi, A., Tan, O., Gil-Flamer, J., Huang, D. (2009). Retinal blood flow detection in diabetic patients by Doppler Fourier domain optical coherence tomography. Opt. Express 17, 4061-4073.

Wang, Y., Fawzi, A.A., Varma, R., Sadun, A.A., Zhang, X., Tan, O., Izatt, J.A., Huang, D. (2011). Pilot study of optical coherence tomography measurement of retinal blood flow in retinal and optic nerve diseases. Investig. Ophthalmol. Vis. Sci. 52, 840-845.

Wells, P. N. T. (1969). A range-gated ultrasonic Doppler system. Med. Biol. Eng. 7, 641-652.

Wereley, S. T. and Meinhart, C. D. (2010). Recent advances in micro-particle image velocimetry. Annu. Rev. Fluid Mech. 42, 557-576.

White, F. M. (1999). Fluid Mechanics, 4th Edition, WBC/Mc Graw-Hill, Boston.

Wilkes, J. O. (2006). Fluid Mechanics for Chemical Engineers with Microfluidics and CFD. Pearson Education.

Wu, L. (2004) Simultaneous measurement of flow velocity and Doppler angle by the use of Doppler optical coherence tomography. Opt. Lasers Eng. 42, 303-313.

Wu, J. and Gu, M. (2011). Microfluidic sensing: state of the art fabrication and detection techniques. J. Biomed. Opt. 16(8), 080901.

Yeh, Y. and Cummins, H. Z. (1964) Localized fluid flow measurements with an He-Ne spectrometer. Appl. Phys. Lett. 4, 176-178.

Yue, J., Rebrow, E. V. and Schouten, J. C. (2014). Gas–liquid–liquid three-phase flow pattern and pressure drop in a microfluidic chip: similarities with gas–liquid/liquid–liquid flows. Lab Chip 14, 1632–1649.

Zabit, U. (2010). Optimisation of a self-mixing laser displacement sensor. Thesis dissertation.

Zakian, C., Dickinson, M and King, T. (2005). Particle sizing and flow measurement using self-mixing interferometry with a laser diode. J. Opt. A: Pure Appl. Opt. 7, S445-S452.

Annexes

Annex 1: Electronic circuitry relative to the infrared laser Thorlabs L785P090.

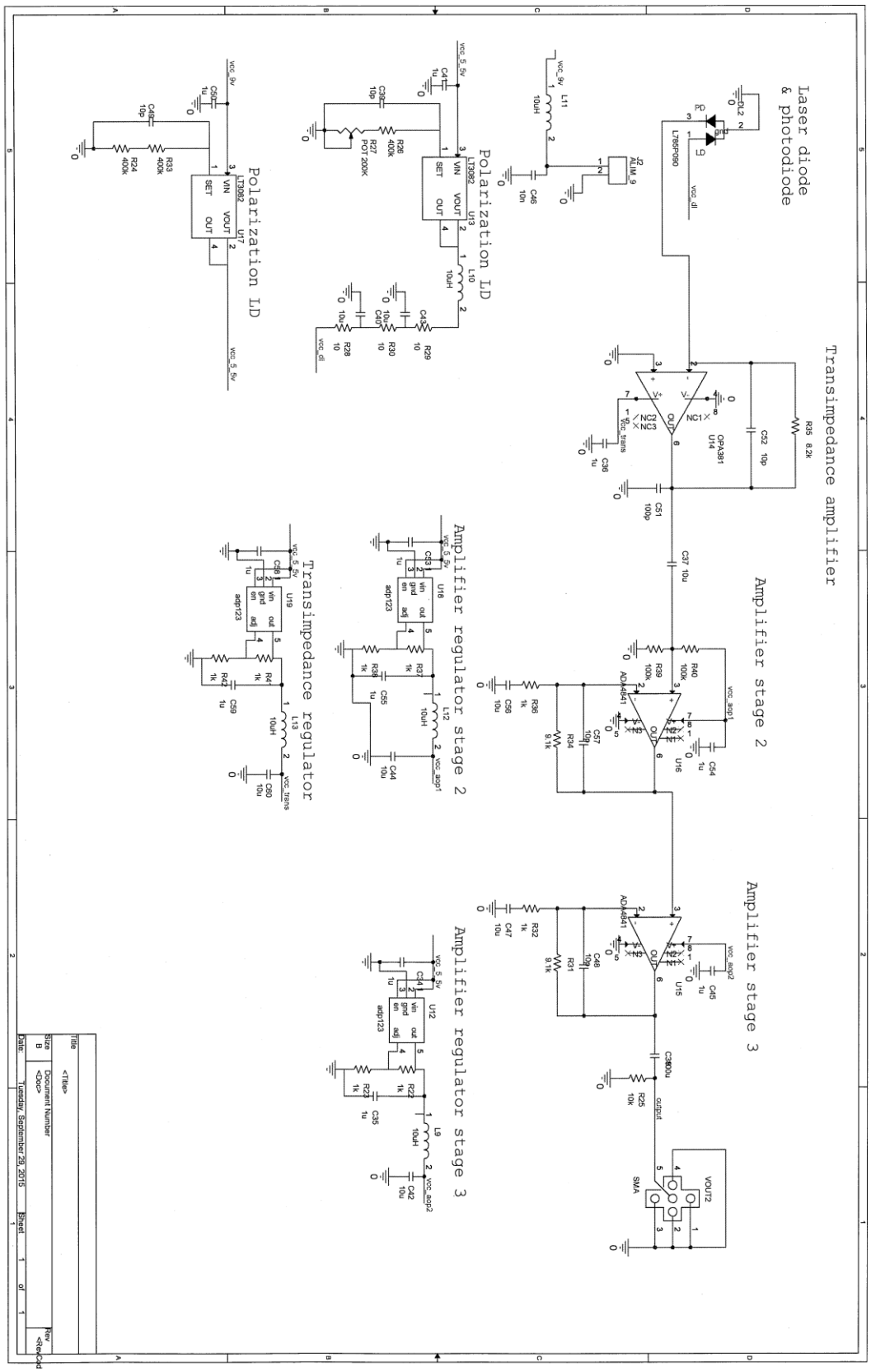

Annex 2: Electronic circuitry relative to the blue-violet laser Panasonic DL5146-101S.